

Copyright
by
Michael Gostein
1997

**Dynamical Effects in Dissociative Adsorption:
Quantum State-Resolved Studies of
H₂ Scattering from Pd and Cu**

by

Michael Gostein, B.S., M.A.

Dissertation

Presented to the Faculty of the Graduate School of
The University of Texas at Austin
in Partial Fulfillment
of the Requirements
for the Degree of

Doctor of Philosophy

**The University of Texas at Austin
May, 1997**

**Dynamical Effects in Dissociative Adsorption:
Quantum State-Resolved Studies of
H₂ Scattering from Pd and Cu**

**Approved by
Dissertation Committee:**

Greg O. Sitz, Supervisor

Manfred Fink

John W. Keto

Charles B. Mullins

John M. White

Acknowledgements

The experiments described in this dissertation were part of a project begun by my advisor, Prof. Greg O. Sitz, to study quantum-state resolved effects in molecule-surface scattering. Construction of the experimental apparatus began a year or two before I started my graduate studies.

I participated in building up the apparatus along with fellow students Jennifer Siders, Michael Bryan, Hadi Parhikhteh, Chad Cotton, and Elizabeth Watts. Some of my initial experiments were performed with Hadi Parhikhteh, and some of the later ones with Elizabeth Watts, and Prof. Sitz participated actively in all stages of the projects. I want to thank the students mentioned above, and those who worked on other projects, Marcia Isakson and Rudy McGlothlin, for making the Sitz lab a fun place to work.

I truly enjoyed working with Prof. Sitz and I deeply appreciate his support and guidance during my graduate studies. He takes teaching seriously, is always fair and considerate in treating his students and colleagues, and truly inspires enthusiasm for science. I consider him not only a teacher but a friend.

I am also very grateful to the other members of my dissertation committee, Profs. Manfred Fink, John Keto, Mike White, and especially Buddie Mullins, for frequent consultations about the progress of my work.

In addition, I thank the University of Texas at Austin for generously supporting me with fellowships during three of my years of graduate study.

And, for the last five years, my wife Abby was a constant source of support, encouragement, and love.

Dynamical Effects in Dissociative Adsorption: Quantum State-Resolved Studies of H₂ Scattering from Pd and Cu

Publication No. _____

Michael Gostein, Ph.D.

The University of Texas at Austin, 1997

Supervisor: Greg O. Sitz

The effects of molecular rotation and vibration in the dynamics of H₂ scattering from Pd(111) and Cu(110) were studied using molecular beam and laser spectroscopy techniques. These studies test state-of-the-art theoretical simulations of molecule-surface interactions, a fundamental understanding of which is relevant to diverse fields in science and technology.

Experiments on the rotational state dependence of H₂ dissociation on Pd(111) were motivated by recent theoretical results concerning the concept of dynamical steering. This concept has been invoked to explain the enhancement of sticking at low translational energy for H₂ incident on certain metals. It suggests that sticking should also be enhanced for low rotational energy in these systems.

The experiments presented here qualitatively confirm this prediction. For incident translational energies from 31-95 meV, the H₂/Pd(111) sticking coefficient goes down as the rotational quantum number J is raised from 0 to 3. It then increases for $J=4$ and 5, which is consistent with rotational energy also

helping directly overcome the activation barrier. A fraction of the scattered H₂ molecules are also rotationally excited. This occurs directly upon scattering but is activated by the surface temperature, not the incident translational energy. This behavior is not explained by current theoretical treatments and requires further exploration.

Experiments on the vibrational state dependence of H₂ scattering from Cu(110) and Pd(111) were motivated by continued considerations of activation barriers to dissociative adsorption, since vibrational energy assists in surmounting barriers which occur “late” along the reaction path.

The survival probability of H₂ in the rovibrational state ($v=1, J=1$), prepared by stimulated Raman scattering, was measured for scattering from each surface. In both cases the ($v=1, J=1$) survival probability is smaller than that of the ground vibrational state, in accord with expectations for a late barrier. On Cu(110) it decreases from 0.67 ± 0.09 to 0.28 ± 0.05 over the translational energy range 77-280 meV, in good agreement with recent theoretical calculations. On clean Pd(111), it is only a few percent. Vibrational relaxation was also observed on Pd(111), in a process that involves transfer of some vibrational energy to the Pd substrate. The relaxation channel may be electronically nonadiabatic and deserves further theoretical and experimental investigation.

Contents

List of Tables	ix
List of Figures	x
Part I Overview	1
Chapter 1 Why Molecule-Surface Scattering?	2
Part II Rotational Effects - H₂ on Pd	7
Chapter 2 Introduction	8
2.1 Dynamical Steering	8
2.2 J-Dependent Sticking	9
2.3 Experimental Tests	11
Chapter 3 Experimental Apparatus	13
3.1 Molecular Beam System	13
3.2 Laser Spectroscopy	14
3.3 Distinguishing Incident and Scattered Molecules	16
3.4 Sample Preparation	17
Chapter 4 Measurement Technique and Results	20
4.1 Program of Measurements and Normalization Method	20
4.2 Representative Rotational Spectra	22
4.3 Model and Analysis	25
4.4 Extracted Model Parameters	27
Chapter 5 Discussion of Results	30
5.1 J-Resolved Sticking Coefficients	30
5.2 Rotational Relaxation	35
5.3 Rotational Excitation	36
5.4 Contribution from Recombinative Desorption	41
5.5 Systematic Errors	44
Part III Vibrational Effects - H₂ on Cu and Pd	48
Chapter 6 Introduction	49
6.1 Late Barriers in Activated Dissociative Adsorption	49

6.2 H ₂ /Cu	50
6.3 H ₂ /Pd	54
Chapter 7 Experimental Apparatus	56
7.1 State Preparation and Detection	56
7.2 Sample Preparation	58
Chapter 8 H₂ on Copper	60
8.1 Representative TOF Curves	60
8.2 Determining Incident and Scattered Velocities and Transforming TOF Spectra from Density to Flux Weighted	63
8.3 Survival Probability versus Incident Translational Energy	65
8.4 Absolute Survival Probability Measurement	68
8.5 Discussion	71
Chapter 9 H₂ on Pd	78
9.1 TOF Curves for Clean and H-Covered Pd	78
9.2 Absolute Survival Probability on Clean and H-Covered Pd	81
9.3 Vibrational Relaxation	84
Part IV Conclusion	92
Chapter 10 Summary, Conclusions, and Future Work	93
10.1 Summary of Part II - Rotational Effects	93
10.2 Summary of Part III - Vibrational Effects	95
10.3 Future Work on the State-Resolved Scattering Experiments	97
10.4 Future Directions in Surface Science	102
Appendix A H₂ REMPI and Raman Transitions	105
Appendix B Response versus Scattering Angle in Shadow Experiments	106
Appendix C Density to Flux Transformation of TOF Spectra	110
References	115
Vita	122

List of Tables

4.1: Number of measurement sets and range of nozzle temperatures used to determine the J-resolved H ₂ /Pd(111) sticking and state-changing probabilities.	28
4.2: Rotational state-resolved sticking coefficients and rotational state changing probabilities for H ₂ scattered from Pd(111) at T _s = 423 K.	28
8.1: Parameters for fit of H ₂ (v=1, J=1) survival probability on Cu(110) versus incident translational energy.	68
9.1: Energy disposal in H ₂ (v=1, J=1) vibrational relaxation on Pd(111).	89

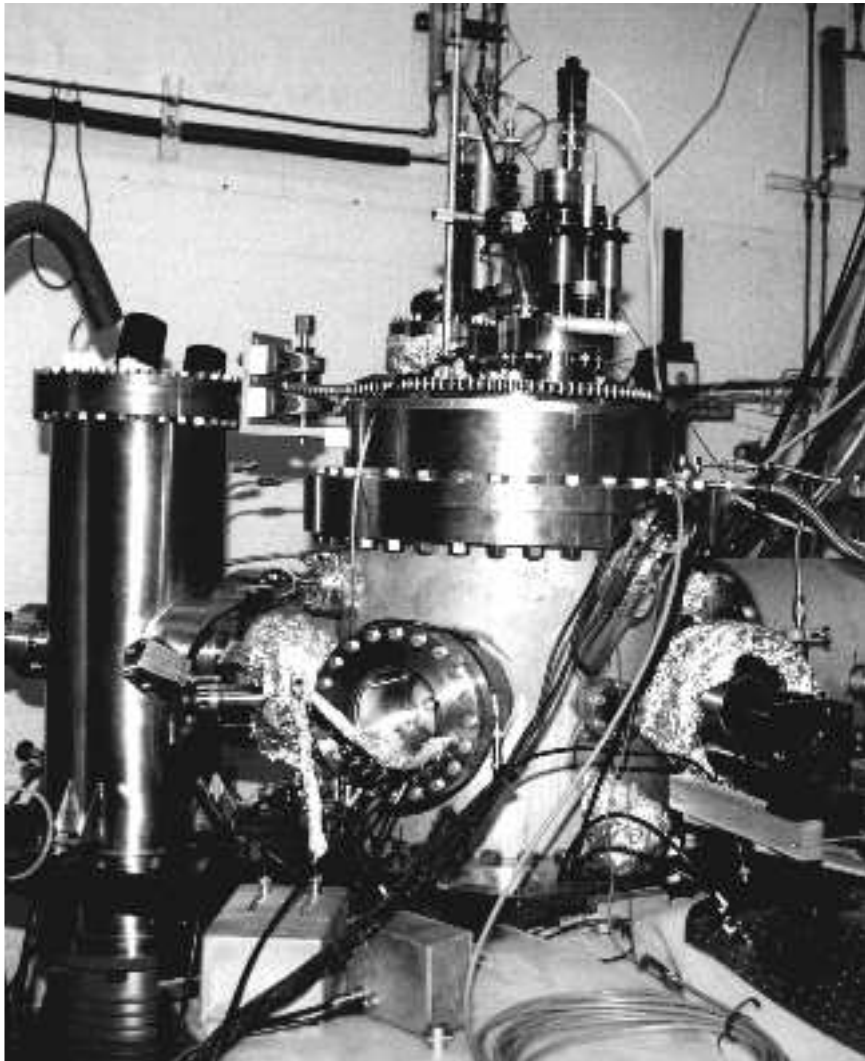
List of Figures

2.1: Theoretical sticking probability of H ₂ on Pd(100) as a function of incident kinetic energy and initial rotational state.	10
3.2: Schematic diagram of the experimental apparatus.	14
4.1: Representative rotational distributions for H ₂ scattered from Pd(111).	24
5.1: H ₂ /Pd(111) sticking coefficient and as a function of incident translational energy and rotational state J.	31
5.2: H ₂ /Pd(111) sticking coefficient versus rotational quantum number J at $E_i = 74$ meV.	32
5.3: Comparison of state-averaged H ₂ /Pd(111) sticking coefficients measured by Beutl and coworkers with predictions from state-resolved results reported here.	34
5.4: Rotational excitation coefficients for H ₂ on Pd(111) at $T_s = 423$ K.	37
5.5: Representative TOF data from which surface temperature dependent rotational excitation coefficients were determined.	38
5.6: Arrhenius plot of rotational excitation coefficients versus inverse surface temperature showing apparent activation energy for excitation.	39
5.7: One-dimensional H/Pd potential energy diagram illustrating energetics for desorption and diffusion.	43
6.1: Theoretical dissociation, vibrational excitation, and vibrational relaxation probabilities for H ₂ ($v=0$) and ($v=1$) scattered from Cu(100).	51
8.1: Representative TOF curves for H ₂ ($v=1, J=1$) scattered from Cu(110) at three different translational energies.	61
8.2: Incident and scattered peak times in pump/probe experiment versus probe laser distance from the surface.	64
8.3: Survival probability versus incident translational energy for H ₂ ($v=1, J=1$) on Cu(110).	66
8.4: Spatial profile of flux incident on and scattered back from Cu(110) in the H ₂ ($v=1, J=1$) state.	70
8.5: Comparison of H ₂ ($v=1, J=1$) loss probability on Cu(110) with theoretical calculations and previous experiments.	74
9.2: Spatial profiles of incident and scattered flux for H ₂ ($v=1, J=1$) scattered from Pd(111), both clean and H-covered.	82
9.3: TOF curves for H ₂ ($v=1, J=1$) incident on Pd(111), showing vibrational relaxation to $v=0$ manifold.	85
A.1: Energy level diagram showing H ₂ REMPI and Raman transitions.	105
B.1: Geometry for determining angular response function of detection system when using wire-shadowed aperture.	107

B.2: Angular response of detection system in shadow geometry.	108
C.1: Distance traversed through probe volume by a scattered molecule.	110
C.2: Example of density to flux transformation of TOF spectrum.	114

Part I

Overview



Chapter 1

Why Molecule-Surface Scattering?

Chemical reactions on solid surfaces play an important role in many branches of science and technology. In the chemical industry, for example, heterogeneous catalysis on the surfaces of metal and oxide powders is widely used to promote and gain selectivity in chemical reactions. Catalysts are an essential part of this industry and there is a constant effort to develop and improve them. Heterogeneous catalysis may also play an important role in the environment, such as in the effects of reactions on aerosol or ice particle surfaces on atmospheric chemistry. And, in the electronics industry, knowledge of the details of surface chemical reactions used in the patterning of integrated circuits is becoming more important as the size of electronic devices continues to shrink. As a result of their widespread importance, the nature of surface chemical reactions has been studied intensely for the past three decades.

A principle research goal has been to build up predictive power in analyzing these reactions. This is intrinsically complicated because surface reactions are, by nature, many-body problems, involving many electrons and nuclei. Furthermore, in any one chemical system a variety of physical processes must be considered, such as the adsorption of species onto the reactive surface, their dissociation, diffusion across the surface, reaction with other species, and subsequent desorption, as well as changes in the chemical/electronic state of the surface and rearrangement of the surface atoms during the entire process. The fundamental nature of each of these processes has typically been studied independently to simplify the problem.

Of the surface chemical processes listed above, one of the most important is that of dissociative adsorption, in which a molecule in the gas phase strikes a surface and dissociates into two adsorbed atoms. This is often the initial step in a surface-catalyzed chemical reaction, as it brings the reactants to the surface. Consequently there has been a great deal of theoretical and experimental effort aimed at understanding the dynamics of this step. [1,2]

In general, chemical reactions may be classified as one of two types: those that are activated and those that are not. Activated processes require input of energy for the reactants to surmount a repulsive barrier which initially prevents reaction, even though the process as a whole releases energy, while unactivated processes require no energy input. Therefore activated processes typically occur slowly while unactivated processes occur readily. Many gas-surface systems display activation barriers to dissociative adsorption. An important theoretical and experimental goal has been to investigate the nature of these barriers, why they arise, and the dynamical mechanisms by which they are overcome.

Both theory and experiment have concentrated on explaining the fundamental phenomena of dissociative adsorption as observed in certain model gas-surface systems. Typically these systems are small molecules, particularly diatomics such as H_2 , N_2 , NO , CO , etc., interacting with various low Miller index faces of single crystal metals and semiconductors. The reaction of H_2 with metals has been particularly important, because H_2 is the simplest molecule to treat theoretically.

The theoretical approach to the dissociative adsorption problem, as for many other problems in chemical dynamics, has been to consider first the total energy of the system as a function of the positions of all the atoms, referred to as the potential energy surface (PES), and then, using the PES, to calculate the

dynamics for given initial conditions. Both steps in this program are complicated by the number of atoms involved, and simplifying approximations, such as neglecting some degrees of freedom, must be made. An implicit assumption in this program is that the total energy may be regarded as only a function of the atomic coordinates, i.e. that the electronic degrees of freedom equilibrate much faster than the nuclear motion, which is the Born-Oppenheimer approximation.

Due to steady progress in both computational power and analytical techniques, the sophistication of theoretical simulations of molecule-surface scattering dynamics has increased greatly in recent years. The current state-of-the-art in these calculations permits evaluating the PES for a diatomic molecule in terms of all six molecular degrees of freedom and calculating the dynamics on this six-dimensional PES quantum mechanically. Density functional theory (DFT) with the generalized gradient approximation (GGA) is used in calculating the PES and a coupled channel or wave packet approach is used to calculate the dynamics. [1,3,4,5] The six degrees of freedom are the molecule/surface separation, the atom/atom separation in the diatomic molecule, the two impact coordinates of the molecule on the surface, and the two angles describing the molecular orientation. Motion of the surface atoms is still either neglected or treated in a lower degree of precision, however.

In the theoretical simulations, the initial conditions of a molecule-surface scattering event may be precisely controlled, and the effect of these conditions on the outcome of the scattering may be explored. Thus, for example, the effects of initial velocity, incidence angle, and rotational and vibrational motion on a molecule's behavior when colliding with a given surface may be examined. Certain dynamical behaviors are found to be characteristic of particular features in the calculated potential energy surface.

In order to test the theoretical predictions, and to uncover new behavior, it is desired to perform experiments which provide information on the molecule-surface interaction forces and dynamics. One typical approach to exploring these forces and dynamics, as in many physical problems, is to perform a scattering experiment.

Scattering experiments of relevance to gas-surface chemistry usually employ supersonic molecular beams directed at single-crystal samples of the target material in ultra-high vacuum (UHV). The mean velocity of the molecular beam is easily adjusted by varying the ratio of reactant gas to inert seed gas in the beam source, as well as the temperature of the nozzle from which the beam emerges. The velocity distribution in the beam is very narrow because the expansion from the nozzle is supersonic. Therefore these experiments can probe the effects of the molecule's incident velocity and angle on the scattering and the reaction probability. Laser spectroscopy may also be used to measure the rotational and vibrational state distributions of the incident and scattered molecules, and thus probe the effects of the scattering on the internal molecular motion during the collision.

The goal of the present work was to study experimentally the effect of the molecule's *initial* rotational and vibrational motion on the scattering event, and to make the most precise comparisons with theory possible by measuring the reaction probabilities of molecules in particular rotational and vibrational states. To this end, a molecular beam surface scattering apparatus was used with laser spectroscopy for quantum state resolved detection, and, in some experiments, for quantum state preparation in the molecular beam.

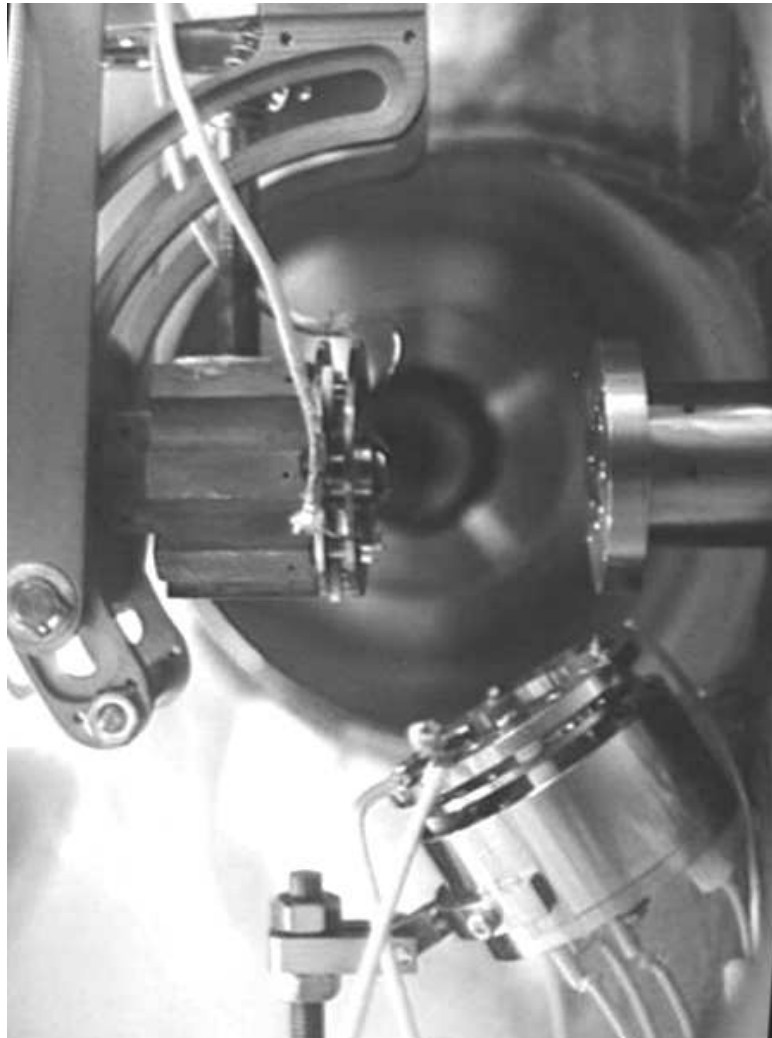
For this work, the reaction of H₂ with Pd and Cu single crystals was studied. The H₂/Pd and H₂/Cu systems have been well studied previously both

experimentally and theoretically. The former is an example where dissociation occurs readily, while the latter is a classic example of a system with a high activation barrier to dissociative adsorption. Recent experimental and theoretical results in these systems have shown strong effects due to rotational and vibrational motion of the incident molecules, as will be discussed in the chapters that follow. The present work was undertaken to explore these effects with greater precision and provide a more stringent check against theory. Because of the unique experimental approaches adopted, new behaviors were also uncovered during these studies which cannot be explained within the current theoretical state-of-the-art.

The experiments on the rotational motion effects were carried out solely for H₂ dissociation on Pd and are discussed in Part II of the dissertation, chapters 2 through 5. The experiments on vibrational motion effects were carried out for H₂ on both Cu and Pd and are discussed in Part III, chapters 6 through 9. Part IV contains the concluding chapter, Chapter 10, which summarizes the results and conclusions of both sets of experiments. It also suggests directions for future work on these projects and in the molecule-surface scattering field in general.

Part II

Rotational Effects - H₂ on Pd



Chapter 2

Introduction

This section of the dissertation, Chapters 2 through 5, discusses the experiments performed on the effects of rotational motion in the dissociation of H_2 on Pd. These experiments were motivated by recent theoretical calculations concerning the role of dynamical steering in this system. This chapter gives a brief introduction to the theoretical discussion of these effects, a summary of some previous experiments performed to test them, and the motivations for the present work. In Chapter 3 the experimental apparatus used in the present work is described, and in Chapters 4 and 5 the results of the experiments are discussed.

2.2 Dynamical Steering

The concept of dynamical steering emerged recently to explain certain trends observed in nonactivated dissociative adsorption. [4,6,7] In the cases of H_2 adsorption on, for example, Pd [8], W [9], and Pt [10], molecular beam experiments have shown that, at low incident kinetic energy, the sticking coefficient actually decreases as the kinetic energy is raised. In the past, this trend has often been interpreted in terms of a precursor-mediated adsorption mechanism, in which adsorption occurs by first the trapping of the incident particles into the physisorbed state, followed by a dissociative step. [11] Because trapping into the physisorbed state is favored at low kinetic energy, the sticking coefficient goes down as the kinetic energy is raised. This mechanism is almost certainly correct in the case of the dissociative adsorption of alkanes on transition metals, for example. [12,13] But for H_2 on metals, such as in the examples listed above, an alternative explanation seems called for, since H_2 physisorption is

generally weak [14,15] and its lightness results in small trapping probabilities on metals. An alternative explanation of the H₂/metal sticking behavior has recently been proposed, in which the incident H₂ molecules are dynamically steered along the lowest energy paths towards favorable adsorption geometries during their approach to the surface. The steering forces enhance the dissociation probability for molecules approaching the surface slowly enough. As the kinetic energy is raised beyond this range, the molecules do not have enough time during the collision to be steered to the dissociation configuration, so the sticking coefficient goes down.

High-dimensional dynamical simulations on *ab initio* potential energy surfaces have demonstrated the dynamical steering effect for H₂ on Pd [4,5], W [6], and Rh [7]. These calculations also show a strong coupling between the surface and the rotational degree of freedom of the incident molecule, with the interaction acting to rotate the molecule into a favorable adsorption geometry.

2.4 J-Dependent Sticking

An additional feature of the theoretical work done by Gross, Wilke, and Scheffler on the H₂/Pd system [4,5] is their prediction that the H₂ sticking coefficient should depend sensitively on the initial rotational quantum number. Figure 2.1 shows their calculated values for the sticking coefficient of H₂ on Pd(100) as a function of initial rotational quantum number J_i and incident kinetic energy E_i . At the lowest incident kinetic energy, where the steering mechanism should be dominant, the figure shows that the sticking coefficient drops, in general, as either the kinetic energy or the rotational state is raised. Their interpretation is that in the low energy range, increasing either the kinetic energy or the rotational energy inhibits the ability of the steering effect to guide the molecule to dissociation. The predicted dependence of the sticking on rotational

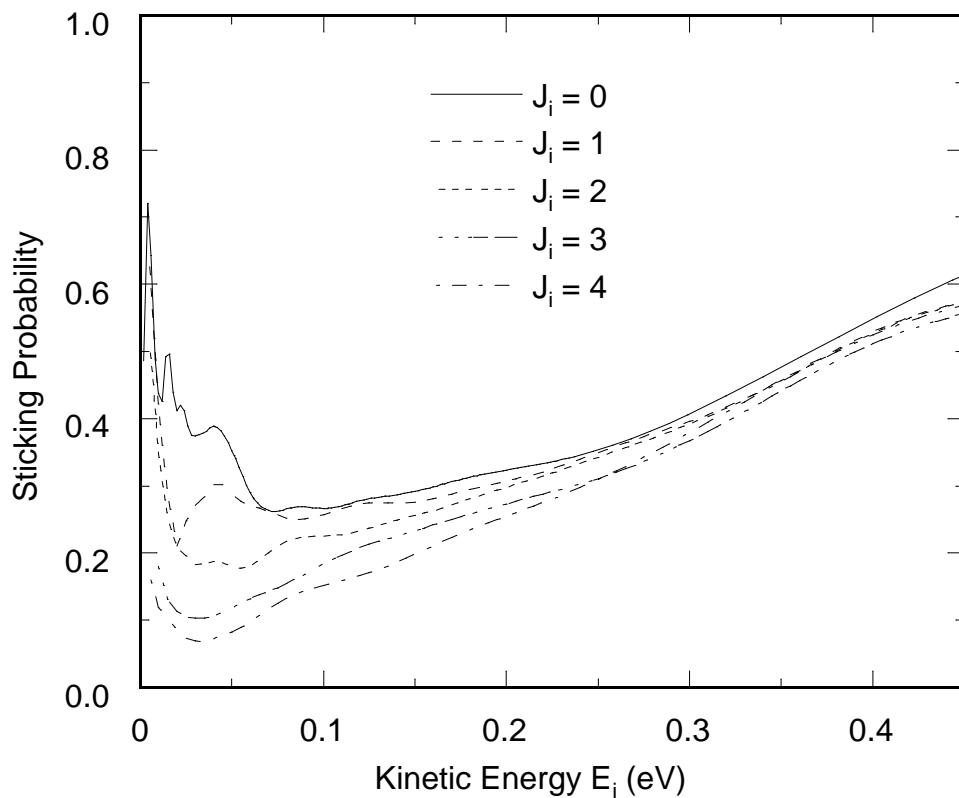


Figure 2.2: Theoretical sticking probability of H_2 on Pd(100) as a function of incident kinetic energy and initial rotational state. Results are courtesy of Axel Gross and appeared in Ref. 5.

state was consistent with the observation of rotational cooling in recombinative desorption of H_2 from Pd(100) [16], which, by the principle of detailed balance, implies lower sticking coefficients for higher J states.

Note in Fig. 2.1 that, in the high energy range, the sticking coefficient does go up with increasing kinetic energy, contrary to the trend at low energy. This is because at the high energies the suppression of the steering effect, which guides the molecules around the activation barriers, is already complete, but increasing

the translational energy helps the molecules to directly overcome the activation barriers.

Also note in Fig. 2.1, although they will not be considered in detail here, the oscillatory features in the sticking probability as a function of translational energy. These features are typical of quantum mechanical dynamics and arise from a number of sources. One source is the opening of new diffraction (scattering) channels as the translational energy is raised. [4,17,18] Another is resonances that occur when the incident translational energy matches the energies of frustrated vibration and rotation states of the molecule at the surface. [6]

2.6 Experimental Tests

The prediction of rotational state dependent H_2/Pd sticking coefficients was directly confirmed in adsorption by Beutl, Riedler, and Rendulic, who found in seeded beam experiments that the $H_2/Pd(111)$ sticking coefficient decreased substantially as the average rotational energy of the incident molecular beam was increased. [19] In a later experiment on H_2/Pt , they actually determined state-resolved sticking coefficients for $J=0, 1, \text{ and } 2$ by cleverly using different ortho and para H_2 mixtures. [20] Sticking coefficients for higher rotational states probably cannot be obtained using this method, however, which relies on detecting differences in the average sticking coefficient for beams of different rotational temperatures. The populations in the higher states are not large enough to significantly affect the average sticking coefficient. Also, these results are based on the assumption that the ratio of ortho and para molecules in the beam is not altered during passage through the beam source. Though the authors have reason to believe this assumption is correct, they were not able to check it.

Rettner and Auerbach also briefly addressed the rotational state dependence of the H_2/Pd sticking coefficient using laser spectroscopy for state-

selective detection in a molecular beam experiment. [21] They measured the relative reflectivity, $R(J)$, for H_2 in different J states scattered from clean versus hydrogen saturated Pd(100). They found the ratio $R(J)_{clean}/R(J)_{saturated}$ increased with J over the range $J=0$ to 3, for incident translational energies of 50 meV and 70 meV. This suggests that the sticking coefficient on the clean surface drops as J is increased, supporting the prediction of Gross, Wilke, and Scheffler regarding the role of rotation in inhibiting adsorption. However, they measured sticking coefficients that are higher than those predicted by Gross *et al.* for Pd(100) by approximately a factor of two. In addition, they questioned the detailed structure calculated by Gross *et al.* for sticking versus translational energy, which they did not observe experimentally. [22]

The present work was undertaken to further investigate the role of rotational motion in H_2 /Pd adsorption. Experiments were performed to measure the sticking coefficient of H_2 on Pd(111) as a function of initial rotational quantum state. These experiments are similar to those performed by Rettner and Auerbach, but the measurements have been extended to a larger range of J and translational energy, and, in addition, the possibility of rotational state changing collisions at the surface has been included in the analysis. The results of the present experiments show an interesting trend which generally supports the dynamical steering model. In addition, there are some unique experimental findings which require further experimental and theoretical investigation.

Chapter 3

Experimental Apparatus

In this chapter the experimental apparatus used in all the scattering experiments will be discussed, along with details particularly relevant to the H₂/Pd rotational motion experiments. Details relevant to the experiments on vibrational motion will be discussed in Chapter 7 of Part III.

3.2 Molecular Beam System

A schematic diagram of the experimental apparatus, some details of which have been described previously in the literature [23], is shown in Figure 3.2. A supersonic H₂ beam exits a pulsed nozzle, operating at 10 Hz, the temperature of which was varied between 150 K and 800 K for these experiments. The beam is skimmed and then chopped by a high-speed rotating disk in the differentially pumped buffer chamber. It enters the differentially pumped ultra-high vacuum (UHV) scattering chamber through a specially shaped aperture, which will be discussed further below, and scatters off a Pd(111) crystal within a few degrees of normal incidence.

The chopper disk has slits of two different sizes and the nozzle firing time can be chosen to select either of the slits. When the narrower slit is used, the flux of the beam source onto the target is $\leq 1 \times 10^{12} / \text{cm}^2$ per pulse, corresponding to ≤ 0.00065 monolayers (ML) per pulse given the Pd(111) site density $N_A = 1.53 \times 10^{15} / \text{cm}^2$. These pulses have a temporal full width at half maximum of about 10 μs when they reach the Pd target (when pure H₂ is used in the beam source, at room temperature). When the larger slit is used, the pulse width and flux per pulse are increased by a factor of 20. The larger slit is used only for brief

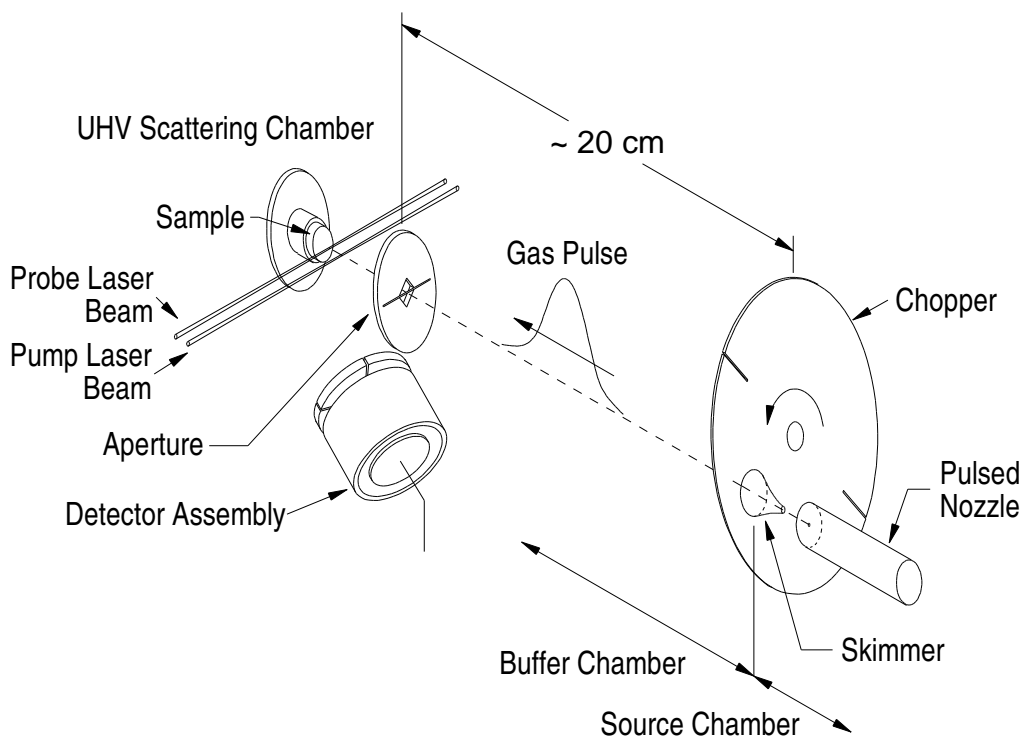


Figure 3.4: Schematic diagram of the experimental apparatus.

periods to quickly build up a saturated layer of hydrogen on the Pd surface at low temperature.

3.4 Laser Spectroscopy

The incident and scattered H_2 molecules are detected by (2+1) resonance-enhanced multi-photon ionization (REMPI). [24] The ionizing laser crosses the molecular beam perpendicularly, as shown in Figure 3.4, 2 mm from the Pd target. The laser operates at 10 Hz, as does the nozzle, and has a pulse length of ≈ 10 ns. The probe radiation is tuned over the range 201.6 nm to 203.3 nm to ionize H_2 in the ($v=0$, $J=0-5$) states via the Q branch of the (0,0) vibrational band. (See Appendix A for a diagram illustrating the probe transitions.) Ions created by the

laser are swept to a microchannel plate in the bottom of the detector assembly shown in Figure 3.4, and the amplified charge per pulse is recorded by a data acquisition computer. The laser firing time can be adjusted with respect to the nozzle and scanned under computer control to measure a time-of-flight (TOF) spectrum. This allows us to measure the velocity of the incident beam. The laser frequency can also be scanned under computer control to measure the rotational spectrum.

The pump laser beam shown in Fig. 3.1 is not used for the experiments described here, but only for those described in Part III.

The velocity resolution in the TOF spectra depends on the ratio of the chopper slit opening time, 6 μs , to the flight time of the molecules between the chopper and the probe laser, about 92 μs for an incident translational energy of 73 meV. Thus the velocity resolution ranges from about 4% to 8% over the range of incident translational energies studied, 31 meV to 94 meV.

At the output of the scattering chamber, the ultraviolet probe radiation is directed onto a white card and the resulting blue fluorescence is measured with a photodiode. The intensity is recorded during data acquisition and used to correct the ion signal for variations in probe power as the dye laser frequency is scanned. Using neutral density filters to adjust the probe power over a wide range at a given frequency, it was found empirically that the measured ion signal is proportional to the photodiode signal raised to the power 1.6, and this relation is used in correcting the spectra.

The neutral density filters are also used during the experiments to keep the probe power below levels which saturate the ion detection system. If the probe power is too high, excessive levels of ionization result in a subtle but significant nonlinearity in the response of the ion detection system which makes it difficult to

simultaneously compare strong and weak features in the spectra. (This fact was discovered after many months of effort trying to explain bizarre results.) A linear operation regime for the detection system was identified by measuring the output signal as the chamber was backfilled with H₂ and the pressure measured with an ion gauge.

The microchannel plate in the ion detection system can also be easily saturated by scattered uv light from the probe laser. The intense uv light ejects electrons from the channel plate and initiates an electron cascade. To prevent saturation, the channel plate gain is switched rapidly with a home-built high-voltage pulse circuit which discriminates against detector response during the laser firing time. [25]

3.6 Distinguishing Incident and Scattered Molecules

We wish to selectively probe with the laser either molecules incident upon the surface or those scattered back from it. These cannot be distinguished using only the laser firing time, because the round-trip flight time of the molecules from the laser focus to the surface and back again, $\approx 1 \mu\text{s}$, is much smaller than the pulse width of the incident H₂ beam, $\approx 10 \mu\text{s}$. To probe solely the incident molecules, the sample manipulator (attached to the rotating lid of the scattering chamber) is simply moved to remove the Pd target from the molecular beam. To probe solely the scattered molecules when the target is in the scattering position, a clever trick was used. A thin wire, of diameter 0.38 mm, was placed horizontally across the final molecular beam collimating aperture. This aperture is a square hole 4.75 mm on a side, tilted so that its diagonal is parallel to the probe laser, as shown in Figure 3.4. By focusing the probe laser into the “shadow” created by the wire, the incident molecular beam is completely rejected (ideally), and only molecules which have scattered off the surface into the shadow are detected. [26] Since the

molecular beam is not perfectly collimated, however, and the probe laser is not perfectly aligned with the shadow, there is a small response to the incident molecules even with the probe in the shadow. This is approximately 3% of the full response to the incident beam measured just outside the shadow, and is therefore negligible for the results discussed here.

As a result of the finite size of the molecular beam and the positioning of the probe laser in the shadow, only molecules which scatter off the target within a certain range of angles with respect to the surface normal will be detected. The analysis in Appendix B shows that this range is approximately 5 to 80 degrees, and that the response of the detection system is approximately uniform for angles between 10 and 60 degrees. The square shape of the aperture was chosen to achieve this uniformity, the importance of which will be discussed below in Section 4.5.

3.8 Sample Preparation

The Pd(111) disk used in these studies is 7 mm in diameter and 2 mm thick. It is heated and cooled from the back side by electron bombardment and liquid nitrogen, respectively. The crystal temperature is measured with a chromel/alumel thermocouple inserted into a hole spark-drilled in the side of the crystal.

To prepare a clean, well-ordered surface in vacuum, the following procedure is used. First the crystal is sputtered for 30 min with 340 eV Ar⁺ ions, at a current of about 0.8 μ a, in the presence of 6×10^{-8} Torr of air leaked into the chamber. Air is used as a convenient source of oxygen to oxidize any carbon which may be adsorbed on the surface. During this time the crystal is held at 300° C, which is above the desorption temperatures for N₂ [27] and CO [28].

Then the sputter source and air leak are turned off, and the crystal is heated to 600° C for 10 minutes, to anneal it and also desorb any adsorbed oxygen. [29]

Following this procedure, the crystal exhibits a sharp (1×1) LEED pattern, indicating that the surface is crystalline and well ordered. No impurities are detected on the surface with Auger spectroscopy, which will be sensitive to small concentrations of most impurities except carbon. Small surface coverages of carbon cannot be detected on Pd with Auger spectroscopy, because of the overlap near 275 eV of carbon and palladium features in the Auger spectrum. This fact, and proposed schemes for producing or verifying carbon-free Pd surfaces, have been discussed considerably in the literature. [30]

The cleaning recipe discussed above is believed to result in a carbon-free surface because of the exposure to molecular oxygen during sputtering. This position is supported by the following experiment. Large amounts of adsorbed carbon were intentionally placed on the Pd surface by exposure to acetylene and subsequent heating of the surface. Following the large carbon exposure, there is a clear change in the Auger spectrum, with the peak at 275 eV becoming about 10% larger relative to the strongest Pd peak at 330 eV, just as reported in Ref. 30. If the crystal is then heated to 300 °C in the presence 6×10^{-8} Torr air for 5 minutes, the Auger spectrum reverts to its original state, indicating that much of the carbon has been removed. Since this 5 minute oxidation procedure is effective in removing significant amounts of carbon, it seems reasonable that effectively all of the carbon is removed during the 30 minutes of sputtering and oxidation used in the cleaning procedure.

In the course of the experiments, measurements are made for beams scattered both from a clean surface and from a hydrogen saturated surface. For the scattering measurements from the clean surface, the surface temperature T_s is held

at 423 K, which is well above the H₂/Pd desorption temperature of ≈350 K. Equating the average beam flux of 0.0065 ML/s with the H₂/Pd desorption rate

$$r_{des} = v_{des} \exp\left(-\frac{E_{des}}{kT}\right) (\theta)^2 N_A, \quad (3.2)$$

where $v_{des} = 1.3 \times 10^{-1} \text{ cm}^2\text{-s}$ [31] and $E_{des} = 0.91 \text{ eV}$ [32], a steady-state coverage of less than 0.001 ML at $T_s = 423 \text{ K}$ is expected, considering loss of hydrogen from the surface due to desorption alone. If bulk absorption is also considered, we would expect the surface H coverage to be even lower, which will be discussed further below in Section 4.4. For measurements from a hydrogen saturated surface the Pd target is kept at 100 K. Considering both desorption and bulk absorption, the steady state hydrogen surface coverage at this temperature is expected to be near unity for the given beam flux.

The base pressure in the UHV system is typically 7×10^{-10} Torr, with the residual gas being mostly composed of about equal parts H₂, H₂O and CO. To ensure that the surface is as free of C and O as possible, all scattering experiments on the clean surface are carried out within 90 minutes of the surface cleaning procedure outlined above. During this time the surface is kept at $T_s = 423 \text{ K}$ which is above the desorption temperature for H₂O [33] and high enough to prevent significant CO adsorption given the CO/Pd desorption kinetics. [28,34] With the hydrogen beam source on, the pressure in the scattering chamber may rise to 2×10^{-9} Torr of H₂ in some circumstances.

Chapter 4

Measurement Technique and Results

This chapter presents the measurement technique and basic results for the H₂/Pd J-dependent sticking coefficients and state-changing probabilities. The first section outlines the program of measurements used to measure and normalize the rotational spectra of the incident and scattered molecules, and in the next section representative data are presented. Following this, the model used to analyze the data is discussed. Results of the analysis are presented in the last section in tabular form, and discussed in more detail in the next chapter.

4.2 Program of Measurements and Normalization Method

The essence of the measurement technique is as follows. For given incident molecular beam conditions, i.e. nozzle temperature and gas mixture, the number of molecules incident upon the clean surface in each J state as well as the number scattered back from it in each J state is measured. These measurements are then repeated for different beam conditions which produce a very different incident rotational state distribution but the same measured translational energy. Combining these results and using the model discussed in Section 4.3, the probabilities that molecules incident in each J state dissociate and stick to the surface, scatter back in a higher J state, or scatter back in a lower J state, for the given incident translational energy, are extracted from the data. This entire procedure is then repeated for several different values of the translational energy.

In order to determine the fraction of the total incident flux that scatters back from the clean surface in each J state, there must be a way of scaling the measured scattered intensities to the incident ones. To do this, the assumption is

made that when the surface is cooled to 100 K and saturated with hydrogen atoms, the reflectivity to incident hydrogen molecules will be unity, because the net adsorption is zero. (Calculations with the model discussed in Section 5.4 show that the rate of bulk absorption is negligible, compared to the incident flux, at 100 K.) Thus, following each measurement of the rotational state spectrum for molecules scattered from the clean surface, the surface is cooled to 100 K and saturated with hydrogen, and then the spectrum is measured again. The two measurements are then normalized together so that the sum of the intensities in all J states from the molecules scattered off the saturated surface is unity. Thus the normalized values for the clean surface scattering equal the fraction of the total incident flux which scatters off the surface without dissociating and ends up in each particular J state. Note that no assumptions about the rotational state distribution of molecules scattered off the hydrogen saturated surface have been made, only that the total effective reflectivity of the saturated surface is unity because the surface sites are filled.

Experiments have suggested, however, that hydrogen can directly absorb into subsurface Pd(111) sites, even if the surface sites are filled. [35] But from the large exposures necessary to observe subsurface site population in these experiments, we can conclude that the probability for direct sticking into these sites is $< 10^{-4}$, and may therefore be neglected for the purposes of the experiment.

An additional assumption that is made in using this normalization scheme is that the angular distribution of scattered molecules is similar for the clean surface at 423 K and the saturated surface at 100 K. If the angular distributions differ markedly from each other, then the normalization will not be entirely correct, because of the limited uniformity in the angular response of the detection system. This is discussed further in Section 5.5.

It is assumed that the contribution of dissociation followed by recombinative desorption to the measurements of the spectra of molecules scattered from the clean surface may be neglected. This is because as the laser wavelength is scanned to measure the intensities in each J state, the laser firing time is kept fixed at the peak arrival time of the scattered molecular beam pulse at the laser focus. At this time, the overwhelming contribution to the measured signal is from molecules which have directly scattered off the Pd target without dissociating, rather than those which have dissociated on the surface, recombined, and desorbed. This is made clear by comparing the flux of directly scattered molecules with that of desorbing molecules. The beam flux is roughly 1×10^{12} molecules per cm^2 arriving in each $10 \mu\text{s}$ pulse, giving a peak flux of $\approx 1 \times 10^{17} / \text{cm}^2\text{-s}$. If half of these molecules stick to the surface, the peak flux of directly scattered molecules will be $\approx 5 \times 10^{16} / \text{cm}^2\text{-s}$. The half of the beam pulse which sticks corresponds to 0.00033 ML, so the peak surface coverage θ_{max} during the beam pulse cannot be much more than the steady state value of 0.001 ML given above. The desorption rate, using Eq. (3.2), is then $2.7 \times 10^{12} / \text{cm}^2\text{-s}$. This is four orders of magnitude smaller than the rate of direct scattering near the peak arrival time of molecules at the target.

4.4 Representative Rotational Spectra

Below are presented some sample rotational distributions which illustrate how the sticking coefficients and rotational state changing probabilities are determined.

Figures 4.1a and 4.1b show rotational state distributions measured for an incident beam translational energy of 55 meV. In Fig. 4.1a, 14% N_2 was mixed into the beam and the nozzle temperature was 643 K, so the incident beam has

significant populations for $J=2-5$. In Figure 4.1b the nozzle temperature was held at 212 K, so there is very little population in $J=2, 3, 4,$ and 5 in the incident distribution.

The intensity scales for the measurements on the incident beams in these figures have been normalized so that the sum of the incident populations is unity. The measurements for the scattered distributions have been normalized by the sum of the populations for the beam scattered off the hydrogen saturated surface, as discussed above. Hence the scattered “populations” for $T_s = 423$ K (the clean surface) give the number of molecules scattered back from the clean surface in each J state, relative to the total incident flux. One minus the sum of these populations gives the average sticking coefficient for the beam.

For the rotationally cold incident distribution (Fig. 4.1b), more molecules are scattered back in $J=2$ and $J=3$ from the clean surface at $T_s = 423$ K than were incident upon it. This shows that excitation from $J=0$ to $J=2$ and from $J=1$ to $J=3$ is occurring during scattering. (Nuclear spin statistics require $\Delta J = 2$.)

In Figure 4.1a the initial populations in the $J=2-5$ states are much larger, so the rotational excitation is not apparent. Fig. 4.1a shows that the ratio of scattered populations from the clean surface to incident populations varies with J , and is smallest for $J=0$. This results from rotational excitation, which enhances the populations of the higher J states in the scattered distribution, and from a J -dependent sticking probability. By combining the data of Figures 4.1a and 4.1b, both the J -dependent sticking probabilities and the rotational excitation probabilities can be determined.

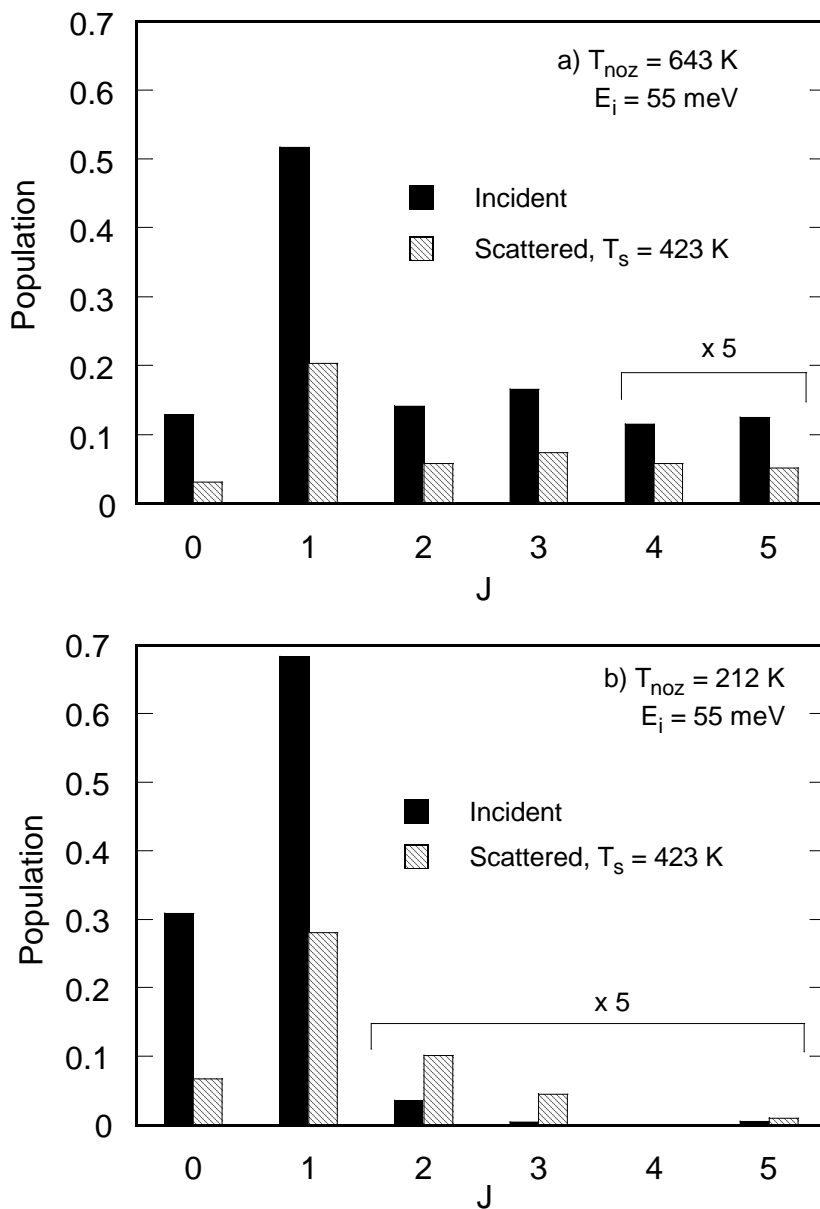


Figure 4.2: Representative rotational distributions for H_2 scattered from Pd(111). Each panel is for a different nozzle temperature but the same translational energy. Panel a) shows a dependence of sticking on J , while b) shows rotational excitation.

In addition, by comparing the ratios of scattered to incident population for $J=0$ and $J=1$ between Figures 4.2a and 4.2b, the magnitudes of the rotational relaxation probabilities out of $J=2$ and $J=3$ may be determined, if the data are of sufficiently high quality. If, for example, the probability for relaxation from $J=2$ to $J=0$ is significant, then the apparent reflectivity in the $J=0$ state will be higher when the $J=2$ population in the incident beam is larger compared to $J=0$.

This analysis will be made quantitative in the next section.

4.6 Model and Analysis

Consider several sets of state distribution measurements, such as shown in Figures 4.2a and 4.2b, that have been made for a particular incident translational energy but different nozzle temperatures, and therefore different incident rotational state distributions. Let $N_I^{(k)}(J)$ and $N_S^{(k)}(J)$ represent the populations in state J for the k^{th} measurement set for molecules incident upon (I) and scattered back from the clean surface (S), respectively. The incident and scattered populations will differ because of sticking and rotational state changing collisions.

The $N_I^{(k)}(J)$ are related to the $N_S^{(k)}(J)$ by the following set of equations:

$$\begin{aligned}
N_S^{(1)}(0) &= N_I^{(1)}(0) \cdot (1 - S_0 - T_{0 \rightarrow 2}) + N_I^{(1)}(2) \cdot T_{2 \rightarrow 0} \\
N_S^{(1)}(2) &= N_I^{(1)}(2) \cdot (1 - S_2 - T_{2 \rightarrow 0}) + N_I^{(1)}(0) \cdot T_{0 \rightarrow 2} \\
N_S^{(1)}(4) &= N_I^{(1)}(4) \cdot (1 - S_4) \\
N_S^{(2)}(0) &= N_I^{(2)}(0) \cdot (1 - S_0 - T_{0 \rightarrow 2}) + N_I^{(2)}(2) \cdot T_{2 \rightarrow 0} \\
N_S^{(2)}(2) &= N_I^{(2)}(2) \cdot (1 - S_2 - T_{2 \rightarrow 0}) + N_I^{(2)}(0) \cdot T_{0 \rightarrow 2} \\
N_S^{(2)}(4) &= N_I^{(2)}(4) \cdot (1 - S_4) \\
&\vdots \\
N_S^{(k)}(4) &= N_I^{(k)}(4) \cdot (1 - S_4)
\end{aligned} \tag{4.2}$$

Here s_J is the sticking coefficient for state J and $T_{J' \rightarrow J''}$ is the probability that a molecule incident upon the surface in state J' will be scattered back in state J'' . Only the even J states, 0, 2, and 4, were included in the equations above. A similar set of equations is used for the $J=1, 3,$ and 5 states. The even and odd J states are not coupled, because of nuclear spin; conversion between even and odd J states may only occur if the molecular bond is broken, and it was shown above that the experiment is sensitive only to molecules which directly scatter without dissociating.

In the above equations, rotational state changing collisions to or from the $J=4$ and $J=5$ states were neglected. This is because the range of rotational distributions accessed in the experiment is not large enough to permit determining these state-changing probabilities independently from the sticking coefficients for the $J=4$ and $J=5$ states. Possible effects of this omission on the results will be discussed below in Section 5.5.

Extracting the sticking coefficients S_J and state-changing probabilities $T_{J' \rightarrow J''}$ from the measured data could be done, in principle, using linear algebra to solve Eqs. (4.2) in a straightforward way. However, random errors in the measurements complicate this procedure because of the way in which certain coefficients can compensate each other and because of the limited change in the incident rotational distributions that can be affected by changing the nozzle temperature. Therefore the equations are solved for the unknowns by iteratively adjusting them to optimize a goodness of fit function, as would be done if the equations were nonlinear. This also allows the easy imposition of physical constraints on the coefficients (such as $0 \leq S_J \leq 1$, etc.).

By analysis of a number of repeated measurements for the same beam conditions, it was determined that the uncertainty in each of the measured $N(J)$'s

is approximately 10% of its value or an absolute value of 0.001, whichever is greater. The 10% uncertainty arises from fluctuations in beam flux, beam expansion conditions, the laser probe pulse characteristics, and so forth. The absolute noise floor of 0.001 arises from electronic noise in the ion detection system and from counting statistics.

In order to determine the effect of the measurement uncertainties on the solutions of the above equations, the equations were first fit to the measured data, and then simulated noise, consistent with the measurement uncertainties given above, was added and the fit was repeated. The variances of the parameters found in the repeated fits with simulated noise were taken to be the uncertainties in the fitted parameters in the reported results. This accounts only for statistical fluctuations, and not systematic error, which is discussed in Section 5.5.

4.8 Extracted Model Parameters

Measurements like those shown in Figure 4.2 were made for a range of incident beam conditions over the translational energy range from 31 to 94 meV. For each energy, 3-4 sets of measurements were made. Table 4.1 lists the minimum and maximum nozzle temperatures used for each translational energy. The nozzle temperatures were held constant to within ± 10 K. The measurements made at the lowest nozzle temperature were done with a pure H₂ beam, while for higher nozzle temperatures the H₂ was antiseeded with up to 25% N₂, as necessary to achieve the desired translational energy. The range of translational energies was limited to that over which sufficiently different rotational distributions could be obtained at constant translational energy by varying the nozzle temperature and seed mixture.

Table 4.2: Number of measurement sets and range of nozzle temperatures used for each translational energy, E_i , to determine the J-resolved $\text{H}_2/\text{Pd}(111)$ sticking and state-changing probabilities. Each measurement set includes a measure of the rotational spectra of the incident molecules, the molecules scattered off the clean surface at 423 K, and the molecules scattered off the saturated surface at 100 K. Representative spectra are shown in Fig. 4.2.

E_i (meV)	Number of Measurements	Lowest T_{noz} (K)	Highest T_{noz} (K)
31 ± 2	3	163	356
55 ± 2	4	212	643
73 ± 3	5	303	653
94 ± 5	4	438	768

Table 4.4: Rotational state resolved sticking coefficients and rotational state changing probabilities for H_2 scattered from $\text{Pd}(111)$ at $T_s = 423$ K. S_J is the sticking coefficient for molecules incident in state J and $T_{J' \rightarrow J''}$ is the probability that a molecule incident upon the surface in state J' will be scattered back in state J'' . Coefficients were determined from measured data using a model discussed in the text.

Model Parameter	Incident Translational Energy (meV)			
	31 ± 2	55 ± 2	73 ± 3	94 ± 5
S_0	0.73 ± 0.02	0.72 ± 0.02	0.76 ± 0.05	0.79 ± 0.02
S_1	0.63 ± 0.02	0.60 ± 0.02	0.62 ± 0.03	0.63 ± 0.02
S_2		0.57 ± 0.06	0.57 ± 0.07	0.67 ± 0.04
S_3		0.47 ± 0.14	0.54 ± 0.13	0.66 ± 0.04
S_4		0.44 ± 0.06	0.56 ± 0.05	0.66 ± 0.02
S_5		0.57 ± 0.05	0.63 ± 0.03	0.69 ± 0.02
$T_{0 \rightarrow 2}$	0.05 ± 0.01	0.05 ± 0.005	0.07 ± 0.03	0.04 ± 0.02
$T_{1 \rightarrow 3}$	0.01 ± 0.001	0.01 ± 0.001	0.01 ± 0.004	0.03 ± 0.006
$T_{2 \rightarrow 0}$		0.03 ± 0.03	0.11 ± 0.03	
$T_{3 \rightarrow 1}$		0.07 ± 0.13	0.09 ± 0.13	

All of these measurements were analyzed using the model discussed above in Section 3.3. The results of the fitting procedure for the sticking coefficients and

rotational state changing probabilities are listed in Table 4.4, along with their statistical uncertainties derived from the model discussed above. The spreads in the translational energies listed in Table 4.4 were determined from the probe velocity resolution discussed in Chapter 3.

Parameters not listed in the table for $E_i = 31$ meV could not be obtained due to insufficient population in the higher J states to obtain meaningful data. The fits to the data for $E_i = 94$ meV always converged on unphysical (negative) values for the rotational relaxation probabilities, even with the simulated noise added, so these parameters were set to zero in the model and have been omitted them from Table 4.4.

The results listed in Table 4.4 are discussed further in the next chapter.

Chapter 5

Discussion of Results

This chapter discusses in more detail the results of the analysis of the H₂/Pd experiments which were briefly presented at the end of the last chapter. The first section discusses the sticking coefficients for H₂ on Pd determined as a function of J, the implications of these results in light of the relevant theory, and a comparison of the results to previous work. The next two sections deal with rotational relaxation and excitation. Following this, the possible complications of the rotational excitation results by recombinative desorption are discussed. The last section summarizes possible sources of systematic error in the experiments.

5.2 J-Resolved Sticking Coefficients

Figure 5.1 shows the J-resolved sticking coefficients, listed in Table 4.4, versus incident translational energy. Error bars have been omitted from the figure for clarity, but uncertainties are listed in the table. The figure clearly shows that the sticking coefficient is a sensitive function of J. The trend shown is a significant decrease in the sticking coefficient as J is raised from 0 to 3, and then, notably, an increase in the sticking coefficient as J is raised to 4 and then 5. This trend is made more clear in Figure 5.2, where the sticking coefficients at an incident translational energy of 74 meV have been plotted versus J. The trend shown in Figure 5.2 for 74 meV is also present at the other energy ranges for which high J sticking coefficients were obtained.

The observed decrease in the sticking coefficients as J is raised from 0 to 3 agrees with the prediction of Gross, Wilke, and Scheffler for H₂/Pd(100) that rotational motion should inhibit sticking, presumably by inhibiting dynamical

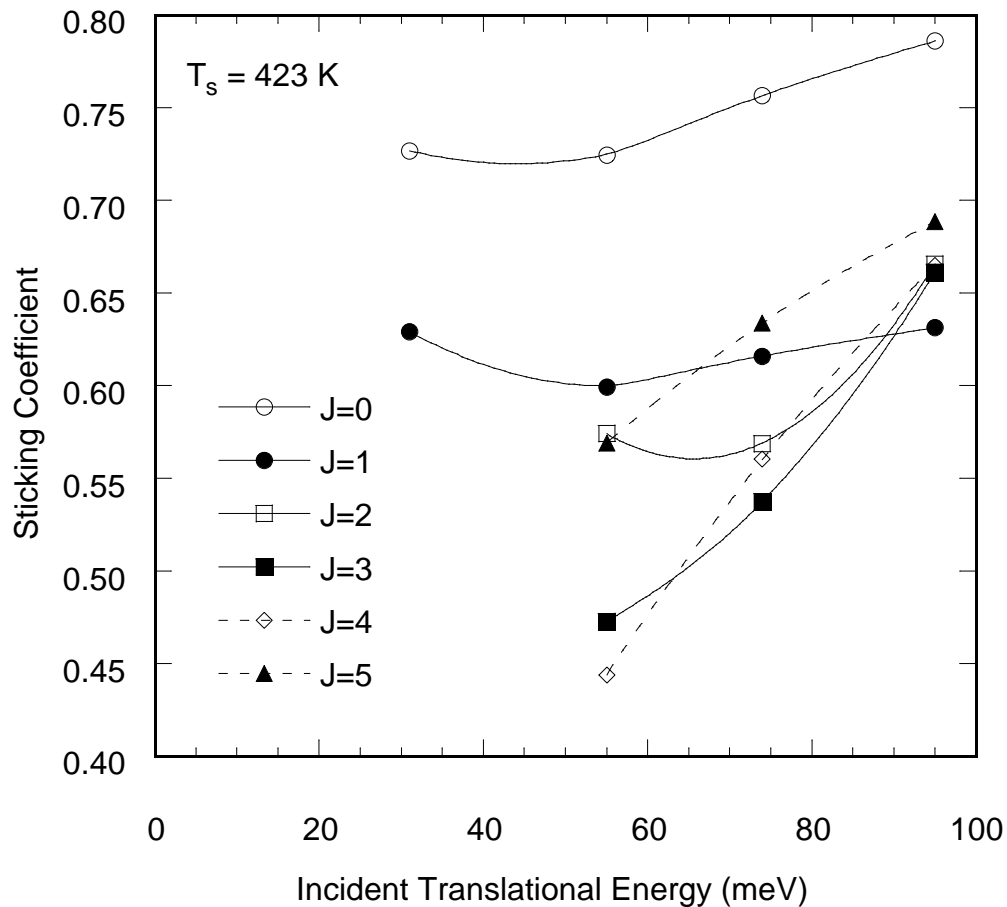


Figure 5.2: $H_2/Pd(111)$ sticking coefficient as a function of incident translational energy and rotational state J .

steering. [4,5] However, their calculations show the sticking coefficient decreasing with J over the range 0 to 6, whereas here an increase in sticking with J as J is raised above 4 is observed.

It is possible that the present observation of sticking coefficients for the $J=4$ and $J=5$ states that are larger than for the $J=3$ state arises from the neglect of

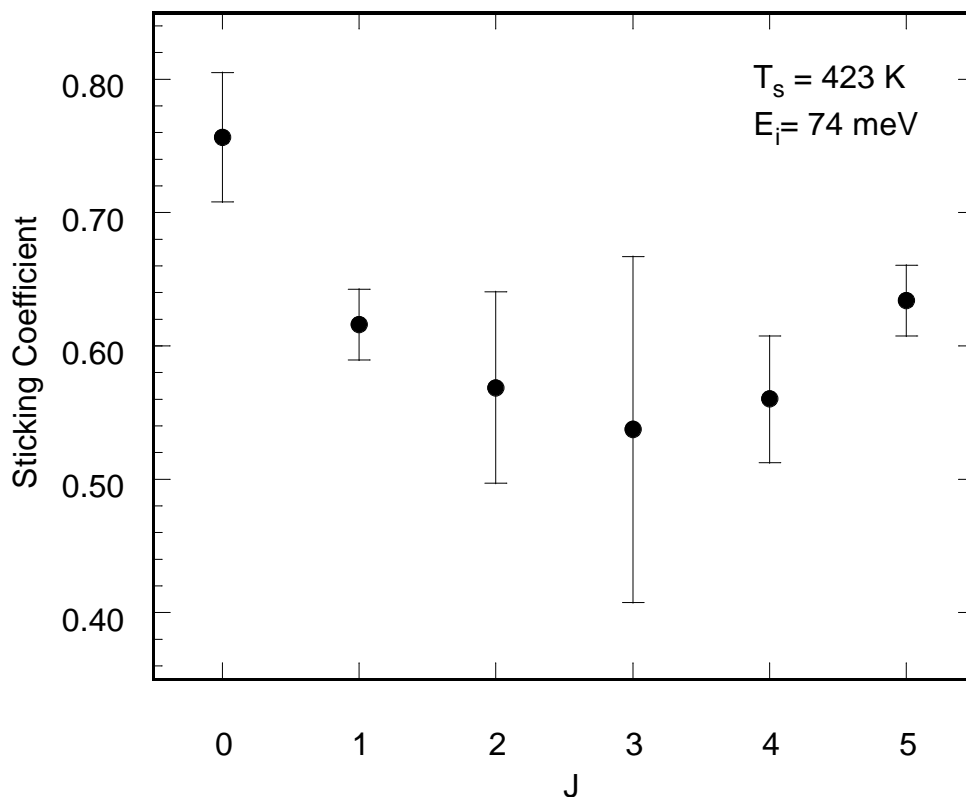


Figure 5.4: $\text{H}_2/\text{Pd}(111)$ sticking coefficient versus rotational quantum number J for incident translational energy $E_i = 74$ meV.

rotational relaxation out of the $J=4$ and $J=5$ states in the analysis discussed above in Section 3.3. This point will be addressed in Section 5.5.

However, the observation of a minimum in the sticking coefficient versus J is not so surprising when compared with the H_2/Cu system. Desorption experiments for D_2 on $\text{Cu}(111)$ performed by Michelsen, Rettner, and Auerbach have also suggested that the sticking coefficient initially decreases with J and then increases. [36] The authors suggested that at low J rotational energy suppresses dissociation by reducing the amount of time the molecule spends in the preferred dissociation orientation, while at high J rotational energy enhances dissociation by

coupling into the reaction coordinate. Theoretical discussion of these points has been summarized by Darling and Holloway. [37]

Furthermore, reaction probabilities which show a minimum as a function of J are also found in gas phase reactions. [38]

Since the translational energy dependence of the sticking coefficients plays an important role in the dynamical steering theory, the measured state-resolved sticking coefficients versus translational energy should be compared with theoretical predictions and also with previous, non-state-resolved measurements.

In their calculations on $H_2/Pd(100)$, Gross and coworkers found a marked increase in the sticking coefficient as the translational energy was reduced below about 25 meV for $J=1-4$, or about 60 meV for $J=0$. [5] The lowest translational energy accessed in the current experiment is 31 meV, so we cannot test the predictions of Gross *et al.* for the $J=1-4$ states. But not much change is seen in the measured $J=0$ sticking probability over the range 31 to 94 meV. However, in comparing the present results to the calculations of Gross *et al.*, it should be noted that their model completely neglects surface atom motion, whereas the sticking coefficients determined here are for a surface temperature of 423 K which is large compared to the bulk Pd Debye temperature of 275 K. [39] In addition, the present results and those of Gross *et al.* correspond to different Pd crystal faces. It is not clear what the effects of these differences should be on the results. Pd(111) was chosen for the present experimental studies, rather than Pd(100) which was studied by Gross *et al.*, because it was readily available.

Figure 5.6 shows a comparison between the rotationally averaged sticking coefficients measured by Beutl, Riedler, and Rendulic for H₂ on Pd(111) using a pure H₂ beam [19] and the values predicted for their experiment using the results for the J-resolved H₂/Pd(111) sticking coefficients determined here. In this comparison, it has been assumed that the rotational temperature of the incident H₂ beam is equal to 0.75 times the nozzle temperature, since Beutl *et al.* state that 75% of the initial rotational energy in their beam remains after the supersonic

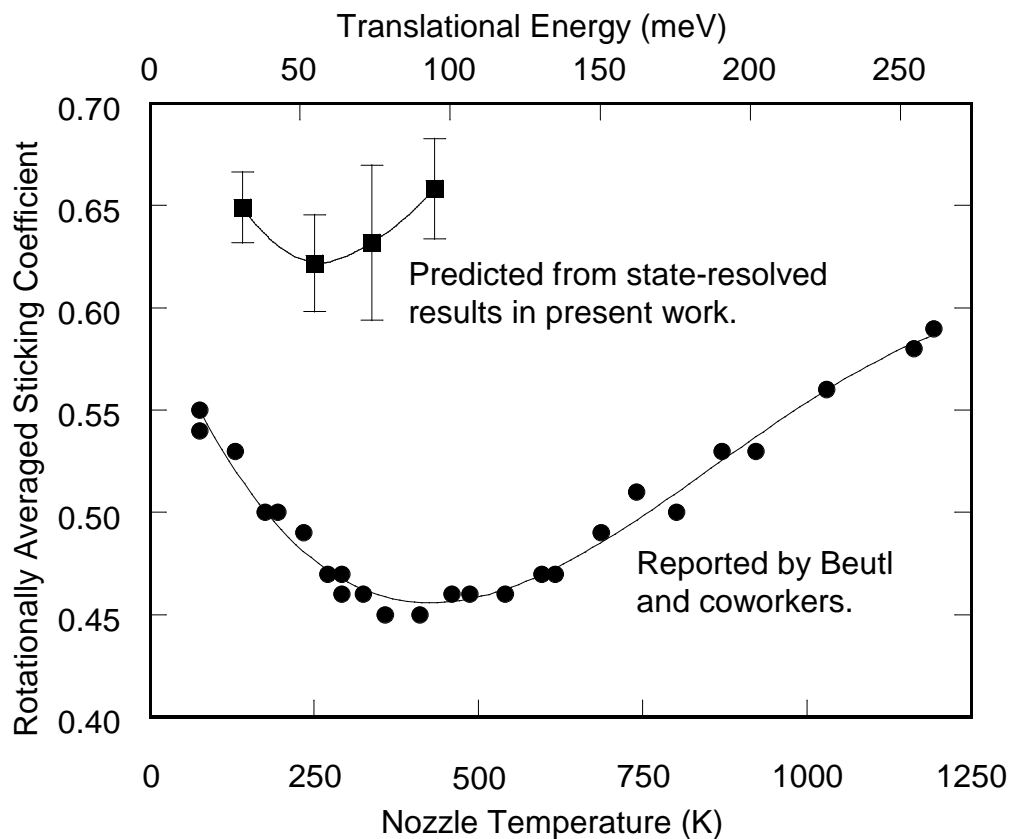


Figure 5.6: Comparison of state-averaged H₂/Pd(111) sticking coefficients measured by Beutl and coworkers [19] with predictions from state-resolved results reported here.

expansion. The relation between nozzle temperature and translational energy has also been taken as given by their data.

The state-averaged sticking coefficients predicted here are significantly higher than those found by Beutl *et al.* However, the predicted values show a dependence on nozzle temperature similar to that observed in their experiment, although the minimum in the sticking coefficient occurs at a different nozzle temperature. It should be noted that their measurements were done for a surface temperature of 220 K, while those reported here were done at 423 K, though it is not clear what effect this difference would have on the results.

5.4 Rotational Relaxation

The parameters $T_{2 \rightarrow 0}$ and $T_{3 \rightarrow 1}$ listed in Table 4.4 show some weak evidence for rotational relaxation from $J=2$ to $J=0$ and $J=3$ to $J=1$, respectively, during the scattering. Only the value for $T_{2 \rightarrow 0}$ at 73 meV is significantly different from zero given the uncertainties, however.

Rotational relaxation is difficult to observe conclusively in the experiment. The populations of the low J states are higher than those of the higher J 's in the thermal incident beams, so relaxation from higher J 's will have only a small effect on the observed "reflectivity" of the low ones. The most favorable case is for relaxation from $J=2$ to $J=0$, since the populations of these two states can be made nearly equal at the highest nozzle temperatures achievable in the experiment. Nonetheless, $J=2$ to $J=0$ relaxation probabilities which are less than about 10% cannot be clearly distinguished from random variations in the observed scattered intensity of $J=0$. Relaxation from $J=3$ to $J=1$ is even more difficult to observe because the incident $J=1$ population is never less than 3 times the $J=3$ population for the range of nozzle temperatures used.

Note that the uncertainties in the relaxation coefficients $T_{2 \rightarrow 0}$ and $T_{3 \rightarrow 1}$ are directly coupled to the uncertainties in the sticking coefficients S_2 and S_3 , because both relaxation and sticking are used in the model to account for the observed loss in these states upon scattering. Hence, if relaxation were omitted from the analysis, the sticking coefficients determined for $J=2$ and $J=3$ would be higher, and the reported uncertainties would be smaller.

5.6 Rotational Excitation

In contrast to rotational relaxation, rotational excitation is clearly observed in the data. At the lowest nozzle temperatures, the incident populations for $J>1$ are very small, so that small excitations from $J=0$ and $J=1$ to higher J states during the scattering may be clearly observed. Excitation from $J=1$ to $J=3$, for example, may be detected for a nozzle temperature of 212 K if the excitation probability is larger than about 0.2%. Figure 4.2b shows an example of a data set which demonstrates rotational excitation: the populations in $J=2$ and $J=3$ are larger in the scattered than the incident flux.

Figure 5.4 shows the rotational excitation coefficients, listed in Table 4.4, versus incident translational energy. The fact that $T_{1 \rightarrow 3}$ is smaller than $T_{0 \rightarrow 2}$ is expected, since the energy gap between $J=1$ and $J=3$, 74 meV, is larger than that between $J=0$ and $J=2$, 44 meV.

Although rotationally inelastic transitions in direct gas-surface scattering are usually thought of as resulting from a transfer of incident translational energy into final rotation [40], this is not the dominant mechanism involved in the present results. The excitation probabilities are roughly independent of incident translational energy. Furthermore, the excitations are observed even for an incident translational energy of 31 meV, which is smaller than both the rotational

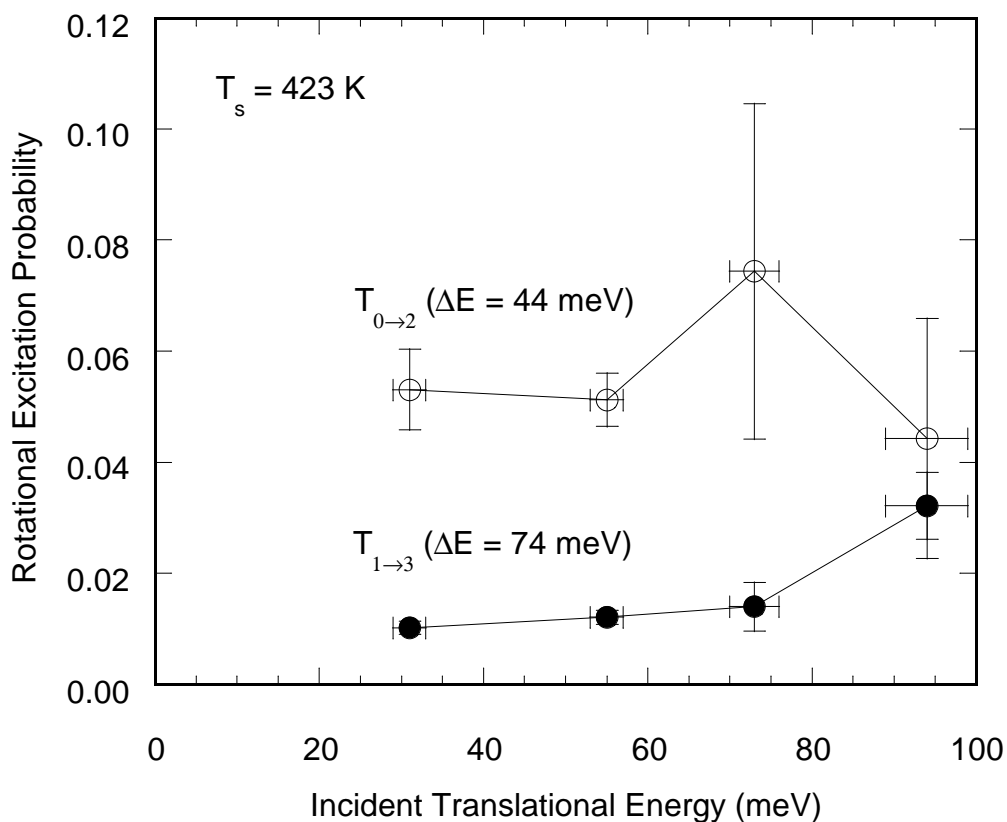


Figure 5.8: Rotational excitation coefficients for H₂ on Pd(111) at $T_s = 423$ K.

transition energies. Consequently, the surface must contribute a substantial portion of the rotational excitation energy to the molecules.

The probability of rotational excitation increases strongly with the surface temperature. This is demonstrated in Figure 5.5 for the $J=1$ to $J=3$ excitation. The figure shows a series of TOF spectra, over a range of surface temperatures, of scattered molecules in $J=3$. The intensity of the signal increases with surface temperature. The zero of the time axis has been set at the peak of the TOF spectra. The incident translational energy is 55 meV and the nozzle temperature is 212 K. At this nozzle temperature, the $J=3$ population in the incident beam is much

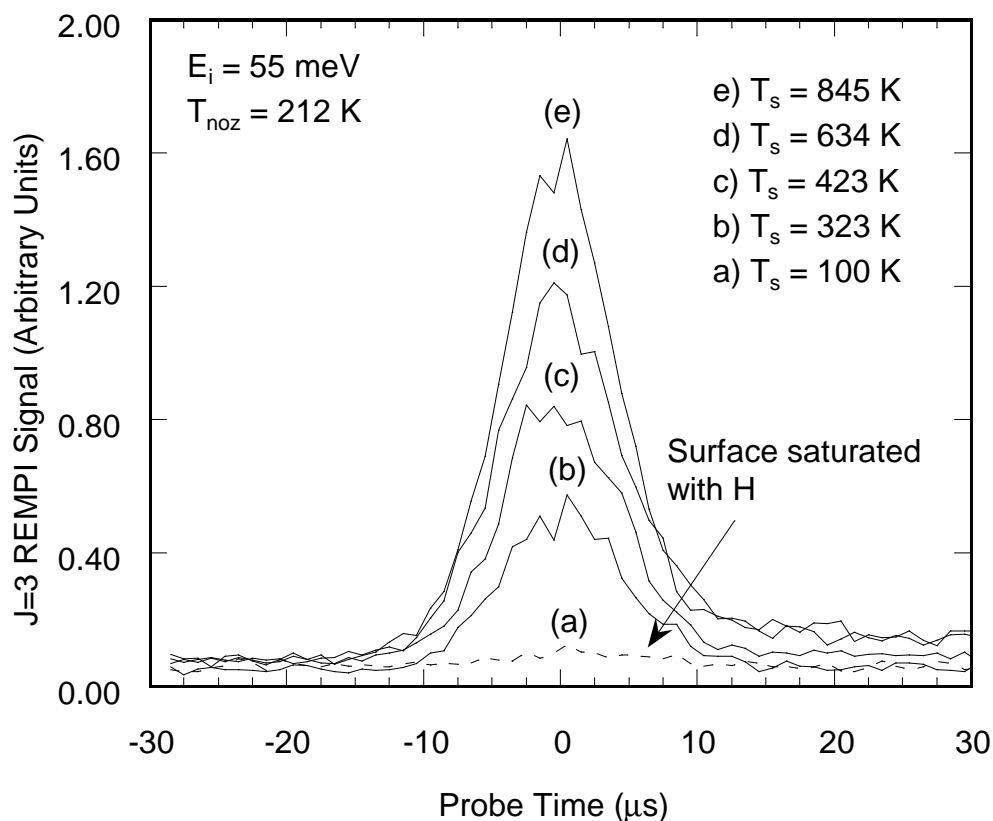


Figure 5.10: Representative TOF data from which surface temperature (T_s) dependent rotational excitation coefficients were determined.

smaller than that in the scattered distribution, as shown in Figure 4.2b, so that essentially all of the $J=3$ signal in Figure 5.5 results from excitation from $J=1$. The small contribution from the scattering of molecules originally incident in $J=3$ is shown by the spectrum taken at 100 K, for which the surface is saturated with H atoms. (Measurements with a hot nozzle show that the reflectivity of the saturated surface for molecules incident in $J=3$ is greater than 0.5.)

Figure 5.6 shows the degree of rotational excitation, taken as the integral under TOF curves such as shown in Figure 5.10, plotted on a log scale versus the reciprocal of the surface temperature. The straight line relationship indicates that

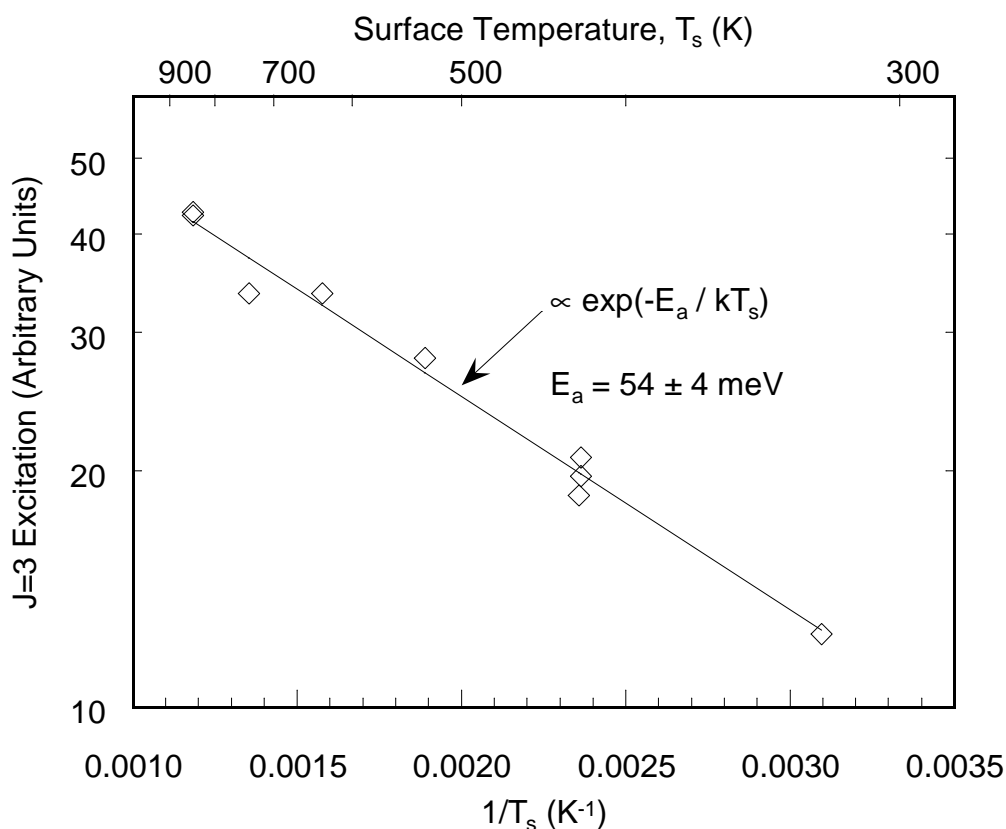


Figure 5.12: Arrhenius plot of rotational excitation coefficients versus inverse surface temperature showing apparent activation energy.

the excitation probability is well represented by an Arrhenius model, with an apparent activation energy of 54 ± 4 meV.

The physical meaning of this apparent activation energy is not yet clear. It is somewhat surprising that it is less than the transition energy for excitation from $J=1$ to $J=3$. Additional experiments might further elucidate the mechanism of the rotational excitation by, e.g., comparing the apparent activation energies in the surface temperature dependence of different rotational transitions or by measuring the final velocities of the rotationally excited molecules. In preliminary studies, it was found that the final kinetic energy of molecules incident in $J=1$ with

40 ± 6 meV kinetic energy and excited into $J=3$ was still 23 ± 7 meV at $T_s = 450$ K. This indicates that, at most, 40% of the 74 meV needed for this rotational transition came from the incident translational energy. In addition, the final kinetic energy in this case was roughly independent of surface temperature over the range 450 K to 850 K, which suggests that the $J=3$ molecules observed were not recombinatively desorbed, as will be discussed further below in Section 5.4.

The observed importance of molecular rotation in the scattering may be considered strong evidence of dynamical steering during the molecule's encounter with the surface. The picture is that as molecules in low rotational states approach the surface, the forces exerted by the surface torque the molecule towards a geometry favorable for dissociation. Many molecules reach this favored geometry and dissociate. Some do not, but still show evidence of the action in that they depart the surface rotationally excited.

An alternative way to describe these results is to say that the molecule-surface interaction potential is a strong function of the orientation of the molecule. For this case dynamical calculations, such as, e.g., those done by Darling and Holloway for the $H_2/Cu(111)$ system [37], have shown that rotational excitation should be expected. Gross and Scheffler have recently calculated rotationally inelastic diffraction probabilities for H_2 on Pd(100), finding values for the rotational excitation coefficients of roughly the same magnitude as those reported here. [17] In these models the rotational excitation energy comes from the molecule's incident translational energy. A recently reported example of this type of excitation is the translation to rotation coupling in the scattering of D_2 from Rh(110). [41]

A unique feature of the present results, however, is that the H₂/Pd(111) rotational excitation is strongly dependent on the surface temperature, and that a large fraction or a majority of the rotational excitation energy comes from the surface, whereas surface excitations are completely neglected in the models mentioned above. Note, however, that Cruz and Jackson predicted a temperature dependence to rotational excitation in their theoretical work on diffraction of H₂ scattering from Cu(100). [42]

5.8 Contribution from Recombinative Desorption

In the discussion above it was assumed that the observed excitation to J=3 at high surface temperature occurs directly upon scattering, and that the contribution of adsorption followed by recombinative desorption is negligible. This is clearly the case for T_s = 423 K, as shown in Chapter 3. However, at higher T_s this point must be considered more carefully, since both the recombinative desorption rate and the rotational temperature of the desorbing molecules goes up with surface temperature.

At T_s = 423 K, the instantaneous desorption flux would be more than 10⁴ times smaller than the total directly scattered flux at the peak arrival time of the molecular beam pulse at the laser, as calculated in Chapter 3. Desorption would then make a negligible contribution to the T_s = 423 K TOF spectrum shown in Figure 5.10, where the J=3 signal corresponds to roughly 1% of the total incident flux (as listed in Figure 5.8 or Table 4.4).

At the highest surface temperature shown in Figure 5.10, T_s = 845 K, it might be expected that the desorption flux into the J=3 state would be comparable to the directly scattered flux, if we were to continue to assume, as in Chapter 3, that adsorbed hydrogen is primarily resident on the surface. However, at the high surface temperatures, the peak surface coverage will be significantly smaller than

assumed in Chapter 3, because of rapid diffusion of H from the surface into the bulk.

To estimate the contribution of desorption to the TOF spectra in Figure 5.10 at the higher surface temperatures, a simple model was employed in which the instantaneous desorption rate as a function of time across the TOF spectrum was calculated. The model took into account the rates of adsorption, solvation into the bulk, and diffusion within the bulk to determine the surface coverage versus time. Using the model, the flux of desorbing molecules in the J=3 state is compared with the flux of incident J=1 molecules directly scattered into J=3. For simplicity, it is assumed that the desorbing molecules have a rotational distribution in equilibrium at the surface temperature, which gives an upper limit on the contribution of desorption to the J=3 signal since the measured rotational temperature in desorption is cooler than the surface temperature. [16]

The energetics for diffusion and desorption are illustrated in Figure 5.7. From the activation energy for recombinative desorption, 0.91 eV [32], we may take the depth of the surface well to be 0.46 eV per H atom. The bulk absorption energy of hydrogen in palladium is 0.39 eV per mole of H₂, in the low concentration limit [43]; hence the bulk H atom well is 0.20 eV below the energy of an H₂ molecule in the gas phase. Bulk diffusion of absorbed H occurs with activation energy 0.230 eV and preexponential 2.90×10^{-3} cm²/s. [96] In this model it has been assumed that the activation energy for solvation, i.e. diffusion from the surface into the bulk, is given roughly by assuming the top of the barrier is at the same energy as the tops of the barriers to diffusion within the bulk. Then the solvation activation energy $E_s = 0.46$ eV. It was assumed that the preexponential for solvation is the same as for bulk diffusion.

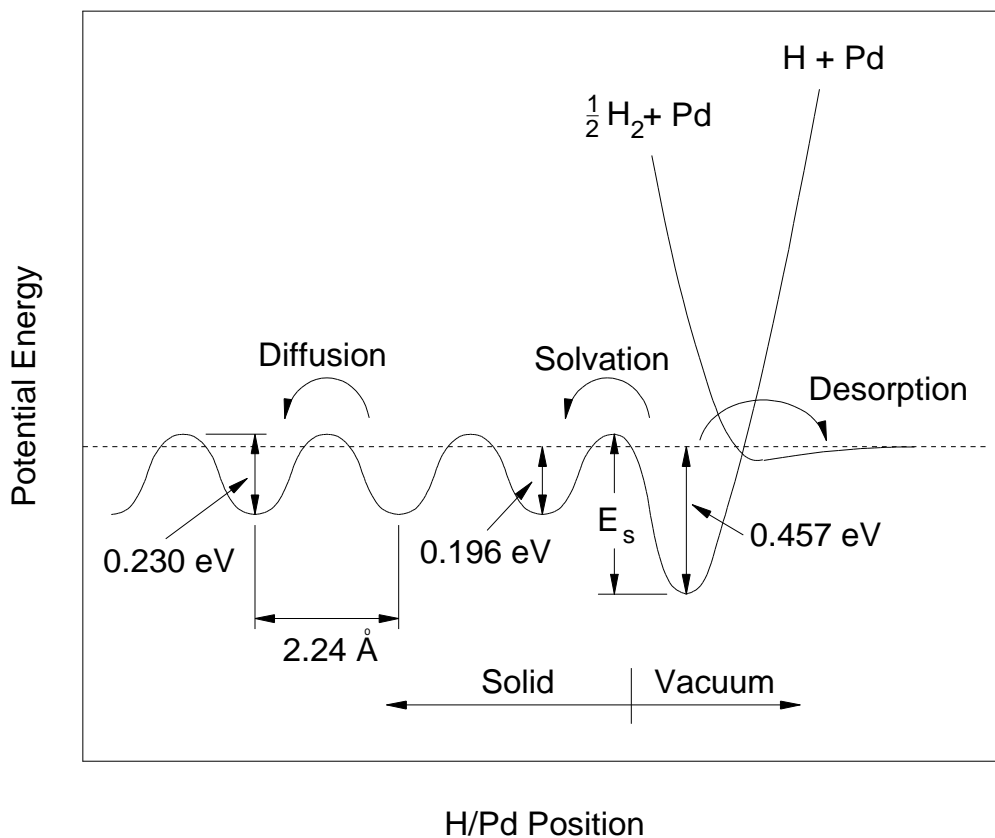


Figure 5.14: One-dimensional H/Pd potential energy diagram illustrating energetics for desorption and diffusion.

Using this model, it is found that, at high temperature, surface-adsorbed hydrogen moves rapidly into the reservoir of sites provided by the bulk, so that the surface coverage is low and the time scale for recombinative desorption is made much longer than the pulse width of the molecular beam, despite the increase in the exponential term of the desorption rate. For the estimated incident flux of $1 \times 10^{12} / \text{cm}^2$ per pulse, the model shows that the integrated contribution of desorption to the $T_s = 845 \text{ K}$ TOF peak in Figure 5.10 is less than $\approx 1\%$. If we let the incident flux be a factor of five larger and assume the solvation activation

energy is 0.56 eV rather than 0.46 eV, both of which would increase the peak surface H coverage, we find the contribution of desorption in the TOF spectrum is still less than $\approx 2\%$. Furthermore, if the model parameters are adjusted to make the desorption flux comparable to the directly scattered flux, then the TOF peaks shift and the shapes of the spectra change as a function of temperature. However, no shifts or changes in shape are observed in the experiment.

Therefore, it is concluded that the dominant contribution to the measured signal in Figure 5.10, even at the higher temperatures, is from direct rotational excitation, as stated above.

5.10 Systematic Errors

In this section two possible sources of systematic error are discussed. The first is differences between the angular distributions of molecules scattered from the clean versus hydrogen saturated surface. The second is the neglect of rotational excitation into or relaxation out of $J=4$ and $J=5$ in the model discussed in Section 4.6. Note that the uncertainties listed in Table 4.4 for the model parameters are statistical uncertainties only, and do not include a consideration of the systematic errors discussed below.

Differences in the angular distributions in scattering from the clean surface at $T_s = 423$ K and the hydrogen saturated surface at $T_s = 100$ K would result in an error in the normalization scheme discussed in Section 4.2. This, in turn, would introduce error into the absolute magnitudes of the reported sticking and state-transfer probabilities. To minimize the error, the detection geometry was arranged so that the detection response versus scattering angle, discussed in Appendix B, is as nearly uniform as possible over the intermediate range of angles.

Nonetheless, the detection response does vary with angle. Perhaps most importantly, the detection response goes to zero for molecules which are directly

backscattered, since they cannot enter the shadow region where the probe laser is positioned. Rough measurements made with the Pd target tilted to a 22.5° angle of incidence, so that the specularly scattered molecules are directed away from the incident beam and the angular distribution can be measured by moving the laser beam, show that the angular distribution of the molecules scattered from the saturated surface is narrower than that from the clean surface. Therefore, in normalizing the rotational state distributions as described in Section 4.2, it is most likely that the intensity of the signal for scattering from the saturated surface was undermeasured, relative to the clean surface, given the poor detection response at small scattering angles. However, this effect cannot be very significant, because the signal measured for scattering at normal incidence from the saturated surface (for which a reflectivity of unity is assumed) is nearly as strong as that in the incident beam. Based on these results, it is estimated that the magnitudes of the reported sticking coefficients may be too low and that of the excitation coefficients too high, but not by more than about 10%, as a result of the systematic error in the normalization.

This conclusion is supported by Rettner and Auerbach's results in their laser-based measurement of sticking coefficients for H_2 on Pd(100). [21] The detection geometry used in our experiment is very similar to that in theirs. To check their laser-based results, they also measured sticking coefficients using the King and Wells technique with a quadrupole mass spectrometer, for which the scattering angular distributions are irrelevant. They found very good agreement between the two methods. Although our scattering chamber is not well equipped to make this check, Rettner and Auerbach's result supports the conclusions above.

The neglect of rotational excitation from $J=2$ to $J=4$ and/or $J=3$ to $J=5$ could result in errors in the sticking coefficients determined for $J=2$ and $J=3$ if the

excitation probabilities are significant. In this case, some of the loss in reflected J=2 and J=3 signal accounted for in the model by sticking would actually arise from excitation into the higher states. However, it is assumed that the excitation probability will decrease as the energy gap between the coupled states becomes larger, which agrees with the observation of smaller excitation probabilities for J=1 to J=3 than for J=0 to J=2 (see Figure 5.8). Therefore, it is expected that $T_{2 \rightarrow 4}$ and $T_{3 \rightarrow 5}$ are less than $T_{1 \rightarrow 3}$, which is $\approx 1\%$, and will be of no significance in the determination of the J=2 and J=3 sticking coefficients.

The neglect of excitation from the J=2 and J=3 states could still be of significance in determining the sticking coefficients from the J=4 and J=5 states, if the population excited into the higher states were comparable to that originally incident in them. However, for the high nozzle temperature measurements, the populations of J=4 and J=5 were $\approx 15\%$ of the J=2 and J=3 populations. Under the assumption that $T_{2 \rightarrow 4}$ and $T_{3 \rightarrow 5}$ are less than 1%, excitation into J=4 and J=5 would not significantly affect the sticking coefficients for these states.

Rotational relaxation out of J=4 and J=5, however, could significantly affect the sticking coefficients for these states, if it is present. Since rotational relaxation from these states was not included in the model of Section 4.6, the reported sticking coefficients for them must be regarded as the sum of the sticking and relaxation probabilities. The relaxation probability was not included in the model because, even at the highest nozzle temperatures, the ratios of populations in J=4 to J=2 and J=5 to J=3 were never large enough to determine the relaxation probabilities given the experimental error. If we assume that the probability of rotational relaxation between two states decreases as the energy gap is made larger, as is the case for excitation, then we are led to discount $T_{4 \rightarrow 2}$ and $T_{5 \rightarrow 3}$, since $T_{2 \rightarrow 0}$, was observed to be at most 0.11 ± 0.03 .

Part III

Vibrational Effects - H₂ on Cu and Pd



Chapter 6

Introduction

The experiments on the effects of vibrational motion in dissociative chemisorption are discussed in this section of the dissertation, Chapters 6-9. Details of the experimental setup are given in Chapter 7, and results of the H₂/Cu and H₂/Pd experiments are then presented in Chapters 8 and 9, respectively. This chapter reviews the theoretical understanding of the vibrational effects, summarizes some of the previous experimental work, and motivates the present work. It begins with a brief comment on “late” barriers in activated dissociative adsorption, which is then followed by a review of selected work on the H₂/Cu and H₂/Pd systems.

6.2 Late Barriers in Activated Dissociative Adsorption

The dissociation of a molecule at a surface may be thought of, in a simplified sense, as requiring two steps: the approach of the molecule to the surface so that reaction can occur, and the breaking of the molecule’s bond by forces which bind its fragments more tightly to the surface than they were bound to each other. When an energetic activation barrier exists in this process, it is convenient to think of it as being either “early” or “late” in the reaction pathway, a concept that has been borrowed from gas-phase chemical dynamics. In this case, an early barrier is one which inhibits the approach of the molecule to the surface, while a late barrier is one which inhibits the breaking of the molecular bond even near the surface.

To overcome an activation barrier, the molecule must have energy in the appropriate degree of freedom. An early barrier is overcome by translational

energy of the molecule towards the surface, while a late barrier is overcome by molecular vibrational energy which, in effect, stretches the bond prior to dissociation. These simplified concepts have framed much of the discussion of activated dissociative adsorption.

6.4 H₂/Cu

The dissociation of H₂ on Cu has been the prototypical example of a system where the activation barrier may be characterized as late along the reaction path. This system has been extensively studied [45,46] and has become a benchmark for both theory and experiment. Experiment has established the general trends in the molecular translational, vibrational, and rotational state dependence of the adsorption process [36,47,48,49,50,51,52,53], and calculations on first-principles potential energy surfaces have verified qualitatively the experimental trends. [54,55,56,57,58] The adsorption is thought to be dominated by vibrationally excited molecules at low translational energy.

There have been numerous theoretical calculations of the H₂/Cu sticking probability as a function of the vibrational state of the incident molecule. Figure 6.1 shows a recent example from the work of Kroes and coworkers. [58] Using density functional theory with the generalized gradient approximation (the current state-of-the-art), they computed the potential energy of the H₂/Cu(100) system as a function of four coordinates: the distance between molecule and surface, the molecular bond length, and the x and y coordinates of the molecule's impact site on the surface unit cell. They left the molecular orientation fixed with the molecular bond parallel to the surface and in the most favorable configuration for dissociation at each impact point on the surface. They then performed a quantum wave packet calculation of the dissociation and vibrationally-inelastic scattering probabilities. The figure shows that the translational energy onset for

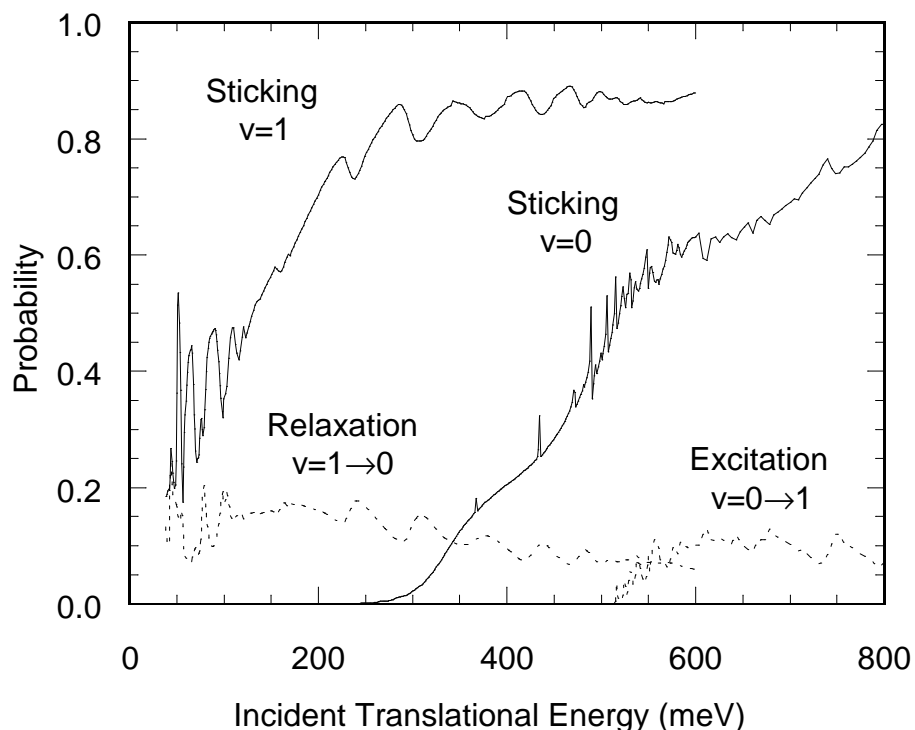


Figure 6.2: Theoretical dissociation (sticking), vibrational excitation, and vibrational relaxation probabilities for H_2 ($v=0$) and ($v=1$) scattered from $\text{Cu}(100)$. Data were provided courtesy of G. J. Kroes and originally appeared in Ref. 58.

dissociation of molecules in the excited vibrational state ($v=1$) is much lower than for ground vibrational state molecules ($v=0$), i.e. that molecular vibration promotes dissociation for a given incident translational energy. This trend is well known from both theory and experiment.

Figure 6.2 also shows the finding of significant probabilities for vibrationally inelastic scattering, i.e. excitation from ($v=0$) to ($v=1$) or relaxation from ($v=1$) to ($v=0$). This results from a coupling of translational and vibrational degrees of freedom in the potential energy surface near the activation barrier to dissociation.

The oscillatory features in the theoretical sticking probability curves are typical of quantum-mechanical dynamics. They arise from several sources, as discussed in Section 2.4, and in principle contain detailed information on the potential energy surface, though they have not yet been observed experimentally.

Although rotational motion was neglected in the calculation discussed above, other calculations have addressed the role of this degree of freedom, which can be significant (as discussed in Part II). Fully six-dimensional calculations have treated all the degrees of freedom simultaneously. [59,60]

The role of vibrational energy in promoting H_2/Cu dissociation has been qualitatively verified by heated nozzle molecular beam experiments, in which partially independent control over the translational and internal degrees of freedom of the incident molecules is obtained. Hayden and Lamont performed some of the early experiments of this type. [48] These were later extended to a larger range of nozzle temperature and translational energy and analyzed more extensively by Rettner, Michelsen, and Auerbach. [49,61] In these experiments, the sticking probability of the molecular beam is found to increase dramatically with nozzle temperature for a given translational energy of the beam, which is fixed by adjusting the H_2/seed gas ratio. These studies demonstrated that H_2 rovibrational excitation can be effective in overcoming the barrier to dissociative adsorption on Cu. It was assumed that this was primarily due to vibrational motion, and Rettner *et al.* fit their data to determine the relative contributions from different vibrational states.

Truly state-specific information was obtained in permeation-desorption experiments using laser spectroscopy. Since, at equilibrium, adsorption and desorption rates are equal according to the principle of detailed balance, these experiments probe what is assumed to be the reverse process of dissociative

adsorption: the recombination of atoms on the surface to form molecules which are desorbed into the gas phase. Kubiak, Sitz, and Zare performed some of the early experiments of this type, which showed a ratio of desorption rates into the ($v=1$) and ($v=0$) states significantly in excess of that expected from a Boltzmann distribution at the surface temperature. [53] This implies, for the reverse process, a higher adsorption probability for ($v=1$) than for ($v=0$). Rettner, *et al.*, performed these experiments in much more detail and mapped out the trends in both the translational energy and rotational and vibrational state dependence of the desorption process. [36,51,52]

However, caution must be used in deducing the adsorption behavior from the desorption results. The adsorption and desorption experiments are not performed at equilibrium and the conditions for the two experiments are different. In general there may be a variety of distinct mechanisms for adsorption and desorption, each of which may have different dynamics. In an experiment, the contribution of each mechanism varies according to the experimental conditions, and the measured dynamics are an average over the contribution of different mechanisms. The beam adsorption experiments are performed for low surface temperatures and very clean substrates, while the permeation-desorption experiments are performed at high surface temperature and with atomic hydrogen delivered to the surface by diffusion through the bulk. It is not clear what effects these differences have on the relative observed dynamics.

In addition, it is difficult to establish the absolute adsorption probabilities from the permeation-desorption experiments, which are best suited to measuring relative rates.

Thus, to further explore the vibrational state dependence of the H_2/Cu adsorption process, in the present work a series of molecular beam experiments

was begun in which vibrational excitation is controlled with laser state preparation. This permits control of both the vibrational and rotational quantum number of the incident molecule independently of the translational energy. The survival probability of H₂ in the (v=1, J=1) state scattered from Cu(110) was measured versus incident translational energy. These results are presented and discussed in the chapters which follow.

6.6 H₂/Pd

The discussion of vibrational effects above has been with reference to a system in which dissociation is activated. For H₂ on Pd, dissociation occurs readily even at low incident translational energy, with sticking coefficients of approximately 0.5 (see Part II), implying the absence of an activation barrier. Nonetheless, vibrational heating of H₂ desorbing from Pd(100) has been observed. [62] From the principle of detailed balance discussed above, this implies that the sticking coefficient of vibrationally excited H₂ on Pd should be larger than that of the ground state molecule. Several authors have tried to reconcile this observation with the apparent lack of an activation barrier.

The resolution of this problem is simply that, while there are many impact parameters of the H₂ molecule on the Pd surface which lead to unactivated reaction paths, activation barriers do exist for unfavorable impact parameters and orientations. Darling and Holloway pointed out that one must therefore consider a distribution of barrier heights to dissociation. [63] If barriers for some sites in the unit cell are characterized as late barriers, then vibrational motion will play a role in both the adsorption and desorption.

To analyze this problem in more detail, Gross and Scheffler recently studied H₂ dissociation on Pd(100) using quantum dynamical simulations on high-dimensional *ab initio* potential energy surfaces, including all six molecular

degrees of freedom. [64] They found that while some reaction pathways are nonactivated, the majority of pathways are activated and an average over impact parameter and orientation gives a nonzero energy barrier to dissociation. Furthermore, they found that the H_2 molecular vibration is softened as the molecule approaches the surface, so that energy initially in the H_2 vibration is available to carry the molecule along the reaction pathway to dissociation, and therefore enhance the sticking coefficient. Their calculations show sticking coefficients for H_2 on Pd that are about twice as large for H_2 ($v=1$) as for H_2 ($v=0$). Their results showed a variation of the translational energy dependence of the sticking with vibrational state similar to that shown in Fig. 6.2 for H_2/Cu .

To directly test these predictions in adsorption, and thus complement the associative desorption experiments, the molecular beam and laser state preparation and detection techniques applied to H_2/Cu were used to measure the survival probability of H_2 in the ($v=1, J=1$) state scattered from Pd(111). These measurements also serve as a useful comparison to the H_2/Cu measurements made with the same technique.

Chapter 7

Experimental Apparatus

This chapter discusses details of the molecular beam scattering apparatus that are relevant to the experiments on vibrational motion to be discussed in Chapters 8 and 9. The vacuum chamber, molecular beam system, and REMPI probe system used in these studies are the same as those employed for the studies on rotational effects which were already described in Chapter 3 of Part II.

For the experiments on vibrational effects to be discussed here, an additional laser, to be referred to as the “pump” laser, is used to prepare H_2 in a vibrationally excited state. This permits preparation of significant amounts of vibrationally excited H_2 regardless of the nozzle temperature, thus allowing independent control of the vibrational and translational degrees of freedom of the incident molecules. In addition, use of the pump laser to prepare excited state molecules results in much greater time resolution in the scattering studies and therefore facilitates unique kinds of measurements, which will be described in subsequent chapters.

The state preparation and detection methods are discussed in the next section, which is then followed by the Cu sample preparation method. The Pd sample used in these experiments is the same as that used in Part II.

7.2 State Preparation and Detection

The pump laser crosses the molecular beam axis parallel to and slightly upstream of the probe laser, as shown in Figure 3.4, typically about 2 mm away from the target. The pump laser system consists of two copropagating laser beams which efficiently excite molecules from the ($v=0, J=1$) state to the ($v=1, J=1$) state

by stimulated Raman scattering. [65,66] (See Appendix A for a diagram of the spectroscopic transitions.) The pump and Stokes light which drive this transition are produced by focusing the linearly polarized second harmonic of a Q-switched Nd:YAG laser, which operates at 1064 nm, into a cell of H₂ at 5 atmospheres pressure and recollimating the residual 532 nm light and Raman-shifted orders which emerge. These are focused onto the molecular beam with a 20 cm focal length lens and timed to hit the temporal peak of the incident ground state molecular beam pulse. The pump laser has a temporal width of approximately 10 ns. Observation of the depletion of the ground state REMPI probe signal when the pump laser is on shows that, within the volume illuminated by the focused pump laser, between 10 and 30 percent of the ground state molecules are promoted to (v=1, J=1). Thus the population in the excited state is increased by orders of magnitude over the thermal background, which might be only 3×10^{-3} even at a nozzle temperature of 1400 K. Note also that only the J=1 state is promoted to v=1.

The excited state (v=1, J=1) molecules are detected with the probe laser using (2+1) REMPI on the Q branch of either the (1,1) or (0,1) vibrational band, at 205.5 nm and 210.6 nm, respectively. (See Appendix A for a diagram of the spectroscopic transitions.) A significantly more intense (v=1, J=1) ion signal can be produced using the (0,1) band. This is because this band has a stronger transition and also because the BBO mixing crystal used to produce the ~200 nm light from the dye laser fundamental and second harmonic is more efficient at the longer wavelength. However, an excessively strong ionization signal can produce a nonlinear response in the ion detection system, as discussed in Chapter 3. For this reason, and because it requires the same laser dye as the ground state (0,0) band, the (1,1) band was used in most of the experiments described below.

The relative delay between the pump and probe lasers is computer-controlled using a home-built delay circuit providing a precision of about 1 ns. By scanning the delay between the pump and probe lasers, a time-of-flight (TOF) spectrum showing the excited state molecules incident upon and then scattered back from the target surface as they pass the probe laser position is recorded. This permits a comparison of the incident and scattered intensities from which the survival probability of the excited state molecules may be determined, as will be discussed below. By tuning the probe laser to other rovibrational states and looking specifically at flight times corresponding to the scattered pumped molecules, rovibrational energy transfer into other states may also be detected, as discussed below.

7.4 Sample Preparation

Both copper and palladium single crystals were used for the scattering studies discussed here. The method of preparation for the palladium sample has already been discussed in Chapter 3. The Cu(110) crystal used in these studies was cut from a nominally (110) oriented copper boule grown in the Physics Department at the University of Texas at Austin in Prof. Jim Erskine's group. It was oriented with Laue x-ray backscattering and then mechanically and chemically polished. [67] Using an electrostatic discharge machine, a hole was drilled in the side of the sample for insertion of a thermocouple during scattering experiments. Once in the vacuum chamber, the Cu crystal surface was cleaned before each experimental run by approximately 30 minutes of sputtering with 300 eV Ar^+ ions followed by 15 minutes of annealing at 600 °C. Auger spectroscopy was used to verify that the surface was free of impurities and LEED was used to verify that the sample surface was crystalline and well ordered following the sample cleaning procedures. The Cu(110) sample was held at room

temperature for the scattering experiments, all of which were performed within approximately two hours of sputter cleaning and annealing the surface, to reduce the effects of surface contamination on the experimental results.

Chapter 8

H₂ on Copper

In this chapter results of the experiments carried out on the H₂/Cu(110) system will be discussed. The general objective of the experiments was to investigate the dynamics of vibrationally excited H₂ molecules scattering from the copper surface. The chapter begins with a presentation of representative TOF curves which demonstrates key features of these spectra, followed by a discussion of the method used to extract the relative flux of incident and scattered molecules from them. Next the translational energy dependence of the survival probability of the excited state molecules deduced from the TOF measurements is presented, along with the method for putting the results on an absolute scale. This is followed by a discussion of the results, their implications for the dissociation probability of the vibrationally excited H₂ on the Cu(110) surface, and a comparison to previous experiments and theory.

8.2 Representative TOF Curves

Figure 8.1 shows several sample TOF spectra for H₂ in the ($v=1, J=1$) state incident upon and scattered back from the Cu(110) sample. Each scan is for a different incident translational energy, which was measured as described below, and the three scans have been offset vertically for presentation in the figure. The translational energy was varied by adjusting the nozzle temperature. The scans shown in the figure were acquired with the pump laser 3.5 mm and the probe laser 0.64 mm from the surface.

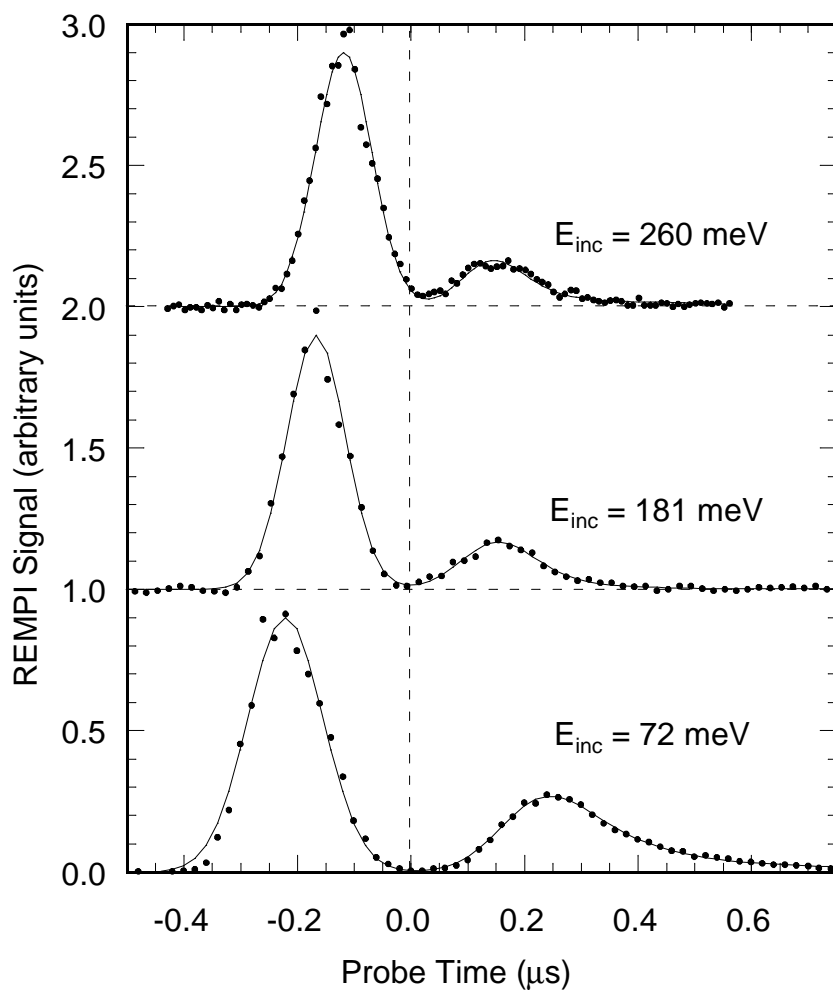


Figure 8.2: Representative time-of-flight curves for H_2 ($v=1, J=1$) scattered from $\text{Cu}(110)$ at three different translational energies. The first peak in each scan is from the incident molecules and the second peak is from scattered molecules. Note the characteristic asymmetric shape of the scattered peak in each scan, resulting from the scattered velocity and angular distributions. Also note that the intensity of the scattered peak goes down as the incident translational energy is raised, due to a lowering of the excited state survival probability. The solid lines are fits to a model discussed in the text.

The first peak in each scan of Fig. 8.2 corresponds to the incident pumped molecules, while the second smaller peak corresponds to pumped molecules scattered back still in the ($v=1$, $J=1$) state. The origin of the time axis is set to the peak arrival time of the incident packet at the surface, determined as described below. The temporal width of the incident peak is determined by the spatial width of the focused pump laser beam. The three scans shown in Fig. 8.2 have all been normalized by the incident peak intensity to compensate for changes in molecular beam flux, laser power, etc.

Note that the peaks in Fig. 8.2 are solely from molecules excited into the ($v=1$, $J=1$) state by the pump laser. While there is a small thermal population in this state at the higher incident translational energies due to the higher nozzle temperature, it can be neglected for the subsequent analysis because it forms an essentially constant background in the TOF spectra, since the time range scanned, e.g. in Fig. 8.2, is small compared to the 10 μ s length of the chopped molecular beam pulse.

The solid lines shown in the figure are fits to a model which has been used to determine the scattered velocity and angular distributions and to convert the TOF spectra from density to flux weighted, as discussed below and in Appendix C. The scattered velocity and angular distributions are responsible for the asymmetric shape of the scattered peaks in the TOF spectra, which have long tails at late times. Molecules which scatter back at lower velocities or larger angles arrive back at the probe laser later than those which scatter back with no change in velocity and directly along the surface normal, giving rise to the asymmetric scattered peak shape.

Note in Fig. 8.2 that the ratio of the scattered to incident peak areas decreases by about a factor of 2 as the incident translational energy is increased

from 70 meV to 260 meV. This decrease can be attributed to a reduction in the survival probability of the excited state molecules as the translational energy is raised, which will be discussed further in Section 8.3.

8.4 Determining Incident and Scattered Velocities and Transforming TOF Spectra from Density to Flux Weighted

The mean translational energy of the incident and scattered packets of pumped molecules are determined, for each nozzle temperature, by translating the probe laser along the molecular beam axis and measuring the TOF peak positions of the incident and scattered molecules as a function of the probe laser distance to the surface. The peak times versus probe position for one such measurement are shown in Figure 8.2. The intersection of the straight line fits in Fig. 8.2 gives the precise position of the surface along the probe laser translation stage as well as the peak arrival time of the incident packet at the surface, the two of which have been taken as the origin of coordinates in the figure. Results from such measurements were also used to set the time origins for each scan in Fig. 8.2. The inverse slopes of the lines in Fig. 8.2 give the incident and scattered velocities, which are determined with a typical statistical uncertainty of 5-10 percent.

In order to determine the survival probability of the excited molecules from the measured TOF spectra, it is important to consider the fact the REMPI probe is sensitive to the *density* of molecules in the probe volume at the time the laser is fired, not the *flux* of molecules crossing the laser axis. Differences in the incident and scattered velocity and angular distributions will affect the observed relative weighting of incident and scattered molecules in the spectra. For example, molecules traveling more slowly remain in the probe region longer than those traveling more quickly, and therefore have a greater likelihood of being detected. Similarly, molecules which traverse the probe laser axis at shallow angles will be

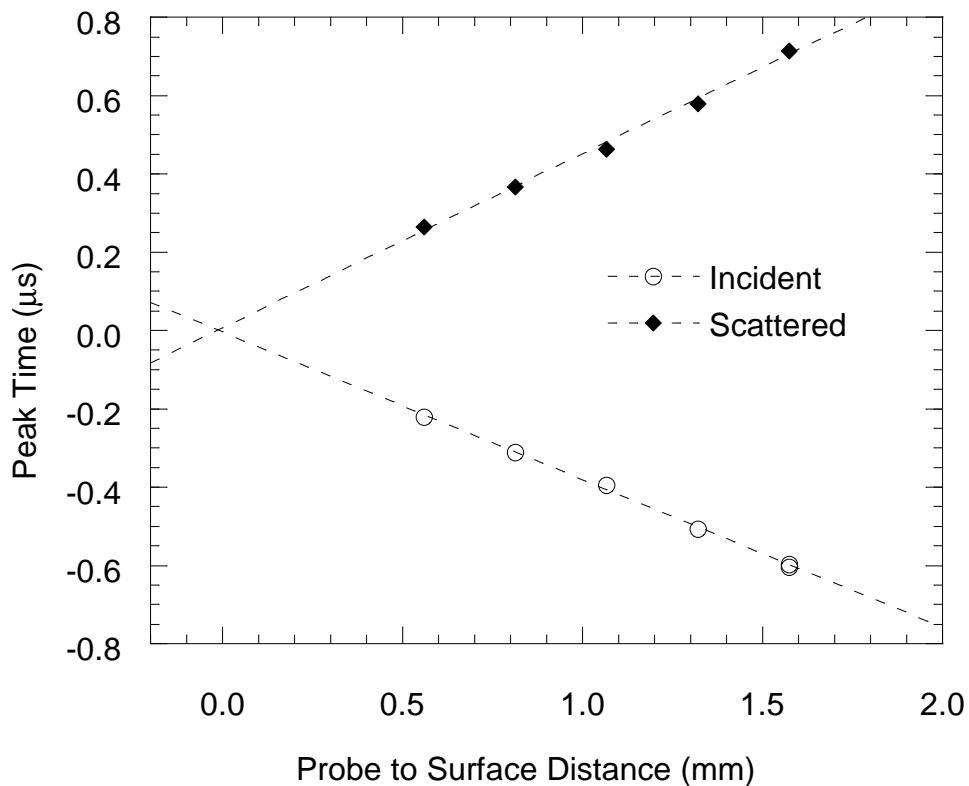


Figure 8.4: Incident and scattered peak times in pump/probe experiment versus probe laser distance from the surface. This type of plot is used to determine incident and scattered velocities and to find the position and time coordinates of the pumped packet arrival at the surface.

detected with greater probability than those which travel along the surface normal. Both of these effects result in an enhancement of the scattered peak relative to the incident peak in the TOF spectra, since the well collimated, monoenergetic incident beam is scattered off the surface into a range of angles and with some loss of translational energy.

To correct for this difference in weighting of the incident and scattered molecules in the TOF spectra, the measured density-weighted spectra are

transformed mathematically into flux-weighted spectra before subsequent analysis. This is done using a model, discussed in Appendix C, which takes into account the mean velocities of the incident and scattered molecules as well as the spread in scattering angle and velocity determined from the shape of the scattered peaks in the TOF spectra. The initial step in this method involves fitting the measured spectra to a smooth function; these are the fits shown in Fig. 8.2.

8.6 Survival Probability versus Incident Translational Energy

To determine the survival probability of the excited state molecules versus their incident translational energy, the ratio of the areas under the scattered and incident peaks in a series of TOF spectra, such as those shown in Fig. 8.2, was first used as a measure of the *relative* survival probability over a range of incident translational energies. [68] (The incident translational energy is varied by adjusting the nozzle temperature.) The *absolute* survival probability was then determined at a single translational energy by integrating over the spatial distributions of the incident and scattered flux [69], as discussed below in Section 8.4, and the relative measurements were scaled by this result. Figure 8.3 shows the resulting plot of survival probability versus translational energy. The pump and probe geometry for the measurements in the figure was exactly as described above for Fig. 8.2, and the incident translational energies were measured at each point as described above. The measured density-weighted TOF spectra were transformed to flux weighted spectra, as discussed above in Section 8.4 and further in Appendix C, before the ratio of scattered to incident peak areas was taken. The plot was then scaled so that the average of the four measurements at the lowest translational energy equals the absolute survival probability value determined at this energy as discussed in Section 8.4.

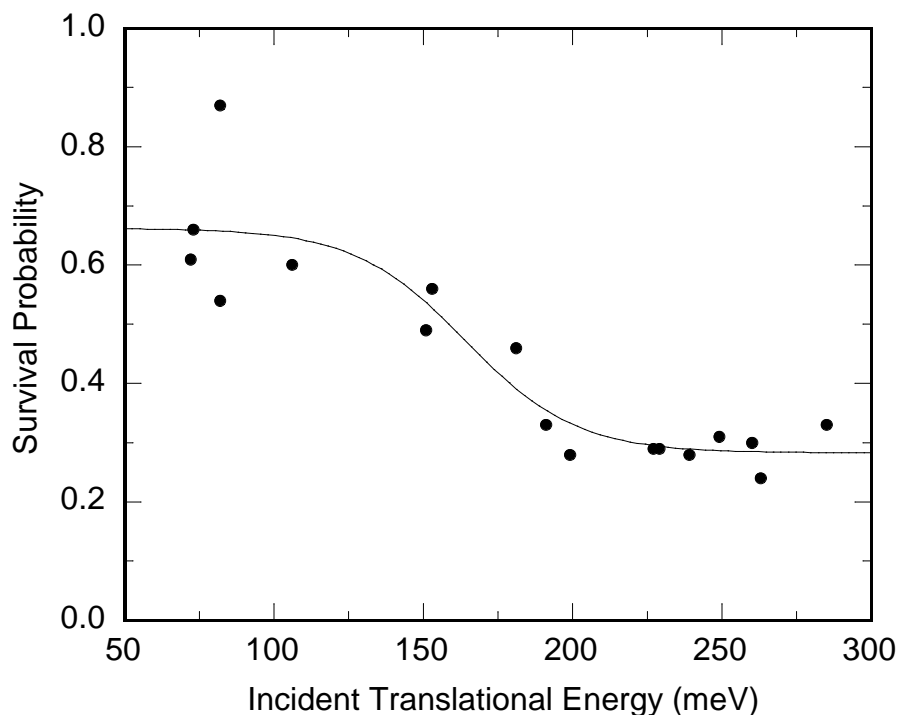


Figure 8.6: Survival probability versus incident translational energy for H_2 ($v=1, J=1$) on $\text{Cu}(110)$. See text for details.

An alternative explanation for the decrease in the scattered to incident ratio in the TOF spectra with increasing energy, besides a decrease in the survival probability, would be that, as the translational energy is raised, there is an increase in the angular spread of the molecules in the plane perpendicular to the probe laser propagation direction. This would reduce the intensity of scattered molecules detected at any particular vertical position of the laser. (See Fig. 3.4.) However, the spatial distribution of scattered molecules in this plane has been measured and was found to decrease by approximately 25% as the incident translational energy was raised from 80 meV to 250 meV. This distribution was measured by scanning the probe laser vertically and taking TOF spectra at a range of heights,

for several translational energies in the range shown in Fig. 8.2. In these measurements the probe laser effectively integrates over the out-of-plane direction because of its proximity to the surface. The decrease in angular spread is in fact to be expected, since the component of velocity normal to the surface is being raised. Since the spatial distribution is weighted more towards the specular angle at the higher translational energies, the decrease in the intensity of the scattered peaks in the TOF spectra as the translational energy is raised must result from a decrease in the survival probability of the incident H_2 ($v=1, J=1$) molecules.

Note, however, that, since the angular distribution of the scattered molecules narrows slightly as the translational energy is increased, but Fig. 8.6 was scaled to the absolute survival probability at only the lowest energy, the survival probability in the figure is overstated by about 25% at the high energy range of the figure.

Given the scatter in the data points in Fig. 8.6, no significance should be attached to the details observed in the structure of the curve, but only to the general trend. The figure shows a steady decrease in the survival probability as the incident translational energy is raised. The solid curve in the figure is a fit of the survival probability to a function of the form

$$P = P_{min} + (P_{max} - P_{min}) \frac{1}{2} \left[1 - \tanh \left(\frac{E_i - E_0}{W} \right) \right]. \quad (8.2)$$

Table 8.2: Parameters for fit of survival probability versus incident translational energy shown in Fig. 8.6 to Eq. (8.2).

Parameter	Value
P_{min}	0.28 \pm 0.05
P_{max}	0.67 \pm 0.13
E_0 (meV)	164 \pm 12
W (meV)	37 \pm 22

This form has been used by other authors [49,70] and is chosen simply as a convenient way to reduce the data. In Eq. (8.2) P is the survival probability at the incident translational energy E_i , P_{max} and P_{min} are the maximum and minimum survival probability, W is the width of the energy range over which a transition occurs, and E_0 is the center of the energy range. The results of the fit to Eq. (8.2) are listed in Table 8.2, including the statistical uncertainties determined from the fit and from uncertainties in the absolute scaling discussed below in Section 8.4. The P_{min} fit parameter has not been corrected for the 25% overestimate of the survival probability at the highest translational energy, which arises from the narrowing of the scattered angular distribution as discussed above. As can be seen from the fit parameters, the excited state survival probability decreases by between a factor of 2 and 3 as the translational energy is raised from 70 meV to 260 meV. These results will be discussed more below in Section 8.5.

8.8 Absolute Survival Probability Measurement

In order to determine the absolute survival probability of the H_2 ($v=1, J=1$) at a given incident translational energy, as discussed above, the probe laser was

scanned vertically (with reference to Fig. 3.4) and a series of TOF spectra were taken at a range of heights with the incident translational energy fixed at 77 meV. [69] Each spectrum was transformed from density to flux weighted, using the method discussed in Appendix C, and the integrals under the incident and scattered peaks in the flux weighted spectra were computed.

Figure 8.4 shows the integrated flux from these spectra plotted versus the vertical position of the probe laser, along with gaussian fits to the incident and scattered profiles used to reduce the data. The spatial profile of the scattered molecules is broader than that of the incident ones, because the molecules scatter off the target into a range of final angles.

Note that each point Fig. 8.4 effectively includes an integration over the coordinate parallel to the laser propagation direction because of the detection geometry. The acceptance angle of the integration along this direction is estimated to be ± 82 degrees from the surface normal, based on the width of the molecular beam (4.8 mm), an estimate of the probe laser interaction length with the beam (8 mm), and the probe to surface distance for the TOF spectra used in making Fig. 8.4 (0.2 mm).

Thus, integrating over the probe laser vertical direction in Fig. 8.4 gives a complete spatial integration of the flux in a plane parallel to the surface. Therefore the ratio of the areas under the fitted scattered and incident curves in Fig. 8.4 is the survival probability of the excited molecules. Using the parameters and uncertainties from the gaussian fits, the survival probability for H_2 ($v=1, J=1$) scattering from Cu(110) at an incident translational energy of 77 meV is 0.67 ± 0.09 . This value was used in scaling the survival probability versus translational energy curve presented in Fig. 8.6, as discussed above.

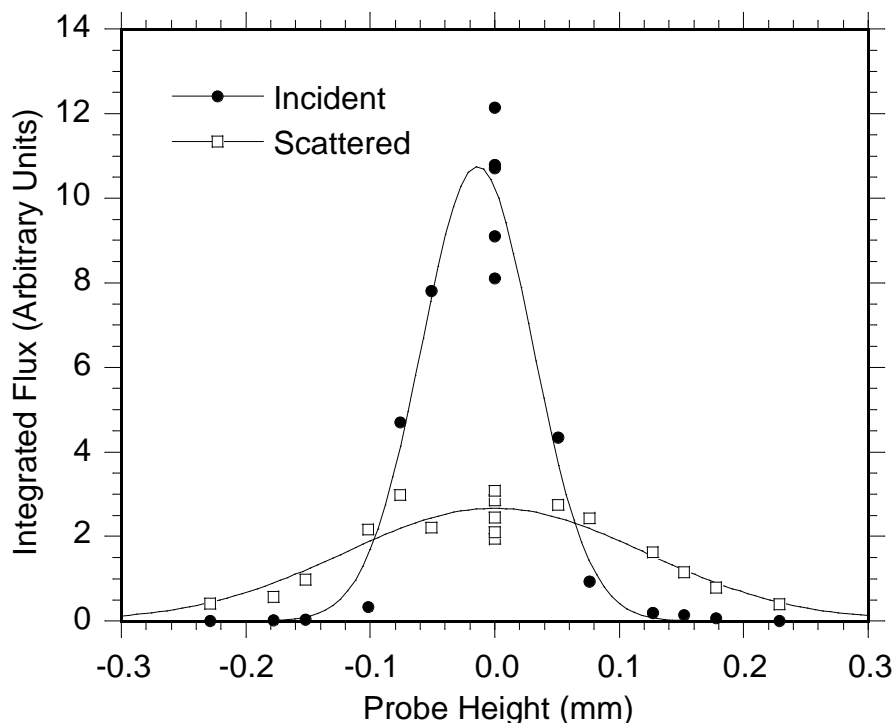


Figure 8.8: Spatial profile of flux incident on and scattered back from Cu(110) in the H_2 ($v=1, J=1$) state, for an incident translational energy of 77 meV. The ratio of the integrals under the scattered and incident profiles gives the survival probability at this energy.

It is important to consider whether differences in angular momentum alignment, e.g. resulting from scattering at the surface, could result in different REMPI rates for the incident and scattered molecules. This would then need to be accounted for in determining the survival probability.

However, this is probably not the case, since two-photon $\Sigma \leftarrow \Sigma$ Q-branch REMPI probing is relatively insensitive to alignment. [71] Also, Q-branch Raman excitation is thought to produce no alignment [72], so any alignment effects at the surface would have to be extreme to induce a measurable alignment in the scattered molecules. As a check on these assumptions, the incident and scattered

pumped H_2 ($v=1, J=1$) signal was measured as a function of the linear polarization direction of the uv probe light, varied with a $1/2$ wave plate, and no variation in signal was found.

8.10 Discussion

The results discussed above show that a significant fraction of the incident H_2 molecules in the ($v=1, J=1$) state do not survive their collision with the Cu(110) target still in this quantum state, and that the surviving fraction goes down as the incident translational energy is raised. What happens to the molecules which are lost? There are three possible loss channels: rotational excitation within the $v=1$ manifold, e.g. ($v=1, J=1 \rightarrow 3$); vibrational relaxation to any odd J state in the ground state $v=0$ manifold; or dissociation (sticking) on the surface. Each of these will be discussed in turn. Note that transfer of population to even J 's is forbidden by nuclear symmetry.

It might initially be assumed that rotational excitation within the $v=1$ manifold would be weak, since experimental studies on ground state H_2 scattered from metals have shown rotational excitation probabilities to be only about 1%. [40] This low level of rotational excitation is in general due to the nearly spherical structure of the H_2 molecule and the high energy spacing between its rotational levels.

In preliminary measurements, however, it was found that rotational excitation of the incident ($v=1, J=1$) molecules to ($v=1, J=3$) accounts for roughly 5% of the ($v=1, J=1$) loss at 260 meV incident translational energy. The rotational excitation energy most likely comes from the molecular translational energy, and the magnitude of the excitation is consistent with theoretical calculations of T-R coupling by Darling and Holloway. [37]

It was planned to measure this rotational excitation probability as a function of incident translational energy and to look for excitation to higher J states as well, but these experiments were not performed. Equipment failure kept the pump laser offline for the last few months of the H_2/Cu studies reported here.

However, it is assumed that the ($v=1$, $J=1\rightarrow 3$) excitation probability increases as translational energy is raised. Then the contribution of this loss over the 77 meV to 260 meV range is not more than the 5% observed at 260 meV. It is also assumed that excitation to higher J values within $v=1$ is negligible, since the excitation probability should go down as the energy gap is increased.

Nonetheless, the role of rotational excitation in the H_2 ($v=1$) scattering from Cu should be addressed by further experiments. The results discussed in Part II showed that the rotational degree of freedom could be significantly involved in the scattering dynamics for H_2/Pd , which is near the barrier to dissociative chemisorption. Since H_2 ($v=1$) on Cu is also probably near the activation barrier, rotational excitation may be significant.

Also, the assumption that the rotational excitation probability increases monotonically with incident translational energy may be called into question by recent work by Hodgson and coworkers. [73] They performed an experiment similar to that discussed here in which they observed the excitation ($v=1$, $J=0\rightarrow 2$) in H_2 incident on Cu(111). They also looked for the transition ($v=1$, $J=1\rightarrow 3$) for translational energies up to 200 meV, but could not observe it within their detection limit. Although the interpretation of their results is complicated by the way they chose to scale their measurements, their data may suggest that the rotational excitation is strongest near the translational energy threshold for removal of the incident vibrationally excited molecules. If this is the case

rotational excitation could be significant in the present results even in the middle of the range of translational energies probed.

What about loss in the excited state due to vibrational relaxation of the incident H_2 ($v=1$) upon collision with the Cu target? This could occur by a number of different mechanisms, each having implications for the dynamics of the molecule-surface interaction.

One possibility is the conversion of molecular vibrational to translational energy during the scattering. This would be consistent with the observation of vibrational excitation in $\text{H}_2/\text{Cu}(111)$ scattering at high incident translational energy [50], since that is essentially the time-reversed process. Also, recent calculations predict a ($v=1 \rightarrow 0$) vibration to translation relaxation probability of about 15% for $\text{H}_2/\text{Cu}(100)$, as shown in Fig. 6.2

Although no attempt was made during the H_2/Cu scattering experiments reported here to observe vibrational relaxation, vibrational relaxation was observed in the H_2 ($v=1$) experiment on Pd. These results are presented in the next chapter, along with a more complete discussion of vibrational relaxation mechanisms which is also relevant to H_2 on Cu.

The sticking probability of the H_2 ($v=1, J=1$) state should be given by the difference between the loss observed in this state upon scattering and the portion of the loss accounted for by rotational excitation and vibrational relaxation. Since these branching ratios were not completely determined, however, the sticking coefficient is not known from the experimental data, only the total loss into sticking and other channels.

Figure 8.10 shows a comparison of the experimental results reported here with the best available theoretical calculations and previous experimental results for H_2 ($v=1$) on Cu. The filled squares show the measured loss in the H_2 ($v=1$, $J=1$) state upon scattering from Cu(110), defined as 1 minus the survival probability given above in Fig. 8.6, versus incident translational energy. The solid line is the sum of the dissociation and relaxation probabilities calculated by Kroes, *et al.* for $H_2/Cu(100)$. [58] The dot-dashed line is a tanh-based function (such as in

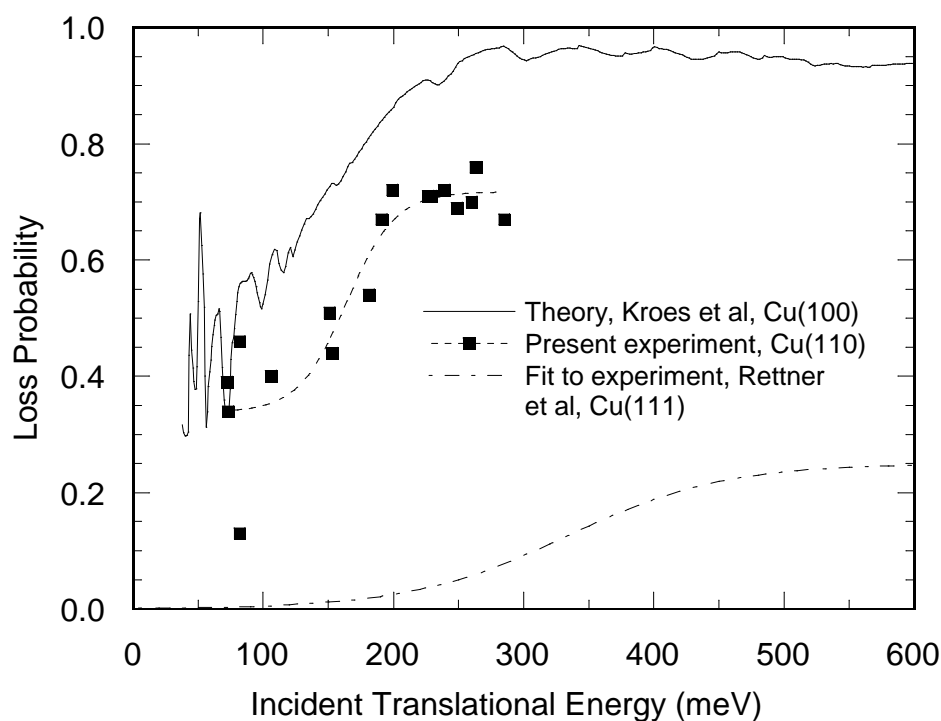


Figure 8.10: Comparison of loss observed in H_2 ($v=1$, $J=1$) state upon scattering from Cu(110) with theoretical calculations and previous experiments. Calculations on $H_2/Cu(100)$ were provided by G. J. Kroes from work in Ref. 58. Previous experimental results were obtained by Rettner, *et al.*, on $H_2/Cu(111)$. [61] See text for details.

Eq. (8.2)) with parameters set as determined by Rettner *et al.* in fitting their H₂/Cu(111) adsorption data. [61]

The agreement between our experimental results and the theoretical calculations by Kroes *et al.* shown in the figure is striking. It may be somewhat fortuitous, however, since these results are for different faces of the Cu crystal and since the effects of rotational motion were neglected in the theoretical calculations. Kroes *et al.* suggest that averaging over initial molecular orientations in their calculations would reduce the magnitude of both the dissociation and relaxation probabilities. Inclusion of molecular rotation might also broaden the transition width of the calculated curve, according to the conclusions of Gross *et al.*, who compared dynamical calculations of different dimensionality. [74]

The threshold and saturation values of the ($v=1$) adsorption probability curve determined by Rettner *et al.* are substantially different than those of the ($v=1, J=1$) total loss curve determined from our results. It is possible that part of the discrepancy results from the excitation and relaxation loss channels available in our experiment in addition to dissociation. However, it seems unlikely that this accounts for the majority of the discrepancy, which is quite large. Also, the calculations of Kroes *et al.* shown in Fig. 6.2 show the vibrational relaxation coefficient being more or less independent of translational energy, so that relaxation probably does not explain the shift in the thresholds between the Rettner *et al.* curve and the present results.

Of course, the Rettner *et al.* curve is determined for a different Cu crystal face than that of our results, but it is not clear whether this explains the differences either. Michelsen and Auerbach did a critical examination of available adsorption and desorption data from other groups for the Cu(100), Cu(111), and Cu(110) crystal faces, fitting all the data to tanh-based adsorption probability functions

(before Rettner, Michelsen, and Auerbach did their own experiments on Cu(111)). [70] Though they did find differences between the crystal faces, the trends are in the opposite direction to explain the discrepancy between the two experimental curves shown above. They found the translational energy threshold for adsorption of H_2 ($v=1$) to be smallest on the (111) face and largest on the (110) face. Also, they found the saturation value of the sticking coefficient to be largest for (111) and smallest for (110).

The fit from the Rettner *et al.* work shown above is from their analysis of adsorption data, which does not include effects due to rotation. From analysis of their H_2 /Cu(111) permeation-desorption data they did obtain both rotationally and vibrationally resolved values of the adsorption probability curve parameters. For ($v=1$, $J=1$), these parameters are not substantially different than those used to make the plot shown above, however.

The adsorption data of Hayden and Lamont [75] for H_2 on Cu(110) show a translational energy onset for sticking from a (presumably vibrationally) hot molecular beam of only about 140 meV, which is in close agreement with the present experimental results presented above. It seems somewhat at odds, however, with the H_2 ($v=1$)/Cu(110) sticking onset of 258 meV determined by Michelsen and Auerbach from analyzing this same (and other) data. [70]

The discrepancies discussed above motivate the approach adopted in the present studies. The combination of heated nozzle adsorption experiments with state-resolved permeation-desorption experiments has clearly established that the translational energy onset for vibrationally excited molecules is lower than that for ground state molecules, which was not addressed in the current studies or discussed above. However, because of the averaging over initial states that is present in the heated nozzle experiments and possible complications in applying

the desorption results to adsorption, the combined adsorption/desorption analysis probably does not give the best possible values for direct, state-resolved adsorption probabilities. The approach adopted here of preparing single rovibrational states in a molecular beam experiment with optical excitation will be able to provide the most exact values.

Chapter 9

H₂ on Pd

This chapter discusses the results of the experiments on H₂ ($v=1, J=1$) scattering from Pd(111). Since dissociation in the H₂/Pd system occurs readily, this system provides an interesting contrast to the experiments done on H₂/Cu, discussed in Chapter 6. In addition, since the Pd surface can easily be made inert to H₂ dissociation by saturation with H atoms, there is a convenient experimental means for checking the absolute survival probability measured in the experiment, as will be discussed below. Also, the fact that the translational energy range of interest in the H₂/Pd system is low means that low nozzle temperatures can be used in the experiments, facilitating the observation of relaxation from the vibrationally excited state to high rotational levels of the ground vibrational state.

This chapter is divided into three sections. The first section presents TOF spectra for the pumped H₂ molecules scattering from the Pd surface and discusses the difference between the clean and saturated surface. In the next section the absolute survival probabilities for these two surface states are computed. Finally, the observation of vibrational relaxation is presented and its implications discussed.

9.1 TOF Curves for Clean and H-Covered Pd

Figure 9.1a shows a TOF spectrum for H₂ in the ($v=1, J=1$) state incident upon and scattered back from clean Pd(111) held at $T_s = 450$ K. The first peak in the figure shows the packet of incident pumped molecules crossing the probe laser on its way towards the target, while the second, much smaller peak shows the molecules scattered back from the target still in the ($v=1, J=1$) state.

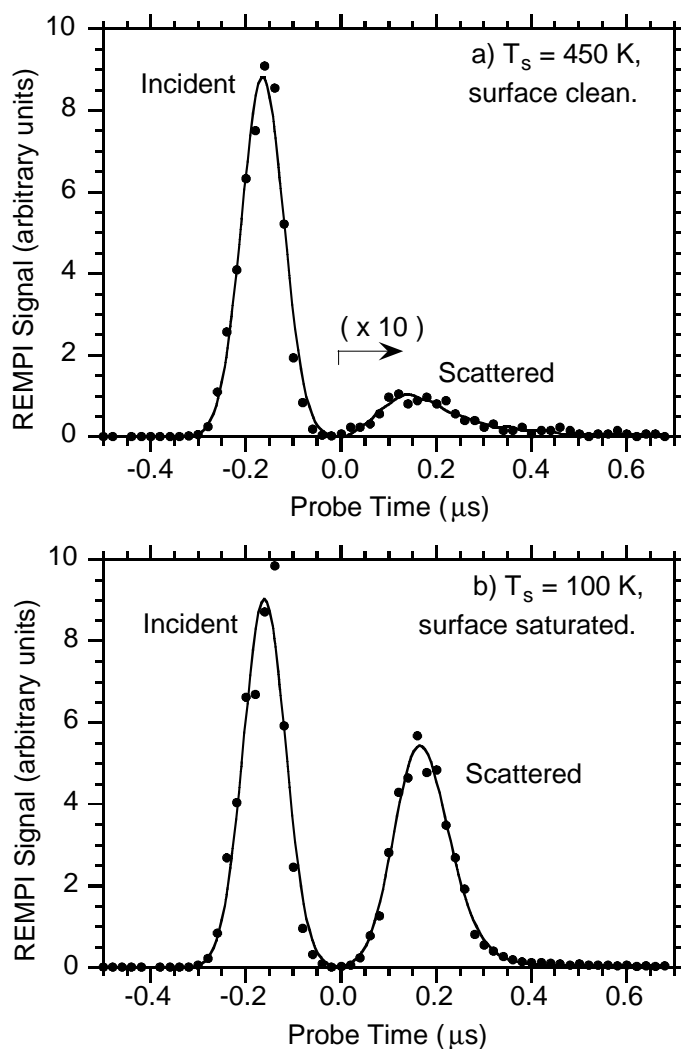


Figure 9.2: Sample TOF curves for H_2 ($v=1, J=1$) scattered from a) clean and b) H-saturated Pd(111) at an incident translational energy of 74 meV. Note that the reflectivity of the clean surface is very low, while that of the saturated surface is high.

The scattered peak is very weak compared to the incident one (note the $\times 10$ scale change), and also very weak compared to that shown for H_2 on Cu in Fig. 8.2.

By contrast, the scattered peak in Figure 9.2b, in which the Pd surface was first cooled to 100 K and saturated with H atoms, is much larger. (The crystal was H-saturated using the method outlined in Chapter 3 of Part II.) This dramatic difference between the two figures suggests very strongly that the loss in H₂ ($v=1$, $J=1$) upon scattering from the clean surface results from an electronic and/or chemical interaction with the surface which is passivated by the adsorbed H atoms.

The mean incident translational energy in both panels of Fig. 9.2, determined as outlined in Section 8.4, was 74 ± 1 meV. The translational energy of the molecules scattered from the H-saturated surface shown in Fig. 9.2b was 69 ± 1 meV, but the translational energy of molecules scattered from the clean surface could not be determined since the signal is so low. The zeros of the time axes in Fig. 9.2 were set to the peak arrival time of incident molecules at the target. The spectra were acquired with the probe laser 0.46 mm from the target surface and with the laser's vertical position (see Fig. 3.4) set to the center of the excited state packet.

The fits shown by the solid lines in Fig. 9.2 were used to prepare the spectra for the density to flux transformation, as discussed in Section 8.4 and further in Appendix C.

The low reflectivity of the clean surface to the pumped molecules appears to be roughly independent of incident translational energy over the range between 22 meV and 151 meV. TOF spectra taken at both ends of this range for the scattering from the clean surface appear very similar to that shown in Fig. 9.2a at 74 meV.

9.2 Absolute Survival Probability on Clean and H-Covered Pd

To determine the absolute survival probability of the H_2 ($v=1$, $J=1$) scattered from the clean and H-saturated Pd surfaces, the spatial integration technique outlined in Section 8.8 was used. A series of TOF measurements, like those shown above in Figure 9.2, was made over a range of vertical positions of the probe laser. The incident and scattered velocities were determined and a flux transform of each of the measured spectra was computed. The integrals under the incident and scattered peaks in the flux-transformed spectra were then tabulated versus the laser height. These data were acquired for an incident translational energy of 74 ± 1 meV and with the probe laser 0.46 mm from the target.

Figure 9.2 shows a plot of the results. Each point in the figure is the integrated flux, at a particular laser height, of either the incident or scattered H_2 ($v=1$, $J=1$) molecules. Data are shown for scattering both from the H-saturated surface (open squares) and from the clean surface (open diamonds). The solid curves in this figure are drawn to guide the eye only.

Taking the ratio of the area under each scattered profile in Figure 9.2 to that of the incident profile gives the survival probability of the excited molecules for the respective state of the surface, clean or saturated. Thus for clean Pd(111) at 450 K the incident H_2 ($v=1$, $J=1$) survival probability is only 0.05 ± 0.01 . The uncertainty in this value is estimated from the reproducibilities of the individual points in Figure 9.2. For the saturated surface at 100 K the ratio of the area under the scattered profile to that under the incident profile is 1.01 ± 0.04 , hence the survival probability, which can be at most 1, is between 0.97 and 1.

The difference in the results for the clean and saturated surface is very striking. Essentially the H-saturated surface is inert to the H_2 molecules incident in the ($v=1, J=1$) state, which are simply reflected. However, upon scattering from the clean surface, almost none of the incident H_2 ($v=1, J=1$) survives. The fact that the survival probability upon scattering from the inert, saturated Pd surface is close to unity also lends confidence that, in the H_2/Cu results presented in the last chapter, the maximum survival probability of only 0.67 represents a true loss of molecules at the surface and not simply a systematic error in integration of the scattered flux.

As in scattering from Cu, there are three possible loss channels for the

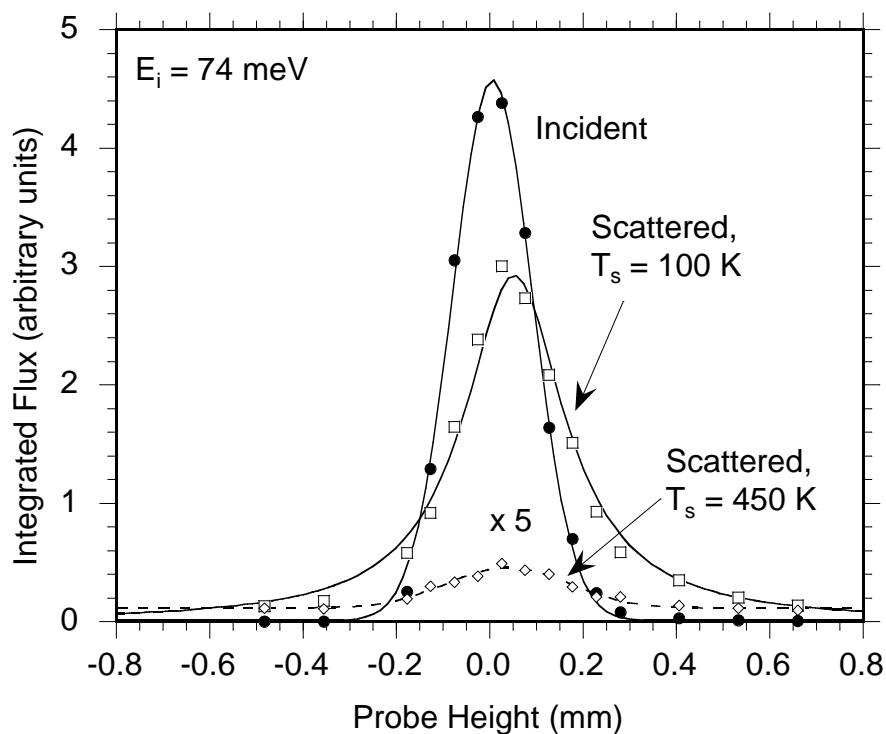


Figure 9.4: Spatial profiles of incident and scattered flux for H_2 ($v=1, J=1$) scattered from Pd(111), both clean and H-covered.

incident H_2 ($v=1, J=1$) upon collision with the clean Pd surface: dissociative adsorption (sticking); relaxation to any odd J in the ground vibrational state $v=0$ manifold; and rotational excitation within $v=1$, e.g. ($v=1, J=1 \rightarrow 3$).

Of these, sticking is almost certainly the dominant channel, since H_2 adsorption on Pd is non-activated and the sticking coefficient for H_2 in the ($v=0, J=1$) state on clean Pd(111) is already 0.62 ± 0.03 . (See Table 4.4 or Ref. 76) The ($v=1, J=1$) sticking coefficient should be even higher, given the excess $v=1$ population observed in permeation-desorption experiments with $\text{D}_2/\text{Pd}(100)$ and applying the principle of detailed balance. [62] Gross and Scheffler also predicted, on the basis of their theoretical calculations on Pd(100), a sticking coefficient for H_2 ($v=1$) more than twice as large as for $v=0$. [64]

However, sticking is not the only loss channel. As will be shown in the next section, vibrational relaxation also accounts for a significant fraction of the observed loss, at least 5% and possibly much more.

Rotational excitation within the $v=1$ manifold, such as observed for H_2/Cu scattering at high incident translational energy, is probably not a significant loss channel in the low translational energy Pd experiments. No scattering into the ($v=1, J=3$) state was observed in the H_2/Pd experiments within the experimental detection limit, which is a few percent of the total scattered flux. Excitation into higher J states is unlikely, since the excitation probability should decrease with the energy gap between the coupled states, and transfer into states with even J need not be considered, since this is forbidden by nuclear spin.

9.4 Vibrational Relaxation

9.4.2 TOF Spectra

To investigate the significance of vibrational relaxation in the H₂/Pd scattering, a series of TOF spectra on different rovibrational states was recorded during the H₂ ($v=1, J=1$) scattering experiment from the clean surface. [77] These are shown plotted together in Figure 9.3. The figure shows spectra recorded for the ($v=1, J=1$) state prepared by the pump laser, as well as for each of the odd J states in the ($v=0$) manifold that are lower in energy than it. Note that these spectra are all plotted with the same vertical axis zero, and are not offset. The incident translational energy of the pumped molecules is 55 ± 1 meV.

The large peak at negative time in the ($v=1, J=1$) spectrum shows the incident pumped molecules, while the small peak at positive time shows the weak scattering from the surface back into this state. The time axis zero has been set to the peak arrival time of the incident pumped packet at the surface, as before. The depletion observed in the ($v=0, J=1$) spectrum arises because this is the ground state from which molecules are pumped to ($v=1, J=1$) by the Raman lasers, and the ground state “hole” corresponds to the ($v=1, J=1$) incident peak.

Vibrational relaxation is evident in the appearance of the small peaks at positive times in the ($v=0, J=5$) and ($v=0, J=7$) spectra, which must arise from relaxation of the pumped ($v=1, J=1$) molecules. The thermal population in the ($v=0, J=5$) and ($v=0, J=7$) states in the molecular beam manifests itself as the baseline offset of these two spectra. Note the shift in the relaxation peaks to earlier time relative to the ($v=1, J=1$) scattered peak. This demonstrates that a significant portion of the vibrational energy disposed of excites translation of the scattered molecules, as will be discussed further below.

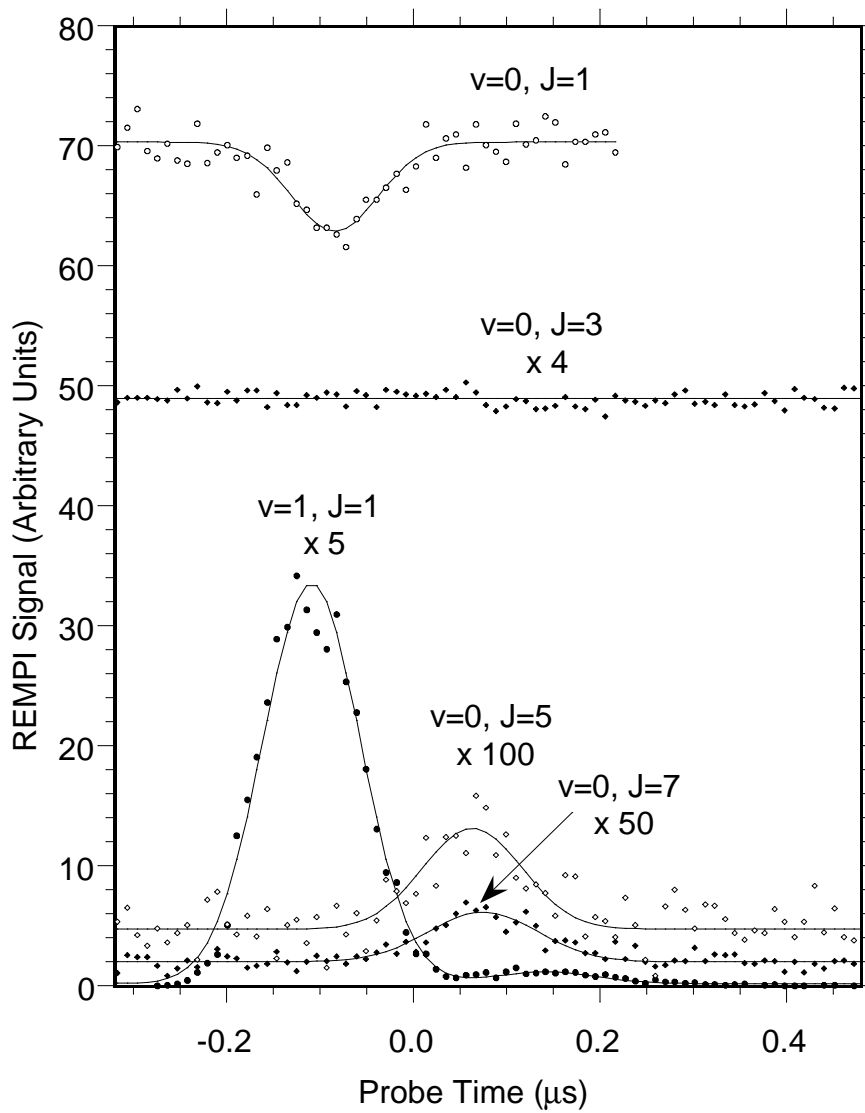


Figure 9.6: Time-of-flight curves for H_2 incident on Pd(111) in $(v=1, J=1)$, showing vibrational relaxation to $v=0$ manifold. Depletion in $(v=0, J=1)$ shows magnitude of population transfer by pump laser. Peaks at positive times in $(v=0, J=5)$ and $(v=0, J=7)$ are evidence of relaxation from $(v=1, J=1)$ into these states.

Since vibrational relaxation from ($v=1, J=1$) to ($v=0, J=5$) and ($v=0, J=7$) is observed, it seems plausible that relaxation to ($v=0, J=1$) and ($v=0, J=3$) should also be present. However, this is much more difficult to observe, because of the high thermal population of these states in the incident molecular beam. The thermal population in ($v=0, J=3$), for example, is about 150 times as large as the relaxation peaks observed in ($v=0, J=5$) and ($v=0, J=7$), as shown in Fig. 9.6. With the signal to noise obtained in the experiment, it was not possible to discern a relaxation peak in the ($v=0, J=3$) spectrum with a signal level smaller than about 1% of the thermal background. For the ($v=0, J=1$) state, the thermal background is even larger, and it is even more difficult to observe a peak due to relaxation.

No relaxation to even J states is expected, since the initial J state is odd and nuclear symmetry prevents coupling even and odd J states in the absence of a highly unlikely nuclear spin flip. To verify this, vibrational relaxation into the ($v=0, J=4$) and ($v=0, J=6$) states, which have low thermal backgrounds, was checked for. None was found.

9.4.4 Relaxation Probabilities

The vibrational relaxation probabilities into each of the observed channels were determined and are listed in Table 9.1, along with other data which will be discussed below. Several steps were taken in compiling this table.

First, corrections were made to the measured TOF spectra in order to put them on the same absolute intensity scale for plotting in Fig. 9.6. The spectra for the ($v=0$) manifold were each corrected for the effects of laser power variation by assuming the intensity is proportional to the square of the uv probe laser power, which was measured with a Scientech calorimeter. No further calibration of the ($v=0$) intensities is needed, since the H_2 (2+1) REMPI rate is nearly independent of rotational state for the Q branch of the (0,0) band used for probing. [78]

However, the REMPI rate can be expected to vary with vibrational band. [78] For the ($v=1, J=1$) spectrum, probed on the Q branch of the (1,1) band, the intensity axis was scaled so that the magnitude of the incident peak would equal the magnitude of the “hole” in the ground state, since these should correspond to exactly the same number of molecules. The size of this correction factor obtained for different experimental runs indicates that, after accounting for variations in probe laser power, the (1,1) band is 1.6 ± 0.2 times stronger than the (0,0) band, which is comparable to the difference in strength between other pairs of vibrational bands in H₂ (2+1) REMPI. [78]

For the ($v=1, J=1$) to ($v=0, J=5$) channel, the relaxation probability was determined in a manner similar to that described above for finding the survival probability of the ($v=1, J=1$) state. The incident and scattered velocities were determined and used to make a density to flux correction. The spatial distribution of incident and scattered flux (i.e. in the plane perpendicular to the lasers) was then integrated over and the resulting integrals were compared.

There was insufficient signal in the experiment to make a similar spatial integration measurement for the ($v=0, J=7$) state. In this case, it was assumed that the angular spread was equal to that measured for ($v=0, J=5$), and the relative scattered peak heights and velocities were used to deduce the relaxation probability for ($v=0, J=7$) from the ($v=0, J=5$) result. (Measurement of the velocities will be discussed below in Section 9.3.3.)

For ($v=0, J=3$) only a limit on the relaxation probability could be set. This was determined from the limit on the height of a relaxation peak set by the signal to noise in Fig. 9.6 and a consideration of the maximum possible velocity of the scattered ($v=0, J=3$) molecules consistent with energy conservation.

The sticking probability of the H₂ ($v=1, J=1$) state should be given by the difference between the loss observed in this state upon scattering from the clean surface and the portion of the loss accounted for by vibrational relaxation. If the relaxation probability to each of the odd- J ($v=0$) states had been determined, then, the H₂ ($v=1, J=1$) sticking coefficient would be known and the prediction of a higher sticking coefficient for the ($v=1$) state relative to ($v=0$) could be tested. Unfortunately, the lack of information on the relaxation to ($v=0, J=1,3$) prevents this, since we can at best guess how the relaxation probability will depend on J .

9.4.6 Energy Disposal

Relaxation of the H₂ vibration from ($v=1$) to ($v=0$) requires disposal of a significant amount of energy — 516 meV. The disposal of this energy into the various possible degrees of freedom has important implications for the dynamics of the scattering and relaxation event.

Some of the vibrational energy is transferred to both the rotational and translational degrees of freedom of the scattered molecule. The transfer of energy into rotation is seen already in that relaxation channels from $J=1$ to both $J=5$ and $J=7$ were observed. The final translational energies of the scattered ($v=0, J=5$) and ($v=0, J=7$) molecules, determined by measuring the scattered peak times as a function of probe laser distance from the surface, were 186 ± 26 meV and 119 ± 35 meV, respectively. These are significantly greater than the translational energy of the incident ($v=1, J=1$) molecules, 55 ± 1 meV. The observed energy gain in rotation and translation is summarized in Table 9.1.

The rotational and translational energy gain of the scattered molecules does not account for all of the vibrational energy lost, however. The difference, listed in Table 9.1, must be disposed of in the substrate. We may consider two

different channels for dissipation of the molecular vibrational energy in the substrate: excitation of phonons and excitation of electronic degrees of freedom.

Since the characteristic energy of the Pd phonons is on the order of 24 meV (the Pd Debye temperature is 275 K [39]), the observed dissipation of 70-180 meV of molecular vibrational energy would require excitation of roughly 3-8 phonons. Excitation of multiple phonons in a molecule-surface collision is expected to be weak [79,80] and relaxation via this channel may therefore be neglected. Also, kinetic energy transfer during a collision between an H₂ molecule and a Pd atom should be weak due to their large mass mismatch.

It seems far more likely that the vibrational energy is dissipated to electrons in the solid. For example, experimental and theoretical work has shown that, for molecules adsorbed on a metal, the molecular vibration can be efficiently coupled to electrons in the metal. If a molecular antibonding orbital lies close in energy to the metal's Fermi level, electrons can move back and forth between the antibonding level and the metal, thus damping the molecular vibration and carrying energy into the solid. [81,82,83] The vibrational relaxation of CO on Cu is a well known example of this mechanism. [84,85,86,87]

But can vibrational relaxation via heating of surface electrons be efficient in a single molecule-surface collision? A consideration of the relevant time scales

Table 9.2: Energy disposal in H₂ (v=1, J=1) vibrational relaxation on Pd(111). The incident translational energy was 55 ± 1 meV. The H₂ vibrational energy lost is 516 meV.

Transition	Probability (%)	Translational Energy Gain (meV)	Rotational Energy Gain (meV)	Energy Loss to Substrate (meV)
(v=1, J=1) → (v=0, J=1)	--	--	1	--
(v=1, J=1) → (v=0, J=3)	< 5.0	--	74	--
(v=1, J=1) → (v=0, J=5)	4.3 ± 1	131 ± 26	202	183 ± 26
(v=1, J=1) → (v=0, J=7)	3.2 ± 1	64 ± 35	380	72 ± 35

and relaxation rates suggests that this is plausible: the vibrational decay times may be comparable to or smaller than the molecule-surface interaction time in a single collision. In the H₂ scattering experiments the interaction time is on the order of a few tenths of a picosecond. For CO on Cu, the vibrational relaxation decay time is only about 2 ps. [84,85,86,87] For H₂ adsorbed on metal surfaces, theoretical calculations show vibrational lifetime broadening to be almost 20 meV, corresponding to a relaxation time of only 33 fs, if the molecule gets close enough to the surface for the energy of its lowest antibonding orbital to cross the metal's Fermi energy. [88,83] This is much smaller than the collision interaction time. Thus relaxation during a single collision seems plausible.

The question of whether metal electrons can be efficiently coupled to molecular vibrations in a single collision has also been addressed with regard to the observed vibrational excitation of NO scattered from silver. Rettner and coworkers, who did the original experimental work, proposed that the excitation did occur via an electronically nonadiabatic mechanism. [89] This was supported by theoretical calculations by Newns. [90] Other workers, however, proposed excitation mechanisms that did not involve excited substrate electrons [91,92], and a consensus still has not been reached on this matter.

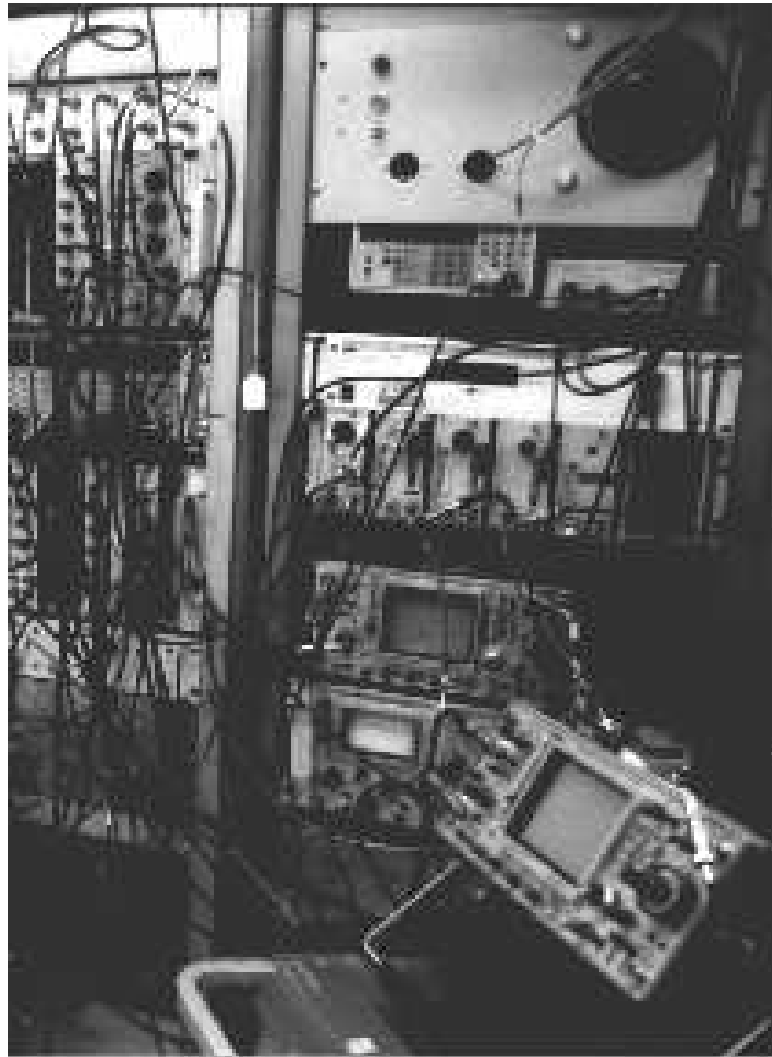
But now return to the present case of H₂ vibrational deexcitation upon scattering from Pd. If there were no transfer of molecular vibrational energy to the substrate, then the relaxation event could be viewed as resulting simply from the dynamics of the incident molecule on a single molecule-surface potential energy surface during the collision. Relaxation would occur in this case if the dissociation barrier is "late" along the reaction pathway, i.e. occurs at an extended value of the molecular bond length, since in this case the potential energy surface results in vibrational and translational degrees of freedom being mixed at the transition

state. Vibrational energy could be converted to translational energy during the collision. This would be analogous to the time-reversed process of the vibrational excitation of a molecule incident in the ground vibrational state with very high translational energy. This type of excitation has been observed for H₂ on Cu(111) [50], which is, as already discussed in Chapter 6, the classic example of a system with a late barrier to dissociation. The additional coupling to rotational motion can be considered within the same framework, involving a potential energy surface which has high spatial anisotropy, as discussed in Part II.

However, the observation that the relaxation mechanism involves significant energy transfer to the surface, and most likely to surface electronic degrees of freedom, indicates that the conceptual framework outlined above is not sufficient to understand the relaxation process observed. State-of-the-art dynamical calculations for the scattering of H₂ from metals have advanced considerably, to the point where all six molecular degrees of freedom can be considered quantum mechanically. However, in these calculations the surface degrees of freedom are not treated and no excited electronic states are considered. The results presented here suggest that electronically excited states may play an important role in the scattering dynamics and must be considered.

Part IV

Conclusion



Chapter 10

Summary, Conclusions, and Future Work

The principle goal of this work was to explore dynamical effects in dissociative adsorption via quantum state-resolved observations of molecule-surface scattering. Effects due to molecular rotation and to molecular vibration were considered in two separate sets of experiments. The results help test state-of-the-art theoretical simulations of molecule-surface scattering. The work is thus part of a larger effort to understand issues in gas-surface chemistry, which has widespread scientific and technological relevance.

Here the results and conclusions of each of the two main sections of the dissertation, Parts II and III, are reviewed. Following this, suggestions for further work on these projects are discussed. Lastly, future directions for surface science research in general are considered.

10.2 Summary of Part II - Rotational Effects

The experiments on the effects of molecular rotation in the dissociation probability of H_2 on Pd were motivated by recent theoretical calculations concerning the role of dynamical steering in this system.

The concept of dynamical steering emerged recently to explain trends observed in the nonactivated adsorption of H_2 on metals, namely the decrease of the sticking coefficient with increasing kinetic energy in the low energy regime. This trend also occurs in adsorption mediated by trapping, but the trapping channel is probably not relevant to H_2 on metals except at extremely low incident energies. According to the dynamical steering concept, the sticking probability of slowly moving molecules is enhanced by the ability of the molecule-surface

interaction forces to steer these molecules to favorable dissociation sites and geometries during the collision.

Theoretical calculations for H₂ adsorption on Pd(100), a system that has nonactivated adsorption pathways, therefore predict a strong dependence of the sticking coefficient not only on translational energy but also on initial rotational energy, because rotational motion can inhibit steering in the same way as translational motion. [4] The inhibition of sticking with rotational energy was qualitatively verified by permeation-desorption experiments and also by beam adsorption experiments carefully constructed to give some state-resolved results.

In the present work the molecular rotation effects in the H₂/Pd(111) system were investigated to explore a larger range of rotational and translational energy than achieved in previous experiments and also to consider the effects of state-changing collisions at the surface.

The rotational state-resolved measurements of the sticking coefficient of H₂ on Pd(111) at T_s = 423 K show a strong variation of the sticking coefficient with initial rotational quantum number. As J is raised from 0 to 3, the sticking coefficient decreases, qualitatively in accord with the theoretical calculations mentioned above. Notably, the sticking coefficient increases again as J is raised to 4 and 5, most likely because rotational energy can be used to directly overcome the activation barriers.

In addition to the strong dependence of the sticking coefficient on rotational quantum number, rotational excitation of the incident H₂ molecules during scattering from the surface was observed. This excitation is strongly activated by the surface temperature, occurs directly upon scattering, and is not activated by incident translational energy. For example, the probability for H₂ excitation from (v=0, J=1) to (v=0, J=3) on Pd(111) at T_s = 423 K is

approximately 1% even at an incident translational energy of 31 meV, which is less than the rotational excitation energy of 74 meV. The excitation probability goes up a factor of 2 as the surface temperature is raised to 845 K.

Both the J-dependent sticking and the rotational excitation suggest that molecular reorientation during collision with the surface plays an important role in the dissociation dynamics, in accord with theory.

However, the activation of the rotational excitation with surface temperature, in a regime where translation to rotation coupling cannot occur, cannot be explained using the current theoretical approach applied to this problem, which neglects surface degrees of freedom.

The simplest explanation of the observed results would be that the incident molecules are rotationally excited by surface atom motion, i.e. by surface phonons. This could be analyzed theoretically if the problem were treated with classical dynamics, rather than quantum dynamics, since then surface motion could be included more easily. A more interesting situation would occur if the rotational excitation resulted from an electronic (i.e. nonadiabatic) interaction with the surface. Suggestions for distinguishing between these possibilities will be discussed below in Section 10.3.

10.4 Summary of Part III - Vibrational Effects

The role of vibrational motion in activated dissociative chemisorption has been the subject of considerable study, and a consensus has emerged that vibrational energy can promote dissociation in systems where the activation barrier is “late” along the reaction path.

The H₂/Cu system is the most widely studied example of a system with a late barrier. The combination of data from heated nozzle adsorption experiments and state-selective permeation-desorption experiments has demonstrated that the

sticking coefficient of vibrationally excited H₂ on Cu is higher than that of ground state H₂, and has gone a long way towards establishing the relative adsorption probabilities from different rovibrational states and supporting general trends found from theory.

To more accurately determine the scattering behavior of H₂ from Cu in a single rovibrational state, a series of experiments using both laser state preparation and laser detection was carried out in the present work.

The results presented here for H₂ ($v=1, J=1$) scattering from Cu(110) show that the excited state molecules have a survival probability of only 0.67 ± 0.09 at an incident translational energy of 77 meV, and that the survival probability goes down by more than a factor of two as the translational energy is raised to 280 meV. The low survival probability at 77 meV suggests that, even at this energy, dissociation and/or vibrational relaxation are efficient. The results are in surprisingly good agreement with the most recent theoretical calculations for the total loss in H₂ ($v=1$) scattering from Cu(100) due to dissociation and relaxation. Further work is needed, however, to experimentally establish the branching ratios into each of the possible loss channels.

The laser state-preparation and detection scheme has also been used to investigate the scattering of vibrationally excited H₂ from Pd, which has recently become of interest because of the fact that vibrational effects are apparent even though dissociation occurs readily at low energies.

The survival probability of H₂ ($v=1, J=1$) was measured for scattering from clean Pd(111) at 450 K and H-covered Pd(111) at 100 K. The H-covered surface is nearly inert to the incident vibrationally excited hydrogen, which reflects back into the ($v=1, J=1$) state with probability between 0.97 and 1.00 for an incident translational energy of 74 meV. By contrast, the reflectivity of the

clean surface to H_2 ($v=1$, $J=1$) is very low over the incident translational energy range 22 meV to 151 meV, having an absolute value at 74 meV of 0.05 ± 0.01 . The contrast between these two results strongly suggests that the loss on the clean surface is due to an electronic/chemical interaction.

A significant fraction of the loss in the excited state upon scattering, at least 5% and perhaps much more, is accounted for by vibrational relaxation. Interestingly, this vibrational relaxation is most likely electronically nonadiabatic, since some of the energy released from vibration is dissipated in the surface, most likely to bulk electrons. Therefore, it may not be possible to account for this relaxation theoretically on the basis of the ground state potential energy surfaces calculated from density-functional theory.

Although relaxation is a significant loss channel, it is probably still the case that most of the loss in the vibrationally excited state upon scattering from the clean surface is due to dissociation. Even the ground state molecules have a high sticking coefficient (see Table 4.4 of Part II) and the sticking coefficient for ($v=1$) is expected to be even higher according to both theory [64] and experimental results in desorption. [62]

However, since the branching ratios between the different loss channels for H_2 ($v=1$, $J=1$) on Pd, primarily dissociation and relaxation, were not completely determined, it is not possible to say from these results whether the sticking coefficient is indeed higher for the ($v=1$) state than for ($v=0$). Further work is needed, and is in progress, to allow more accurate measurement of all the branching ratios.

10.6 Future Work on the State-Resolved Scattering Experiments

The state-resolved H_2/Pd and H_2/Cu scattering experiments begun in this work still have many interesting features left to explore. Some of these will be

described below. Ultimately, use of the techniques developed in this work for studying the scattering of state-prepared molecules will permit very stringent checks against theoretical calculations.

10.6.2 Continuing to Test the Ground State PES and Dynamics Calculations

The main set of goals in continuing these projects is to more completely measure the state-to-state scattering probabilities, to determine the branching ratios into different final states and to get more detail in the scattering probabilities as a function of translational energy. This will provide a more complete check against the PES and dynamics calculations

Perhaps the first place to start in this program should be to look for and measure the magnitude of vibrational relaxation of H_2 ($v=1$) on Cu, just as was done for Pd, and to measure the branching ratios into all possible loss channels of the excited state. Doing so will then permit the state-resolved sticking probability to be determined for the excited state, rather than just the survival probability.

Measuring the branching ratios into each of the possible vibrational relaxation channels will require significant improvements to the experimental setup. The results presented in Section 9.4.2 show that observation of relaxation into the lowest rotational levels of the ground state, which are well populated thermally, is not possible with the signal to noise ratio currently available in the experiment. It is possible that the signal to noise ratio, which is largely determined by shot-to-shot fluctuations in probe laser pulse characteristics, could be improved by some type of normalization technique. Preliminary attempts to achieve this were encouraging, though still inadequate.

Alternatively, the sticking coefficient (rather than survival probability) for the excited state could be determined if a technique capable of measuring small quantities of adsorbed H atoms could be implemented. The most traditional

approach to measuring adsorbate concentrations, that of thermal desorption spectroscopy, probably cannot be applied because the average flux of vibrationally excited molecules in the molecular beam is very small. However, these molecules are concentrated in a small region of the surface, so a technique sensitive to localized adsorbate concentrations might be successful. An optical or electron scattering technique seems most appropriate.

A further goal, in tandem with that of detecting scattering into more of the possible final states, should be to develop the ability to optically prepare a larger range of initial states. For example, all the $J=0-4$ levels of H_2 ($v=1$) could be prepared using Raman pumping if the Stokes light, currently generated by stimulated scattering in a cell of pressurized H_2 , were generated by a tunable light source. The ability to prepare these states would permit a measurement of the J dependence of sticking for H_2 ($v=1$) on Cu, which could be compared with the results for H_2 ($v=0$) on Pd. These might be expected to be similar, since H_2 ($v=1$) is near the energetic threshold for dissociation on Cu.

Using the ability to prepare these additional states would also permit looking for rotational relaxation, which could not be observed sensitively in the experiments described in Part II because of the high thermal populations in the states into which relaxation would occur. However, preparation of H_2 ($v=1, J=3$) would permit a sensitive measurement of the ($v=1, J=3 \rightarrow 1$) relaxation, since the thermal population in ($v=1, J=1$) is exceedingly small.

Yet another benefit of extending the state preparation techniques would be that it would permit the study of angular momentum alignment effects in reaction. Theoretical calculations predict that the sticking coefficient of H_2 on metals should be highest when the molecule approaches with its bond parallel to the surface, so that both H atoms may form bonds to the metal simultaneously, and

lowest when the molecule approaches with its bond perpendicular to the surface. Thus, with angular momentum aligned perpendicular to the surface, so that the molecules perform a “helicopter” motion, the sticking coefficient should be larger than with angular momentum aligned parallel to the surface, giving a “cartwheel” motion. Permeation experiments have demonstrated this effect, with H₂ desorbing from Pd(100) found to be preferentially aligned with angular momentum perpendicular to the surface. [93] The direct effect in adsorption could be tested in our experimental setup. Using Raman transitions with $\Delta J=2$, the ratio of the two angular momentum alignment states prepared in the molecular beam may be varied, permitting the alignment effects to be observed in the reactive scattering.

Another, and probably more distant goal, is to look for resonance structures in the sticking probabilities as a function of incident translational energy, such as those sharp features shown in the theoretical results in Figs. 2.2 and 6.2 and discussed in Section 2.4. This structure depends very sensitively on the calculated potential energy surface and dynamics, and its detailed observation would permit a very stringent experimental test of theory. A number of issues which complicate the experimental observation of this structure have been discussed in the literature. [22]

10.6.4 Looking for nonadiabatic effects

The proposed experiments discussed above are ones which are designed to further test predictions made by the current state-of-the-art in theory. This involves quantum dynamical simulations on potential energy surfaces computed within density functional theory, with an emphasis on molecular degrees of freedom only. Experiments should also be done which address effects not explained within this theoretical framework.

Two such effects were uncovered in the present work which should be explored further: the surface temperature dependent rotational excitation and the loss of vibrational energy to the substrate observed in H₂/Pd scattering. In these processes energy is not conserved within the molecule. Thus explanation of either of them requires a consideration of surface degrees of freedom. The main question to be answered is whether it is nuclear motion or electronic degrees of freedom (i.e. nonadiabatic effects) that are most important.

This question can be addressed experimentally in the case of the surface temperature dependent rotational excitation by looking for the behavior in both H₂ (v=0) and H₂ (v=1) scattering from Cu. If the rotational excitation occurs by energy transfer from surface phonons, i.e. from the surface atoms essentially knocking around the H₂ molecule during the scattering event, then the rotational excitation for H₂ should be similar in magnitude on Cu and Pd, and should not depend much on the vibrational state for H₂ on Cu at low translational energy. The excitation might even be larger on Cu than Pd, since Cu is lighter and thus should transfer kinetic energy to H₂ via collisions more efficiently. However, if the excitation arises from an electronic interaction, it might be expected that it would occur only when the molecule is close to the energetic barrier for dissociation, which is the case for H₂ (v=1) on Cu as well as H₂ (v=0) on Pd, but not for H₂ (v=0) on Cu.

In the case of the H₂ (v=1) vibrational energy transfer to the Pd substrate, some indication of whether the energy transfer is to phonons or electrons could be obtained by doing the experiment again for H₂ (v=1) on H-covered Pd. If energy transfer occurs to phonons, then the relaxation might be expected to be approximately the same for this case as for H₂ (v=1) on clean Pd, or possibly larger, due to the lower mass of the particle with which the gas-phase H₂ would be

colliding (an H atom instead of a Pd atom). However, if the vibrational energy transfer to the surface is dissipated to electronic degrees of freedom, i.e. as the vibrating molecule interacts with the electronic orbitals of the clean surface, it might be eliminated on the H-passivated Pd.

Interpretation of the results of both sets of experiments just discussed to distinguish between phonon and electron interactions might be good starting points for new theoretical studies.

10.8 Future Directions in Surface Science

At the outset it was stated that one of the principle goals of surface science research is to obtain an understanding of the mechanisms of heterogeneous catalysis, and, ultimately, to be able to use that knowledge to design improved catalytic systems.

Much of the fundamental research in gas-surface chemistry over the last thirty years has concentrated on the mechanisms of dissociative adsorption, since this is often the rate-limiting step in a surface-catalyzed chemical reaction. This research has largely focused on an understanding of activation barriers to dissociative adsorption, with both experiment and theory concentrating on the interactions of molecules on clean, single-crystal metal surfaces.

Much has been learned about the basic physics of interactions in these model systems. For example, the relative reactivities of various metals can be at least qualitatively explained theoretically, as can dynamical effects observed in experiments. Theoretical methods continue to improve, and significant progress has recently been made in calculating potential energy surfaces and dynamics. State-resolved experiments such as those discussed in this dissertation will provide very stringent checks on these calculations.

There is also still much to be learned even in these basic interactions. In particular, as discussed above, there is a need for a better theoretical understanding of surface degrees of freedom, both electronic and nuclear, and their role in molecule-surface scattering.

However, still larger steps remain to be taken before real catalytic systems can be well understood. These systems differ from the traditional surface science models in several ways.

One such difference, often referred to as the “pressure gap,” is that the flux of reactant molecules onto the surface is many orders of magnitude higher in catalytic reactors than that used in typical molecular beam UHV surface science studies. In molecular beam experiments the flux is on the order of 10^{-2} - 10^{-3} ML/s, while at atmospheric pressure it is 10^9 ML/s. Reaction mechanisms may be available in the high flux regime that are not apparent in the low flux studies. For example, collisions of molecules with species already adsorbed or trapped on the surface may induce dissociation which would otherwise not occur, such as in the collisional activation of CH_4 dissociation on Ni. [94] In addition, high flux conditions may permit the population of high-concentration adsorbate phases with greatly enhanced reactivity. An example is the oxidation of CO on O-covered Ru, which proceeds most readily when the O coverage is near 1 ML. [95] The O-Ru bond energy decreases with increasing coverage, facilitating the oxidation reaction. [96]

Furthermore, many real catalysts actually consist of solids of several different components, whose behavior is different than that of the individual constituents. [97,98] In addition, the presence of poisoning or promoting adsorbate species can also greatly alter reactivities, by, for example, changing surface electronic structure. [99] These are very important subjects to address,

because the most likely method of improving catalysis is by tailoring the composition of the catalyst material itself.

And, while the traditional model surface science systems include well defined single crystal surfaces, most catalysts are polycrystalline and contain numerous defect sites and grain boundaries which may have greatly enhanced reactivity. This fact has long been recognized, of course, and experimental and theoretical studies have attempted to address it by studying reactions at step edges and defect sites.

Thus, in the author's opinion, the following are especially important areas for continued study in the program of improving heterogeneous catalysis: the stability and reactivity of high-coverage phases, collision-induced reaction mechanisms, electronic structure and reactivity of alloy and bimetal surfaces, effects of poisoners and promoters, and effects of surface morphology. Each of these areas is still amenable to study by UHV surface science techniques, including molecular beam scattering. The basic model systems used to study them, however, will be of slightly greater complexity than the clean, flat, single crystal metals on which much of surface science has so far been based.

Appendix A

H₂ REMPI and Raman Transitions

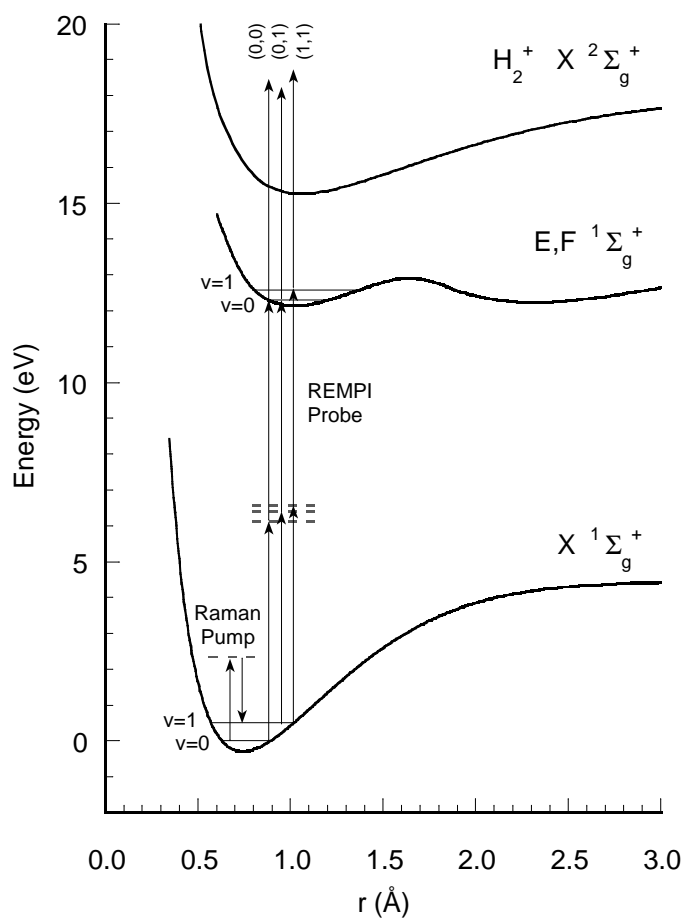


Figure A.2: H₂ REMPI and Raman transitions used. Probing proceeds by (2+1) REMPI through the E,F state. The REMPI vibrational bands are denoted by (v',v''), where v'' and v' are the vibrational quantum numbers in the ground and E,F states, respectively. Each band consists of a manifold of lines between different rotational levels. Only Q-branch lines, with $\Delta J=0$, were used.

Appendix B

Response versus Scattering Angle in Shadow Experiments

In the experiments using the wire-shadowed aperture to distinguish between incident and scattered molecules, the probe system has a detection sensitivity that depends on the scattering angle. Relations for this function will be derived here.

Figure B.1 shows the relevant geometry. The molecular beam is assumed to be incident upon the target at normal incidence and to be perfectly collimated. The figure shows a hypothetical trajectory for a molecule which passes through the aperture, strikes the target at position $(0, y_0, z_0)$ on the surface, and scatters with total scattering angle θ and azimuthal angle ϕ as shown.

Let $P(y_0, z_0, \theta, \phi)$ be the probability that this molecule is subsequently ionized by the probe laser and detected. It is given by

$$P(y_0, z_0, \theta, \phi) = A \cdot \int_0^{\infty} ds [I_P(s)]^2, \quad (\text{B.2})$$

where A is a normalization constant that includes the laser power, ionization cross section, ion collection efficiency, etc., s is the distance from the point of scattering along the scattered trajectory, and $I_P(s)$ is the probe laser intensity at s . We take the REMPI cross section to depend on I_P^2 since it is a two-photon process. For $I_P(s)$ we use the relevant expressions for a gaussian beam [100] with beam waist $\omega_0 = 100 \mu\text{m}$, which is the measured waist of our beam. We have written the above equation as though the probe laser were continuous and the integrand were independent of time, when in fact the laser is pulsed. However, this can be neglected because the duration of the molecular beam pulse is much longer than

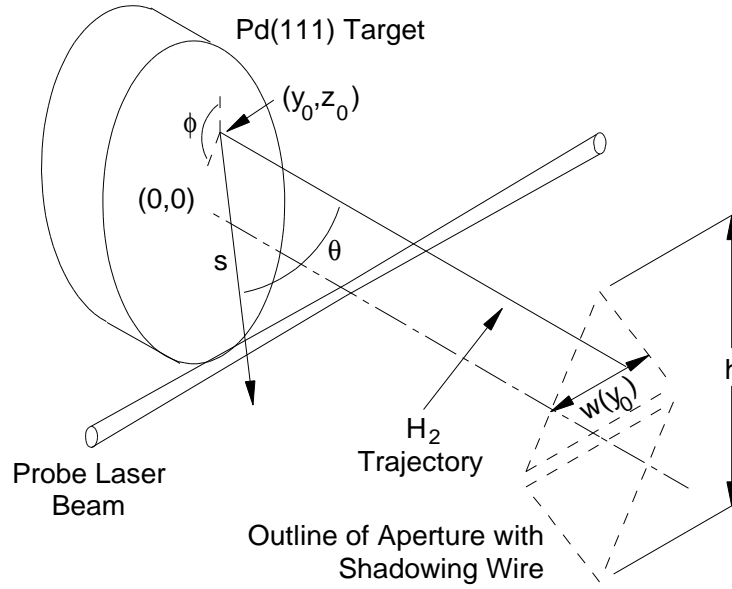


Figure B.2: Geometry for determining angular response function of detection system when using wire-shadowed aperture.

the flight time of the molecules from the target to the probe laser focus, so that the molecular beam pulse may be regarded almost as continuous with respect to the laser. At the instant the laser fires there will always be molecules that have left the chopper at an appropriate time to reach the probe focus, regardless of scattering angle.

The relative response of the detection system to molecules scattering with angles θ and ϕ , integrated over all impact sites on the surface which are illuminated by the molecular beam, is given by

$$R(\theta, \phi) = \int_{-h/2}^{h/2} dy \int_{-w(y)/2}^{w(y)/2} dz P(y, z, \theta, \phi), \quad (\text{B.4})$$

where h is the height of the aperture and $w(y)$ is the width of the aperture at height y . We take $w(y)=0$ over the portion obstructed by the wire.

We now make the simplifying assumption that the scattering is symmetric about ϕ . Then we can define the average response of the detection system versus scattering angle, measured from the normal, as

$$R^{avg}(\theta) = \frac{1}{2\pi} \cdot \int_0^{2\pi} R(\theta, \phi) d\phi . \quad (\text{B.6})$$

We have calculated this function for the aperture dimensions given above in Chapter 3. It is shown in Figure B.4. The poor response at very low scattering angles is due to the placement of the probe laser in the shadow made by the wire across the beam aperture: molecules which scatter along the surface normal cannot enter the shadow region and be detected. The shape and orientation of the

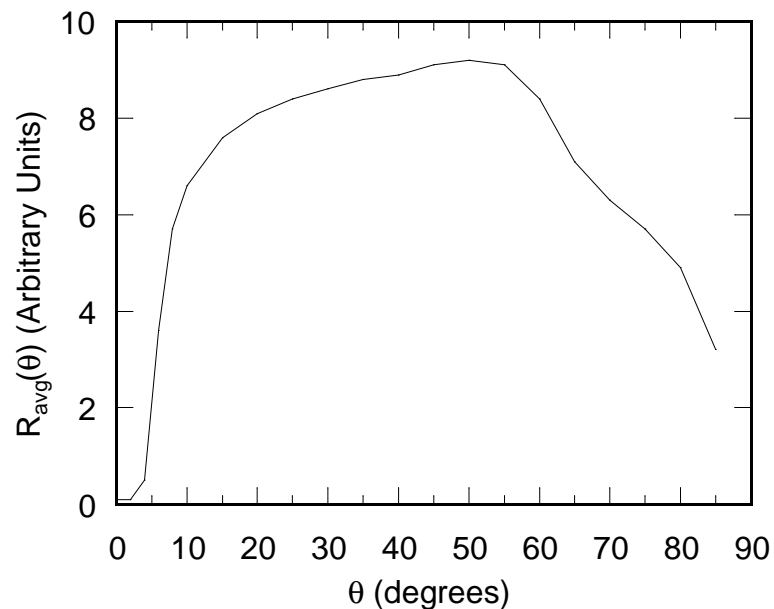


Figure B.4: Angular response of detection system in shadow geometry.

aperture, as well as the probe laser to surface distance, were chosen to achieve the approximately uniform response of $R^{avg}(\theta)$ at intermediate angles which is shown in Figure B.4.

Appendix C

Density to Flux Transformation of TOF Spectra

Here a mathematical procedure for transforming the measured, density-weighted time-of-flight (TOF) spectra to flux-weighted spectra is given. In comparing just the integrals under the incident and scattered peaks in a TOF spectrum, the density to flux correction can be estimated, to fairly good approximation, by considering only the difference between the incident and scattered velocities. This is easily determined. However, to more completely understand the effects of the scattered velocity and angle distributions on the actual shapes of the TOF spectra, and to integrate the flux as accurately as possible, the procedure discussed below was developed.

Both velocity and angle effects can be considered in terms of one relevant parameter, $v_{\perp}^{scat} = v \cos(\theta)$, the projection of a scattered molecule's velocity, v ,

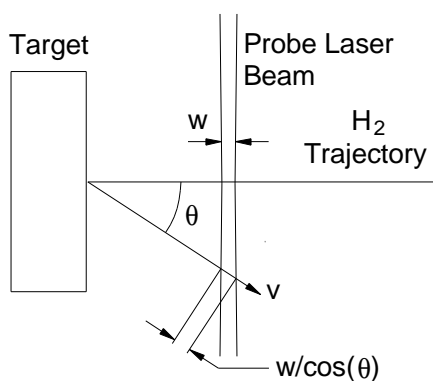


Figure C.2: Distance traversed through probe volume by a scattered molecule.

onto the plane perpendicular to the laser axis. Here θ is the angle the molecule's trajectory makes with the surface normal. The probability for a given scattered molecule to be detected is proportional to $1/v_{\perp}^{scat}$. This is because the time a scattered molecule spends in the laser probe volume is proportional to the distance it traverses through the probe volume divided by its velocity. The distance traversed is $w/\cos\theta$, as shown in Figure C.2, where w is the effective width of the probe laser beam.

Since the angle and velocity spread of the incident molecules is much smaller than that of the scattered molecules, it will be assumed in the following that the incident velocity and angle spreads have negligible effects on the TOF spectra. Only the effects of the scattered velocity and angle distributions, and the incident spread in arrival times, will be considered.

To begin, consider the TOF spectrum that would be obtained if the incident molecules had zero spread in arrival time at the target, in addition to zero spread in angle and velocity. The incident peak in the TOF spectrum would then be a delta function. The density weighted TOF spectrum would be given by

$$I_D^0(t) = A_1 \cdot \delta(t - t_0^{inc}) + A_2 \cdot f(v_{\perp}^{scat}(t)) \cdot \frac{v_{inc}}{v_{\perp}^{scat}(t)}. \quad (C.2)$$

The first term above represents the incident peak in the TOF spectrum, and the second term describes the shape of the scattered peak, which has a nonzero width due to the distribution of scattered velocities. The incident packet hits the target at $t = 0$, and $t_0^{inc} \equiv -d/t$ is the time the incident packet crosses the probe laser, where d is the distance between the laser and the surface. $f(v_{\perp}^{scat})$ is the probability distribution for molecules to scatter back from the surface with a projection of

their velocity onto the plane perpendicular to the laser axis of v_{\perp}^{scat} , and $v_{\perp}^{scat}(t) = d/t$ is the projected velocity required for a scattered molecule to appear at time t in the TOF spectrum. A_1 and A_2 are normalization constants. The factor of $v_{inc}/v_{\perp}^{scat}(t)$ in the second term of eq. (C.2) accounts for the dependence of the scattered molecules' detection probability on their velocity, relative to the detection probability of the incident molecules.

The flux-weighted TOF spectrum is equivalent to eq. (C.2), but without the extra velocity factor in the second term, i.e.

$$I_F^0(t) = A_1 \cdot \delta(t - t_0^{inc}) + A_2 \cdot f(v_{\perp}^{scat}(t)). \quad (C.4)$$

To simplify eqs. (C.2) and (C.4) we substitute in

$$C(t) \equiv A_2 \cdot f(v_{\perp}^{scat}(t)) \cdot \frac{v_{inc}}{v_{\perp}^{scat}(t)} \quad (C.6)$$

to obtain

$$I_D^0(t) = A_1 \cdot \delta(t - t_0^{inc}) + C(t) \quad (C.8)$$

and

$$I_F^0(t) = A_1 \cdot \delta(t - t_0^{inc}) + \frac{v_{inc}}{v_{\perp}^{scat}(t)} \cdot C(t). \quad (C.10)$$

Since, in practice, there is a nonzero spread of incident arrival times at the target, the observed density and flux weighted spectra would be the convolutions of the ideal spectra given by the equations above and the incident time-of-arrival distribution $S(t)$. The observed density-weighted spectrum is then

$$I_D(t) = \int_{-\infty}^{\infty} S(t') \cdot I_D^0(t - t') dt' \quad (C.12)$$

and its flux transform is

$$I_F(t) = \int_{-\infty}^{\infty} S(t) \cdot I_F^0(t-t') dt' . \quad (\text{C.14})$$

The analysis goal is to determine $I_F(t)$, given the measured $I_D(t)$. This is done by assuming a form for $S(t)$, deconvolving the measured $I_D(t)$ with $S(t)$, multiplying the scattered peak in the result by $(d/t)/v_{inc}$, and reconvolving with $S(t)$ to get $I_F(t)$.

The deconvolution step is not approached directly, because, in practice, a direct deconvolution of the measured data is greatly complicated by noise in the spectra and by the fact that the measured spectra are sometimes cut off before the scattered signal has fallen completely to zero. Instead, $C(t)$ is allowed to be an arbitrary function described by a suitable set of parameters, and the parameters are optimized to make the convolution evaluated in eq. (C.12) fit the measured spectrum as smoothly as possible. $S(t)$ is set to a gaussian whose height and width match those of the incident pulse in the measured spectrum. Once $S(t)$ and $C(t)$ have been determined, eqs. (C.10) and (C.14) can be used to calculate the corresponding flux transformed spectrum.

Note that the function $C(t)$ obtained in this process contains information on the velocity and angle distributions of the scattered molecules, which may be of interest in its own right. [101]

Figure C.2 shows an example of the density to flux transformation. The figure shows a TOF spectrum for H_2 ($v=1, J=1$) scattered from Cu(110). The solid symbols are the measured data points. The solid line is the function $I_D(t)$, fit smoothly to the data by fixing $S(t)$ appropriately and then determining $C(t)$ by nonlinear least squares fitting. The dashed line shows the deconvolved spectrum $I_D^0(t)$, and the dotted line shows the final flux-transformed spectrum, $I_F(t)$. Note that the effect of the transformation was to increase the scattered signal at early

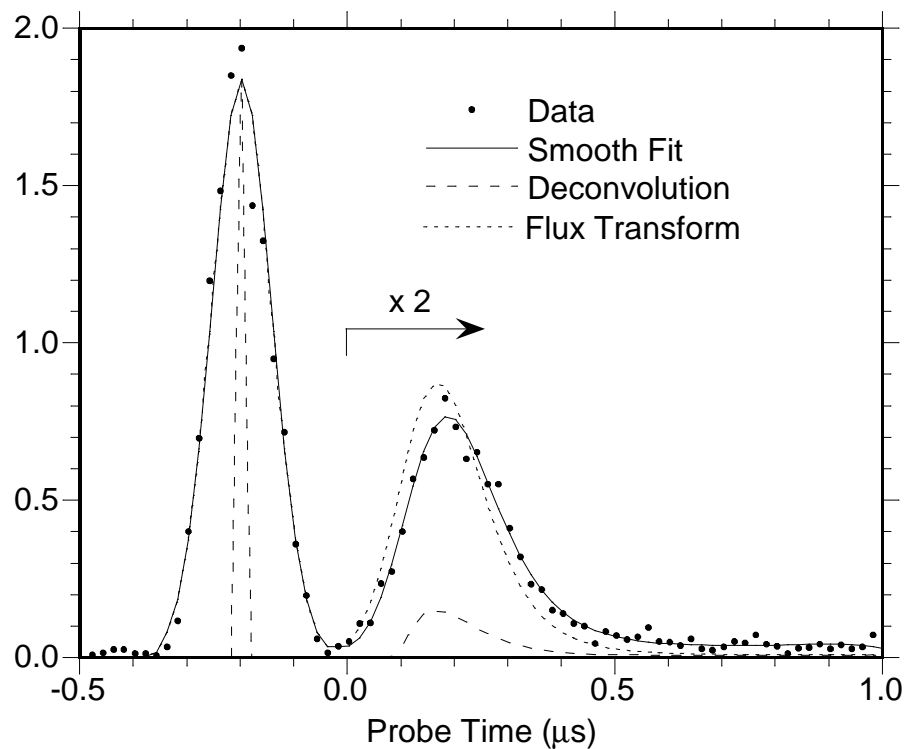


Figure C.4: Example of density to flux transformation of TOF spectrum. See text for details.

times, since here the faster molecules are undercounted in the measured spectrum, and to decrease the signal at late times, where the slower molecules are overcounted.

References

- [1] G. R. Darling and S. Holloway, *Report Prog. Phys.* **58**, 1595 (1995).
- [2] *Dynamics of Gas-Surface Interactions*, edited by C. T. Rettner and M. N. R. Ashfold (Royal Society of Chemistry, London, 1991).
- [3] M. C. Payne, M. P. Teter, D. C. Allan, T. A. Arias, and J. D. Joannopoulos, *Rev. Mod. Phys.* **64**, 1045 (1992).
- [4] A. Gross, S. Wilke, and M. Scheffler, *Phys. Rev. Lett.* **75**, 2718 (1995).
- [5] A. Gross, S. Wilke, and M. Scheffler, *Surf. Sci.* **358**, 614 (1996).
- [6] M. Kay, G. R. Darling, S. Holloway, J. A. White, and D. M. Bird, *Chem. Phys. Lett.* **245**, 311 (1995).
- [7] A. Eichler, G. Kresse, and J. Hafner, *Phys. Rev. Lett.* **77**, 1119 (1996).
- [8] K. D. Rendulic, G. Anger, and A. Winkler, *Surf. Sci.* **208**, 404 (1989); Ch. Resch, H. F. Berger, K. D. Rendulic, and E. Bertel, *Surf. Sci.* **316**, L1105 (1994).
- [9] H. F. Berger, Ch. Resch, E. Grösslinger, G. Eilmsteiner, A. Winkler, and K. D. Rendulic, *Surf. Sci.* **275**, L627 (1992); D. A. Butler, B. E. Hayden, and J. D. Jones, *Chem. Phys. Lett.* **217**, 423 (1994); P. Alnot, A. Cassuto, and D. A. King, *Surf. Sci.* **215**, 29 (1989).
- [10] G. Anger, H. F. Berger, M. Luger, S. Feistritzer, A. Winkler, and K. D. Rendulic, *Surf. Sci.* **219**, L583 (1989).
- [11] K. D. Rendulic and A. Winkler, *Surf. Sci.* **299/300**, 261 (1994).
- [12] C. B. Mullins and W. H. Weinberg, in *Surface Reactions*, edited by R. J. Madix (Spring-Verlag: Berlin, 1994).
- [13] D. Kelly and W. H. Weinberg, *J. Vac. Sci. Technol. A* **14**, 1588 (1996).
- [14] *Physisorption Kinetics*, H. J. Kreuzer and Z. W. Gortel (Spring-Verlag: New York, 1986), pp. 5-9.

- [15] S. Andersson, and L. Wilzén, *Phys. Rev. B* **38**, 2967 (1988).
- [16] L. Schröter, R. David, and H. Zacharias, *Surf. Sci.* **258**, 259 (1991); *J. Vac. Sci. Technol. A* **9**, 1712 (1991).
- [17] A. Gross and M. Scheffler, *Chem. Phys. Lett.* **263**, 567 (1996).
- [18] A. Gross, *J. Chem. Phys.* **102**, 5045 (1995).
- [19] M. Beutl, M. Riedler, and K. D. Rendulic, *Chem. Phys. Lett* **247**, 249 (1995).
- [20] M. Beutl, M. Riedler, and K. D. Rendulic, *Chem. Phys. Lett.* **256**, 33 (1996).
- [21] C. T. Rettner and D. J. Auerbach, *Chem. Phys. Lett.* **253**, 236 (1996).
- [22] C. T. Rettner, D. J. Auerbach, A. Gross, and M. Scheffler, *Phys. Rev. Lett.* **77**, 404 (1996).
- [23] J. L. W. Siders and G. O. Sitz, *J. Chem. Phys.* **101**, 6264 (1994).
- [24] E. E. Marinero, C. T. Rettner, and R. N. Zare, *Phys. Rev. Lett.* **48**, 1323 (1982); E. E. Marinero, R. Vasudev, and R. N. Zare, *J. Chem. Phys.* **78**, 692 (1983).
- [25] M. Gostein and G. O. Sitz, *Rev. Sci. Instrum.* **66**, 3389 (1995); **65**, 3036 (1994).
- [26] This clever trick was suggested by C. Rettner.
- [27] K. Kunimori, T. Kawai, T. Kondow, T. Onishi, and K. Tamaru, *Surf. Sci.* **59**, 302 (1976).
- [28] R. J. Behm, K. Christmann, and G. Ertl, *J. Chem. Phys.* **73**, 2984 (1980).
- [29] H. Conrad, G. Ertl, J. Küppers, and E. E. Latta, *Surf. Sci.* **65**, 245 (1977).
- [30] See, e.g., R. D. Ramsier, K.-W. Lee, and J. T. Yates, Jr., *J. Vac. Sci. Technol. A* **13**, 188 (1995), and references therein.

- [31] K. Christmann, *Introduction to Surface Physical Chemistry*, (Springer-Verlag, New York, 1991), p. 70.
- [32] H. Conrad, G. Ertl, and E. E. Latta, *Surface Sci.* **41**, 435 (1974).
- [33] M. Wolf, S. Nettesheim, J. M. White, E. Hasselbrink, and G. Ertl, *J. Chem. Phys.* **92**, 1509 (1990).
- [34] T. Engel, *J. Chem. Phys.* **69**, 373 (1978); H. Conrad, G. Ertl, J. Koch, and E. E. Latta, *Surf. Sci.* **43**, 462 (1974).
- [35] G. E. Gdowski, R. H. Stulen, and T. E. Felter, *J. Vac. Sci. Technol. A* **5**, 1103 (1987); G. E. Gdowski, T. E. Felter, and R. H. Stulen, *Surf. Sci.* **181**, L147 (1987).
- [36] H. A. Michelsen, C. T. Rettner, and D. J. Auerbach, *J. Chem. Phys.* **98**, 8294 (1993).
- [37] G. R. Darling and S. Holloway, *J. Chem. Phys.* **101**, 3268 (1994) and references therein.
- [38] See, e.g., J.-B. Song and E. A. Gislason, *Chem. Phys.* **202**, 1 (1996) or J.-B. Song and E. A. Gislason, *J. Chem. Phys.* **103**, 8884 (1995) and references therein.
- [39] *Solid State Physics*, N. W. Ashcroft and N. D. Mermin (Saunders Company, Philadelphia, 1976), p. 461.
- [40] L. Mattera, "Rotational Inelastic Scattering," in *Atomic and Molecular Beam Methods*, Vol. 2, ed. by G. Scoles, (Oxford University Press, New York, 1992).
- [41] D. Cvetko, A. Morgante, A. Santaniello, and F. Tommasini, *J. Chem. Phys.* **104**, 7778 (1996).
- [42] A. J. Cruz and B. Jackson, *J. Chem. Phys.* **91**, 4985 (1989).
- [43] D. M. Nace and J. G. Aston, *J. Am. Chem. Soc.*, **79**, 3619 (1957).

- [44] J. Völkl and G. Alefeld, "Diffusion of Hydrogen in Metals," in *Topics in Applied Physics Vol. 28: Hydrogen in Metals I*, ed. by G. Alefeld and J. Völkl, (Springer-Verlag: New York, 1978).
- [45] B. E. Hayden, in *Dynamics of Gas-Surface Interactions*, edited by M. N. R. Ashfold and C. T. Rettner (Royal Society of Chemistry, London, 1991).
- [46] H. A. Michelsen, C. T. Rettner, and D. J. Auerbach, in *Surface Reactions*, edited by R. J. Madix (Springer-Verlag, Berlin, 1994).
- [47] G. Anger, A. Winkler, and K. D. Rendulic, *Surf. Sci.* **220**, 1 (1989).
- [48] B. E. Hayden and C. L. A. Lamont, *Chem. Phys. Lett.* **160**, 331 (1989); *Phys. Rev. Lett.* **63**, 1823 (1989); *Surf. Sci.* **243**, 31 (1991).
- [49] C. T. Rettner, D. J. Auerbach, and H. A. Michelsen, *Phys. Rev. Lett.* **68**, 1164 (1992).
- [50] C. T. Rettner, D. J. Auerbach, and H. A. Michelsen, *Phys. Rev. Lett.* **68**, 2547 (1992).
- [51] H. A. Michelsen, C. T. Rettner, and D. J. Auerbach, *Phys. Rev. Lett.* **69**, 2678 (1992).
- [52] C. T. Rettner, H. A. Michelsen, and D. J. Auerbach, *J. Vac. Sci. Technol. A* **11**, 1901 (1993).
- [53] G. D. Kubiak, G. O. Sitz, and R. N. Zare, *J. Chem. Phys.* **83**, 2538 (1985).
- [54] J. E. Müller, *Surf. Sci.* **272**, 45 (1992).
- [55] B. Hammer, M. Scheffler, K. W. Jacobsen and J. K. Nørskov, *Phys. Rev. Lett.* **73**, 1400 (1994).
- [56] J. A. White, D. M. Bird, M. C. Payne and I. Stich, *Phys. Rev. Lett.* **73**, 1404 (1994).
- [57] G. Wiesenekker, G. J. Kroes, E. J. Baerends, and R. C. Mowrey, *J. Chem. Phys.* **103**, 5168 (1995); **102**, 3873 (1995).

- [58] G. J. Kroes, G. Wiesenekker, and E. J. Baerends, Phys. Rev. B **53**, 10397 (1996).
- [59] G. J. Kroes, E. J. Baerends, and R. C. Mowrey, Phys. Rev. Lett., *in press*.
- [60] G. J. Kroes, E. J. Baerends, and R. C. Mowrey, *in preparation*.
- [61] C. T. Rettner, H. A. Michelsen, and D. J. Auerbach, J. Chem. Phys. **102**, 4625 (1995).
- [62] L. Schröter, H. Zacharias, and R. David, Phys. Rev. Lett. **62**, 571 (1989); L. Schröter, S. Kuchenhoff, R. David, W. Brenig, and H. Zacharias, Surf. Sci. **261**, 243 (1992); L. Schröter, Chr. Trame, J. Gauer, H. Zacharias, R. David, and W. Brenig, Faraday Discuss. Chem. Soc. **96**, 55 (1993).
- [63] G. R. Darling and S. Holloway, Faraday Discuss. Chem. Soc. **96**, 87 (1993).
- [64] A. Gross and M. Scheffler, Chem. Phys. Lett. **256**, 417 (1996).
- [65] R. L. Farrow and D. W. Chandler, J. Chem. Phys. **89**, 1994 (1988).
- [66] R. Frey, J. Lukasik and J. Ducuing, Chem. Phys. Lett **14**, 514 (1972)
- [67] The chemical polishing recipe used was adapted from section A of J. S. Ahearn, J. P. Monaghan, and J. W. Mitchell, Rev. Sci. Instrum. **41**, 1853 (1970). No electropolishing was done. Use of gaseous HCl was omitted.
- [68] This work was originally published in M. Gostein and G. O. Sitz, J. Vac. Sci. and Technol. A **14**, 1562 (1996).
- [69] This work was originally published in M. Gostein, H. Parhikhteh, and G. O. Sitz, Phys. Rev. Lett. **75**, 342 (1995).
- [70] H. A. Michelsen and D. J. Auerbach, J. Chem. Phys. **94**, 7502 (1991).
- [71] T. F. Hanisco and A. C. Kummel, J. Phys. Chem. **96**, 2982 (1992).
- [72] R. Dopheide and H. Zacharias, J. Chem. Phys. **99**, 4864 (1993).

- [73] A. Hodgson, P. Samon, A. Wight, and C. Cottrell, *Phys. Rev. Lett.* **78**, 963 (1997).
- [74] A. Gross, B. Hammer, M. Scheffler, and W. Brenig, *Phys. Rev. Lett.* **73**, 3121 (1994).
- [75] B. E. Hayden and C. L. A. Lamont, *Phys. Rev. Lett.* **63**, 1823 (1989).
- [76] M. Gostein and G. O. Sitz, *J. Chem. Phys.*, *in press*.
- [77] M. Gostein and G. O. Sitz, *J. Chem. Phys.*, *in preparation*.
- [78] K.-D. Rinnen, M. A. Buntine, D. A. V. Kliner, and R. N. Zare, *J. Chem. Phys.* **95**, 214 (1991).
- [79] V. P. Zhdanov and K. I. Zamaraev, *Catal. Rev. Sci. and Engr.* **24**, 373 (1982).
- [80] R. B. Gerber, L. H. Beard, and D. J. Kouri, *J. Chem. Phys.*, **74**, 4709 (1981).
- [81] B. N. J. Persson and M. Persson, *Solid State Communications*, **36**, 175 (1980).
- [82] B. N. J. Persson and R. Ryberg, *Phys. Rev. Lett.* **48**, 549 (1982).
- [83] M. Persson and B. Hellsing, *Phys. Rev. Lett.* **49**, 662 (1982).
- [84] T. A. Germer, J. C. Stephenson, E. J. Heilweil, and R. R. Cavanagh, *Phys. Rev. Lett.* **71**, 3327 (1993).
- [85] J. C. Tully, M. Gomez, M. Head-Gordon, *J. Vac. Sci. Technol. A* **11**, 1914 (1993).
- [86] M. Morin, N. J. Levinos, and A. L. Harris, *J. Chem. Phys.* **96**, 3950 (1992).
- [87] M. Head-Gordon and J. Tully, *J. Chem. Phys.* **96**, 3939 (1992).
- [88] B. Hellsing and M. Persson, *Physica Scripta* **29**, 360 (1984).

- [89] C. T. Rettner, J. Kimman, F. Fabre, D. J. Auerbach, and H. Morawitz, *Surf. Sci.* **192**, 107 (1987); C. T. Rettner, F. Fabre, J. Kimman, and D. J. Auerbach, *Phys. Rev. Lett.* **55**, 1904 (1985).
- [90] D. M. Newns, *Surf. Sci.* **171**, 600 (1986).
- [91] A. Gross, and W. Brenig, *Chem. Phys.* **177**, 497 (1993); *Surf. Sci.* **289**, 335 (1993).
- [92] G. A. Gates, G. R. Darling, and S. Holloway, *J. Chem. Phys.* **101**, 6281. (1994); G. A. Gates and S. Holloway, *Surf. Sci.* **307**, 132 (1994).
- [93] D. Wetzig, R. Dopheide, M. Rutkowski, R. David, H. Zacharias, *Phys. Rev. Lett.* **76**, 463 (1996).
- [94] S. T. Ceyer, *Science* **249**, 133 (1990).
- [95] See, e.g., C. H. F. Peden, D. W. Goodman, M. D. Weisel, and F. M. Hoffmann, *Surf. Sci.* **253**, 44 (1991).
- [96] C. Stampfl, S. Schwegmann, H. Over, M. Scheffler, and G. Ertl, *Phys. Rev. Lett.* **77**, 3371 (1996).
- [97] See, e.g., A. T. Hanbicki, A. P. Baddor, E. W. Plummer, B. Hammer, and M. Scheffler, *Surf. Sci.* **331**, 811 (1995).
- [98] See, e.g., B. Hammer, and M. Scheffler, *Phys. Rev. Lett.* **74**, 3487 (1995).
- [99] See, e.g., E. Bertel, P. Sandl, K. D. Rendulic, and M. Beutl, *Ber. Bunsenges, Phys. Chem.* **100**, 114 (1996).
- [100] *Quantum Electronics*, A. Yariv (John Wiley and Sons: New York, 1989).
- [101] M. Gostein and G. O. Sitz, in *Laser Techniques for State-Selected and State-to-State Chemistry III*, edited by J. W. Hepburn (SPIE, Bellingham, WA, 1995).

Vita

Michael Gojer was born on July 13, 1968 to Charles and Berta Gojer of Dallas, Texas. He attended Hillcrest High School in Dallas, Texas, from which he graduated as salutatorian. He then went on to attend the Massachusetts Institute of Technology in Cambridge, Massachusetts, graduating in 1991 with a bachelors degree in Physics. While at MIT he developed an interest in chemical physics, doing undergraduate research projects in laser spectroscopy. In the fall of 1991 he began his graduate studies at the University of Texas at Austin, working in the laboratory of Prof. Greg Sitz studying the dynamics of dissociative chemisorption using laser spectroscopy and molecular beams. He married Abby Bernstein in 1993, and the two adopted the combined surname Gostein. In 1994 he received a masters degree in Physics from the University of Texas at Austin and continued on as a Ph.D. candidate.



Permanent address: 10802 Branch Oaks Circle, Dallas, Texas 75230

This dissertation was typed by the author.